GEOCHEMISTRY
OF THE
ETIVE GRANITOID COMPLEX
ARGYLL, SCOTLAND

by

Richard A. Batchelor

A thesis presented for the degree of
Master of Science in the Faculty of Science
at the University of St.Andrews, 1984.

DECLARATION

a). I ...RICHARD A. BATCHELOR... hereby certify that this thesis which is approximately ...32,000... words in length has been written by me, that it is a record of work carried out by me, and that it has not been submitted in any previous application for a higher degree

date ...23rd April '84... signature of candidate

b). I hereby certify that the candidate has fulfilled the conditions of the Resolution and Regulations appropriate to the degree of Master of Science of the University of St.Andrews and that he is qualified to submit this thesis in application for that degree.

date ...23/4/84... signature of supervisor

Copyright Declaration

UNRESTRICTED

In submitting this thesis to the University of St.Andrews I understand that I am giving permission for it to be made available for use in accordance with the regulations of the University Library for the time being in force, subject to any copyright vested in the work not being affected thereby. I also understand that the title and abstract will be published, and that a copy of the work may be made and supplied to any bona fide library or research worker.

"I think that most geologists at some time in their career become interested in granites and, judging from past writings on this topic, it seems that one is allowed considerable poetic licence when dealing with it. This makes me less fearful than I otherwise might have been; at least if I talk nonsense I join a distinguished company. One thing is certain, my mind is certainly not confused by too many facts."

- W.S. Fyfe

in 'Mechanisms of Igneous Intrusions' (1970), p.201 'Some thoughts on granitic magmas'.

C O N T E N T S

ACKNOWLEDGEMENTS

It was John Flett Brown who suggested Etive to me as an area for study, and to him I owe much gratitude for his initial direction and for help in the field. Ed Stephens subsequently took responsibility for my work and his direction and criticism has been appreciated. Peter Bowden lent a sympathetic ear to my wilder speculations. Thin sections were prepared by Andrew Mackie and Andrew Barman, and James Allan contributed to the photographic work. My efforts have been supported all along by Prof. E.K. Walton.

Not forgotten are the people of Lorne who provided access to land, local information and the occasional welcome refreshment: Col. R. Campbell-Preston of Ardchattan, Tim Healey of Ardmaddy, Col. Turnbull of Blarcreen, Maj. and Mrs. Reynolds of Ardachy, Liz MacNaughton formerly of Ardachy, Mr. McClarty forester at Barcaldine, The Forestry Commission at Oban, and West Highland Estates at Oban.

The field work would not have been possible without the effort, patience and companionship of Rosalind Garton, who acted as unpaid field assistant throughout the period of this project, tolerated the idiosyncracies of West Highland weather with fortitude, and met the unwelcome attentions of the native insect life with good English stoicism. Her criticism of the text has also been appreciated. She has tolerated my bouts of 'thesisitis' remarkably well and for this I am grateful.

ABSTRACT

The Etive complex is a composite pluton, 30km long and 20km wide intruded into Dalradian metasediments c.400Ma. It is one of the largest Scottish Caledonian granites and is closely associated in time with the vulcanism of Glen Coe.

The complex is made up of four major zones: satellite and marginal intrusions of diorite and quartz diorite, an outer, annular, fault-controlled Cruachan intrusion, sheets and dykes of Meall Odhar granites, and an inner forcefully-emplaced Starav pluton. These lithologies consist of nine petrographically-distinct rock types: diorite, quartz diorite, Cruachan monzodiorites (dark), monzodiorites and monzogranites, porphyritic and non-porphyritic Starav monzogranites, and Meall Odhar monzogranites and alkali granites.

Geochemical investigation of 56 samples has highlighted futher divisions. Quartz diorites and Cruachan monzodiorites (dark) have similar major element compositions. There is a chemical discontinuity between the southern Cruachan monzodiorites and the northern Cruachan monzogranites. The two Starav types are chemically distinct and are considered two independent intrusions, an outer porphyritic Starav monzogranite and an inner Central Starav monzogranite. Within the porphyritic Starav, three chemically-distinct pulses have been identified which correlate with major topographic features. The Meall Odhar monzogranite is chemically similar to the Starav magmas and is

considered to be ring dyke material injected during the forceful intrusion of the Starav plutons, while the unevolved trace element pattern of the alkali granite is consistent with an origin by partial melting from a felsic granulite.

With the exception of the Cruachan monzodiorites, all the rock compositions appear to be related to a mafic (basaltic) parent by fractional crystallisation of clinopyroxene, olivine, orthopyroxene and hornblende, followed by plagioclase, biotite, apatite and sphene. In-situ fractional crystallisation operated within individual intrusions. Isotope studies indicate the incorporation of a crustal component. The Cruachan monzodiorites have enhanced levels of Al, Zr, Hf, Ba, La, Ce and Na, and lie off the general chemical trend for Etive. Chemical evidence suggests that mixing took place between quartz dioritic magmas and crustal partial melts of syenitic composition.

FOLD-OUT CRYPTOGRAM

REFERENCE SHEET

FOLD-OUT CRYPTOGRAM

REFERENCE SHEET

Fig 1

MAP

ETIVE COMPLEX

key

- Sample points
- MOG
- D
- Q
- Geological boundary
- Chemical discontinuity

D	Diorite
Q	Quartz diorite
CMD	Cruachan monzodiorite
" T_o	— dark variant
" T	— normal
" T_x	— felsic variant
CMG	Cruachan monzogranite
MOG	Meall Odhar granites
PSMG	Porphyritic Starav monzogranite
CSMG	Central Starav monzogranite
F	Fault Intrusion

Glencoe
GLEN COE
RANNOCH MOOR
GRANITE
GLEN ETIVE
GLEN URE
GLEN LIVER
GLEN NOE
GLEN KINGLAS
LOCH ETIVE
Beinn Trilleachan
Ben Starav
Meall Odhar
Taynuilt
Ben Cruachan
A108
fault
CMG
CSMG
PSMG
MOG
CMD
Q
D
F
T
T_x
038 039 040 042-1 043,4 050 051 053 054 036 057,058 037 056 055 052 035 059,060 048-9 045 046-7 064 063-1 029 030 031-2 133 134 136 135 102 033 034 099 100 101,3 105 104 106 093 092 094 137-140 095 014 096 015 016-7 073 072 070-1 069-7 066 065 027 025 026 021-4 028 013 018 128-131 097 123 126-7 098 012 118-120 083,2 084-8 107-8 089 081 080 079 078 074 075 077 076,5 019 110-11 116-7 007-8 113-5 009-11,20 090 006 001-5 091 132 109 A156 A155 A157 A163 A162 A164 A022 A020

LOCATION MAP

Wick
Inverness
SCOTLAND
ETIVE
Oban
StAndrews
Glasgow
Edinburgh
60 mi
0 100 km

Rock name	Cryptogram	Symbol
Diorite	D	D
Quartz diorite	Q	Q
Cruachan monzodiorite(dark)	CMD(dark)	T.
Cruachan monzodiorite	CMD	T
Cruachan granitoid(light)	CMD(light)	Tx
Bonawe granitoid	B	B
Cruachan monzogranite	CMG	A
Porphyritic Starav monzogranite	PSMG	P
-ditto- (felsic)	PSMG	P.
Central Starav monzogranite	CSMG	C
Meall Odhar monzogranite	MOG	M
Meall Odhar alkali granite	MOG	M.

INTRODUCTION

The earliest reference to the geology of the Etive granite complex is by MacCulloch (1817) who noticed that Ben Cruachan and Ben Starav were composed of granite containing "an equal mixture of reddish feldspar and white quartz, with very little mica". He compared this granite to that of Cairn Gorm. The official geological surveys of Etive divided the area into two mapping areas, a northern lobe which included Glen Coe (Bailey and Maufe, 1916,1960) and a southern lobe (Kynaston and Hill, 1908). These workers established the major rock types, namely the Quarry Intrusion diorites, the peripheral Cruachan granitoids, one Starav intrusion in the centre and a leucocratic variant of Cruachan (later described as the Meall Odhar type). This groundwork led Anderson (1937) to map the complex as one whole unit and he was able to establish that the Beinn a' Bhuiridh screen, adjacent to the Quarry diorites in the SE consisted of sheared and metamorphosed andesite lavas. He also established that the leucocratic variant of Cruachan was a separate intrusive suite, named after the Meall Odhar occurrence, and that the Starav intrusion was emplaced by cauldron subsidence of the Cruachan. The outer porphyritic and inner non-porphyritic types represented two pulses intruded in close succession.

Brown (1975) attempted the first geochemical study of Etive granitoids as part of a broader isotope study. His major geochemical conclusion was that all the Etive magmas derived from one primary magma source from which individual pulses underwent varying degrees of crystal fractionation. He noted that barium behaved in an anomalous fashion. He also concluded that the whole Cruachan intrusion represented a cross-section through a tilted differentiated pluton, since SiO_2 values increased northwards. He believed that the high concentration of plagioclase crystals in the southern Cruachan monzodiorites were indicative of crystal settling and consequently this zone represented the floor of a magma chamber.

General studies of Caledonian magmatism have encompassed Etive in the last ten years. Structural studies by Roberts (1974) noted that the Glen Coe cauldron is tilted to the NE due to asymmetrical subsidence. This feature may be related to Brown's hypothesis of a NE tilt (op.cit.) which Droop and Treloar (1981) confirmed, on the basis of PT parameters obtained from the contact aureole mineralogy.Groome and Hall (1974) comment that the Etive magma chamber did not feed the rhyolites which form part of the ORS Lorne lava suite, but probably gave rise to the porphyrite dyke swarm, some of which cut the Cruachan granitoids.

Plant et al (1980) found Mo - Cu - Th anomalies around Etive (based on stream sediment sampling). The structure of the Dalradian rocks around Loch Creran, on the W side of Etive, was studied in detail by Litherland (1980) and the effects of contact metamorphism by Etive granitoids on the country rocks led Droop and Treloar (1981) to confirm that Etive must have crystallised at a relatively high level (3 to 6 km).

Several isotope studies based on Sr, O, Pb, and Nd have been carried out on Etive rocks (Blaxland et al. 1979; Hamilton et al. 1980; Pidgeon and Aftalion, 1980; Clayburn 1981; Harmon et al. 1983; Clayburn et al. 1983) and the findings are detailed in the Discussion, Chapter 5. Some of these results are based on analyses from the same rocks as Brown (1975).

The aims and objectives of this study are to gain an understanding of the petrogenesis of this zoned and composite pluton both in terms of source control and high level effects of crystal fractionation. To achieve this the following approaches have been adopted.

1.To sample as widely as possible each of the constituent granitoid bodies which make up the Etive complex.

2.To investigate each sample petrographically and to describe and name the rock types in terms of their mineralogy and texture.

3.To analyse chemically representative samples for major and selected trace elements.

4.To display the chemical data in such a way as to obtain meaningful information concerning the inter-relationship of each rock type.

5. Where appropriate, to compute fractional crystallisation vectors from chosen mineral compositions and published distribution coefficients in order to interpret crystal-liquid controls on chemical variations.

6.To arrive at an internally-consistent petrogenesis for the Etive rocks as a unit, and further to predict the origin of their source magmas.

REGIONAL GEOLOGY

The host rocks around the Etive intrusion consist of Dalradian metapelites, calc-silicates and psammites (Kynaston and Hill, 1908; Bailey and Maufe, 1960). The structure of the rocks around Loch Creran which bound the west side of Etive consists of NE-trending upright D1 folds which become recumbent to the E. At the head of Loch Creran the D1 fold axes swing to the SE. The regional structure is cut by a major slide (the Benderloch slide) which coincides with a change in facies from the Ardmucknish succession (shallow water facies) to the Creran succession (greywackes) which represents the flanks of the developing Dalradian geosyncline. A further three deformation events did not materially alter the major D1 structure which is likened to a 'mushroom' recumbent to the E, on a NE-SW axis (Litherland, 1980,1982).

The granitoid pluton truncates the regional structure, and schistosity in pelitic schists is destroyed by development of contact hornfels (Brown, 1975). Hence the country rocks had already been deformed by Caledonian crustal movements prior to the intrusion of the Etive granitoids (Chinner, 1978). There is no evidence for post-intrusion deformation within the intrusive plutonic rocks and therefore they can be included in the group of Newer Granites as defined by Read (1961).

The thermal aureole at the contact between the Dalradian metapelite sequences and the Cruachan granitoid varies from 2 to 2.5km wide (Droop and Treloar, 1981). Samples of hornfelsed metapelites and calc-silicates studied by Droop and Treloar (op.cit.) were used to assess the depth of intrusion of the Etive granitoids. Calc-silicates contain Diopside + wollastonite + plagioclase (An_{24-33}) + microcline + clinopyroxene + garnet ($Gross_{31}And_{69}$ - $Gross_{22}And_{78}$) + rare quartz. Maximum pressure calculated for this assemblage was 1.6 $\pm$ 1.0kb. Two metapelites containing cordierite + andalusite gave values of 2 and 1.5 $\pm$ 1kb. Using the Al_2SiO_5 P-T diagram, these values represent the maximum pressure within the andalusite field without sillimanite formation. These authors concluded that the contact aureole of the Etive (Cruachan) intrusion represents a depth of 3 to 7km ($\pm$ 1 to 2kb) with accompanying temperatures of 775 to 800^{o}C. Brown (1975) preferred a depth of 2 to 3km ($\pm$ 0.7 to 1kb), based on normative mineralogy and K/Ar systematics.

The maximum thickness of Lower Old Red Sandstone (L.O.R.S.) lavas in the Lorne plateau is 1250m (Roberts, 1966) and the minimum vertical displacement on the Pass of Brander fault is 1280m (the height of Ben Cruachan which is not capped by lavas). These combine to give a minimum depth of intrusion of 2.5km in the SW. This assumes that the Etive pluton intruded the Lorne lava plateau.If, according to Brown (1975), the Etive complex was tilted about a NW-SE axis with the SW end rising about 3km, then the original depth of intrusion for the SW would have been 5.5km, which is consistent with the findings of Droop and Treloar (1981). Based on calculated pressures for garnet grade

metamorphism of 4 to 7kb, the 475-500Ma Dalradian rocks must have risen at a rate of 0.1 to 0.2mm/a to have reached 5km depth by the time the Etive complex was emplaced at c.400Ma (Clayburn et al. 1983).

Magnetic and gravity anomalies over Etive are unusual in having the highest magnitude anomalies of all the Caledonian granitoids. The low gravity anomaly indicates that there is a large density contrast between the igneous rocks and the country rocks. This suggests there is a large volume of the more siliceous late granite at depth.

Recent gravity data (Hipkin and Hussain, 1983) details the nature of the regional anomaly over Scotland. The change in negative anomaly is rapid from the Dalradian country rocks (-10 to -20mgal) in the W across the Cruachan and Porphyritic Starav granitoid contacts, culminating in a negative "low" over the Central Starav pluton of -46mgal. This low value is only exceeded in Scotland by the Cairngorm massif at -54mgal (Fig 2.1). However, the eastern extension of the granite "low" suggests that a buried pluton lies to the E, which does not support the NE tilting model of Droop & Treloar (1981) and Brown (1975). (Fig 2.1)

The filtered aeromagnetic anomaly is +200nT (Caledonian range -50 to +200) and indicates there is a strong magnetic component to the local rocks. Since the gravity anomaly suggests a large volume of silicic rock which is usually low in magnetite, the magnetic anomaly has been ascribed to recrystallisation and accompanying remagnetisation of magnetite within the schists due

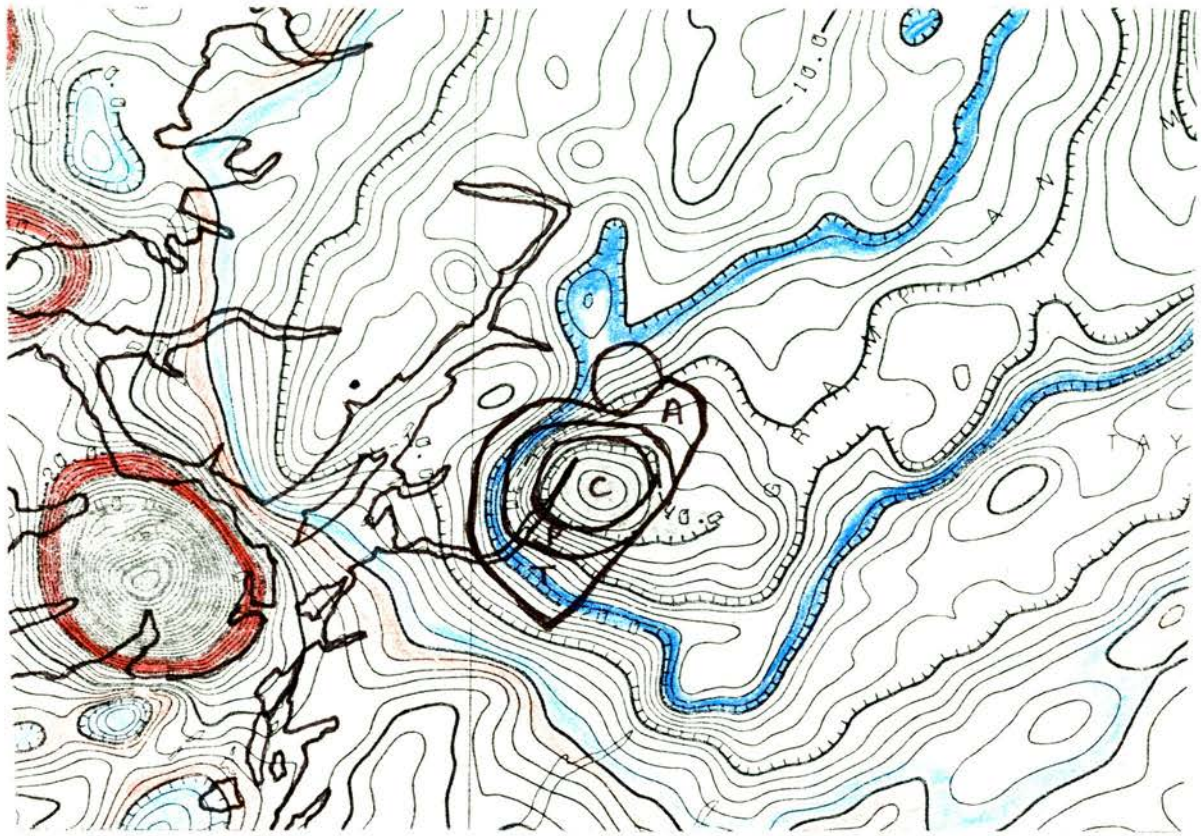

Fig 2.1

Gravity anomaly map of Western Scotland and the Grampian region, with the Etive complex in outline (centre). Blue indicates negative anomalies, with dark blue marking the -20.0mgal contour. Red indicates positive anomalies, with dark red indicating +20.0mgal. The two larger red 'highs' represent Mull and Ardnamurchan Tertiary centres. Etive sits over a regional 'low' which reaches -46mgal under the Central Starav intrusion, exceeded in Scotland only by Cairn Gorm at -54mgal (top right of map). The labels within the Etive outline represent the following cryptograms: T = Cruachan monzodiorite, A = Cruachan monzogranite, P = Porphyritic Starav monzogranite, C = Central Starav monzogranite.

to the intrusion of hot granitic magma (Brown, 1979). Local positive magnetic anomalies occur in the SW were there is a concentration of quartz diorites and monzodiorites. (Data for anomalies comes from Hall and Dagley (1970)). The mineralogical classification of granites by Ishihara (1977) depended upon the occurrence of either ilmenite (in S-type granites) or magnetite and sphene (I-type granites). Since sphene is a common accessory in all Etive rocks (except Central Starav) and magnetite was positively identified during mineral separation work, the magnetite-dominated environment is more likely to explain the positive magnetic anomaly.

2.1 DIORITIC ROCKS

Diorites and quartz diorites occur irregularly as bosses of variable size (0.3-1km) around the perimeter of the Etive granitoid intrusion. Three separate diorite intrusions occur to the N.W. in Glen Creran, one forms Beinn Lurachan in the S.E., one occurs in Glen Ure, another is associated with ultrabasic rocks in Clais-gobhair (Clashgour), and a large arcuate intrusion (8km x 0.5km) occurs on the S.E. margin. This latter body is known as the Quarry Intrusion and was extensively studied by Anderson(1937) and Kynaston & Hill(1908).

This work restricts itself to a brief study of the Glen Ure satellite and draws upon petrographic material used by Anderson(op.cit.) for the Quarry Intrusion.

The Glen Ure body is a quartz diorite (RB049) intruded into the Dalradian metasediments, and is cut by the Cruachan monzogranite (CMG). Dioritic xenoliths can be seen locally within the CMG and a coarse variant of the quartz diorite (RB048) occurs close to its contact with the acid rock. A faint foliation is visible in RB049.

The Quarry Intrusion was intruded between Dalradian metasediments and a belt of foliated and metamorphosed andesite lavas, which in turn are in contact with the Cruachan monzodiorite (CMD). The belt of altered lavas, known as the Beinn a' Bhuiridh screen, is considered to be part of the L.O.R.S. Lorne Plateau lavas which were downfaulted during a period of cauldron subsidence associated with the intrusion of the Cruachan granitoids. The dioritic rocks exploited this faulted region and rose higher into the crust. Veins of the later Meall Odhar granites (MOG) cut the diorites and the CMD, but the relations of the latter two rock types cannot be ascertained. The presence of cloudy plagioclase feldspar and alteration of hornblende to biotite was taken as evidence of contact metamorphism of the diorites by the later CMD (Anderson,1937).

Brown (1975) noted foliation within the Quarry Diorite parallel to its contact with the CMD.

An isolated outcrop of dioritic material (RB131) occurs adjacent to the contact of the CMD and Porphyritic Starav monzogranite (PSMG) at Cadderlie. This isolated occurrence suggests that the diorite is a xenolith transported by the later PSMG.

2.2 CRUACHAN INTRUSION

The outer intrusion of the Etive complex forms an almost complete elliptical outcrop around the inner PSMG. Stratigraphically it appears to consist of one magma pulse, but chemically and mineralogically the intrusion can be divided into a northern lobe of monzogranite (CMG) and a southern lobe of monzodiorite (CMD). An inferred boundary between them is obscured by overburden in the Beinn Sgulaird area (NN050460).

2.2.1 CRUACHAN MONZODIORITE (CMD)

This rock type outcrops in the southern half of the Etive complex as a heterogenous dark grey, medium grained crystalline rock. A partial ring fault is indicated on the Geological Survey 1" map (Sheet 45) on the W. and S.W. margins and could be considered as the continuation of the Beinn a' Bhuiridh screen fault which was associated with cauldron subsidence of the overlying lavas. (Anderson,1937). However this fault is seen to cut the CMD on the western margin (Brown,1975) and the intrusion is seen intruding Dalradian metasediments (Plate 2.1) in a complex interdigitating fashion (Kynaston & Hill,1908). Against the

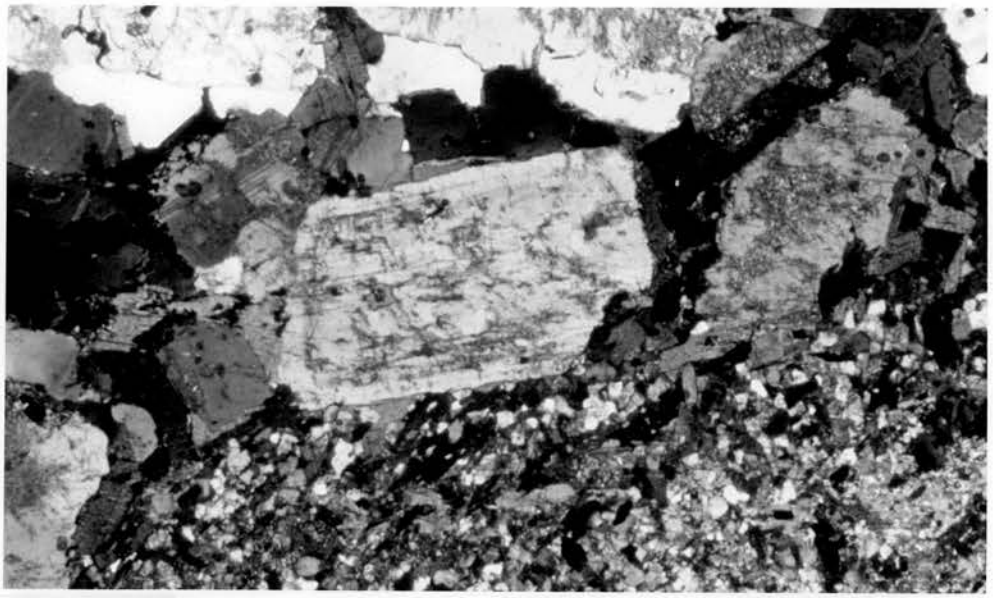

Plate 2.1

RB024. Contact between Dalradian metasediment (fine grained material) and Cruachan monzodiorite. A euhedral plagioclase feldpsar crystal lies against the contact plane.

metasediments the CMD makes a shallow contact angle which dips in towards the centre of the Etive complex. In contrast the dips on the eastern margins are steep.

The CMD is cut by porphyrite dykes (RB011, RB097, RB130) which trend NE-SW, and by veins and sheets of MOG.

2.2.2 CRUACHAN MONZOGRANITE (CMG)

The northern lobe of the Cruachan intrusion is composed of a pink, medium to coarse grained monzogranite whose relation to the monzodiorite in the south is uncertain. The inferred zone of transition or contact is poorly exposed in the Beinn Sgulaird area (NN050460).

Further north in Glen Etive it underlies the lower horizon of the Glen Coe rhyolite lavas (RB050) and locally contains greisen veins (RB058) and metasedimentary xenoliths (RB056). The presence of greisen veins suggests that this part of the CMG was close to the roof of the intrusion.

The fact that modal quartz increases northwards led Brown(1975) to suggest that this succession represented the vertical component of a differentiated pluton and that the whole intrusion had been tilted in a north-easterly direction. This interpretation is consistent with the variation in bulk chemistry south to north, and with the geometry of the Starav intrusions whose geometric centres

are each offset northwards relative to the geographical centre of the Etive complex. However further petrographic and chemical data has shown that CMG also occurs in the SE, (RB107v, RB109, JFBA157), forming an inferred arcuate margin to the CMD.

2.3 MEALL ODHAR GRANITES (MOG)

The type locality is a 3km long arcuate exposure of pink granite which outcrops between Meall Odhar (NN188462) and Stob Dubh (NN165482) in the NE part of the Etive intrusion, E. of Glenceitlein (NN148479). This 'pink' granite outcrops irregularly as sheets and dykes elsewhere in the Cruachan intrusion, and is most abundant in the CMD of the south and west.

Kynaston & Hill (1908) noted that the 'pink ' granite was seen to pass imperceptibly into the CMG in some places and in others it formed distinct bands and patches. As sheets it forms the summit of Ben Cruachan (NN065305), Beinn Sgulaird (NN050455), and other prominent peaks in the SW, and dips at 9-15 degrees in towards the Starav intrusion. Nowhere does it cut the Starav rocks. Anderson (1937) noted that in the Glen Noe area (NN052348) abundant 'pink' sheets intrude the CMD which locally become fine grained and dioritic. He attributed each occurrence of 'pink' granite to the Meall Odhar type, and considered it to have been intruded contemporaneously with the Cruachan type, and earlier than the Starav rocks.

Bailey & Maufe (1960) noted that in the northern outcrops, the MOG does not chill against the CMG and that close to the contact, the CMG contains more biotite than normal. These authors considered the MOG to represent ring dyke material generated after cauldron subsidence of the Starav block.

Samples collected for this study show a variety of textural features. In the south, E. of Bonawe Quarry (NN031340) bifurcating fine grained dykes of MOG cut the dark CMD and exhibit chilled margins (RB010). Beyond Craig, on the W. shore of Loch Etive, a coarse variant was collected (RB098A), and further north (RB128) dark CMD is cut by a 10mm white vein composed of quartz and alkali feldspar with granophyric texture. On the west side of Etive, a sheet of 'pink' granite (RB026) is medium grained and has a saccharoidal texture. Petrographic examination indicates the existence of two distinct types; an alkali granite and a monzogranite. The monzogranite represents the type Meall Odhar rock.

This variety in form is reflected in the chemistry, which shows a bimodal distribution. The implications of this are discussed in Chapter 5

2.4 STARAV MONZOGRANITES

The central part of the Etive complex is occupied by an elliptical granitoid body composed of an outer porphyritic zone and an inner non-porphyritic area. The transition between the two is narrow and has been considered as gradational over a distance of 0.5km (Bailey & Maufe, 1960; Anderson, 1937). However, on mineralogical evidence Brown(1975) considered them as separate intrusions. He noted the almost complete absence of sphene in the Central intrusion, in contrast to its relative abundance in the porphyritic facies.

2.4.1 PORPHYRITIC STARAV MONZOGRANITE (PSMG)

The porphyritic facies contains megacrysts of pink alkali feldspar up to 3cm long which diminish in size and number inwards, away from the outer contact with the Cruachan intrusion.

The contact between the PSMG and Cruachan types shows signs of forceful intrusion, as evidenced by foliation of the CMD (RB077), cataclasis of the felsic minerals (RB061,RB081) in the marginal PSMG, and haematised veins within the Cruachan. Kynaston & Hill (1908) noted sharp contacts with the exception of one exposure on the east flanks of Beinn Sgulaird (NN050455) where they claim that the contact is gradational over about 20m. In this area apophyses of coarse PSMG are in sharp contact with Cruachan granitoid (RB134) (Plate 2.2)

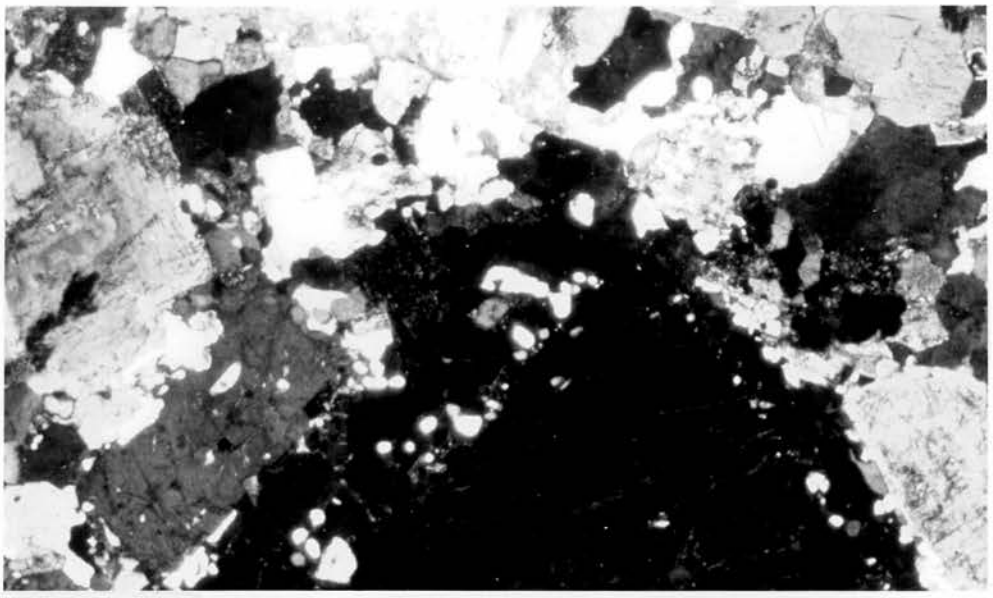

(Plate 2.2)

RB134. Contact between Cruachan granitoid and Porphyritic Starav monzogranite. Blebs of exsolved quartz have formed around the perimeter of an alkali feldpsar crystal which belongs to the Starav intrusion.

N.W. of Cadderlie, Anderson (1937) noted that there is a sharp contact between the PSMG and the MOG, and that the Starav is non-porphyritic for a few cm away from this contact.

Aplite veins (RB016, RB031) and pegmatite (RB095, RB096) occur in this intrusion. Amphibole content averages 3%, though near Glen Kinglass (RB082) it occurs concentrated in a pegmatite. This latter sample was found loose and no source outcrop could be found. A coarse accumulation of amphibole is also seen in RB075 from Glen Kinglass.

2.4.2 CENTRAL STARAV MONZOGRANITE (CSMG)

This type forms the centre of the Etive complex, in particular the high ground of Ben Starav and Beinn Trilleachan. Evidence from phenocryst distribution and some chemical variation suggested to Anderson (1937) and Kynaston & Hill (1908) that it was consanguinous with the outer porphyritic type. Brown (1975) noted schlieren textures in the transition zone and the almost complete absence of sphene in the central facies. Schlieren texture was found (RB140) within 10m of the inferred contact zone. Large scale jointing can be seen trending NNE (ie. perpendicular to "contact") in the transition zone (RB092) and haematised feldspar with veining occurs at (RB094). A deep cleft in the E. face of Beinn Trilleachan is utilised by a stream, in the bed of which multiple parallel jointing occurs in a

zone of intense haematised alkali feldspar and coarse pegmatite formation (RB137).

Chemical data considered in Chapter 4 strongly suggests that the two Starav granitoids are independent pulses of magma, and that the above mentioned fracture zone represents the contact between the two.

PETROGRAPHY

Introduction

Petrographic descriptions are arranged for each major rock type in order of apparent intrusive sequence. The samples described are considered to be representative of their type. Local variations or particular features are noted in the Sequence of Crystallisation section.

Modal analyses are all based on 2000 points. In the case of some accessory minerals whose abundances were low, values in brackets represent the actual counts per 2000. Where accessory minerals were present but not quantifiable, these are marked with an asterisk (*).

All photomicrographs were taken at a magnification of x10 except where stated otherwise.

DIORITES

3.1.1 Rock Description

The dioritic rocks (labelled D on the map, Fig 1), contain augitic pyroxene (often rimmed by hornblende), biotite, plagioclase, microperthitic alkali feldspar and occasionally quartz. Quartz is more abundant in the outer facies of the Quarry Intrusion, which led Anderson (1937) to describe it as a quartz diorite. The grain size is variable due to the occasional presence of augite/hornblende phenocrysts (5-8mm) and plagioclase laths (up to 5mm). The groundmass grain size averages <2mm.

The Glen Ure satellite intrusion, composed of a fine grained quartz diorite, contains a sparse population of augite/hornblende phenocrysts which increase in number closer to its contact with the Cruachan monzogranite (CMG). A faint foliation of mafic minerals is evident.

3.1.2 Mineralogy

3.1.2.1 Sample RB049 (Glen Ure) (Plate 3.1.2)

Accessory Minerals

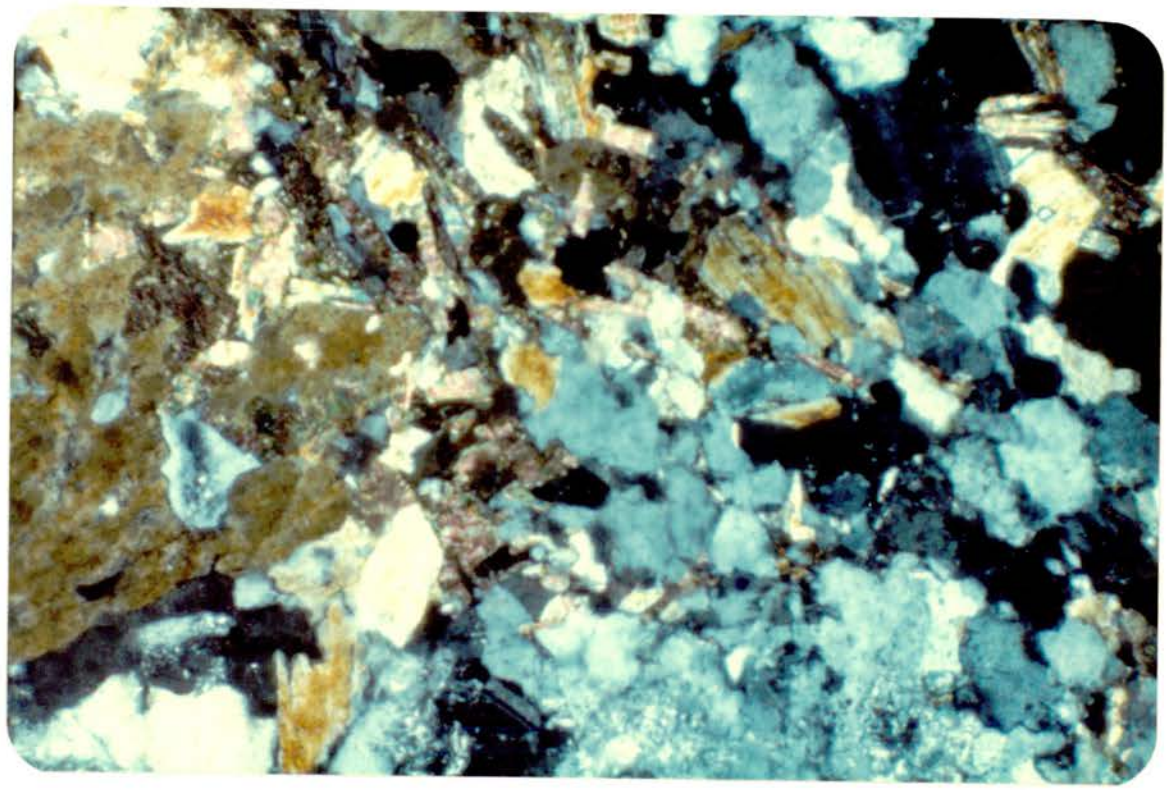

3.1.2 Diorite, Glen Ure. (RB049)

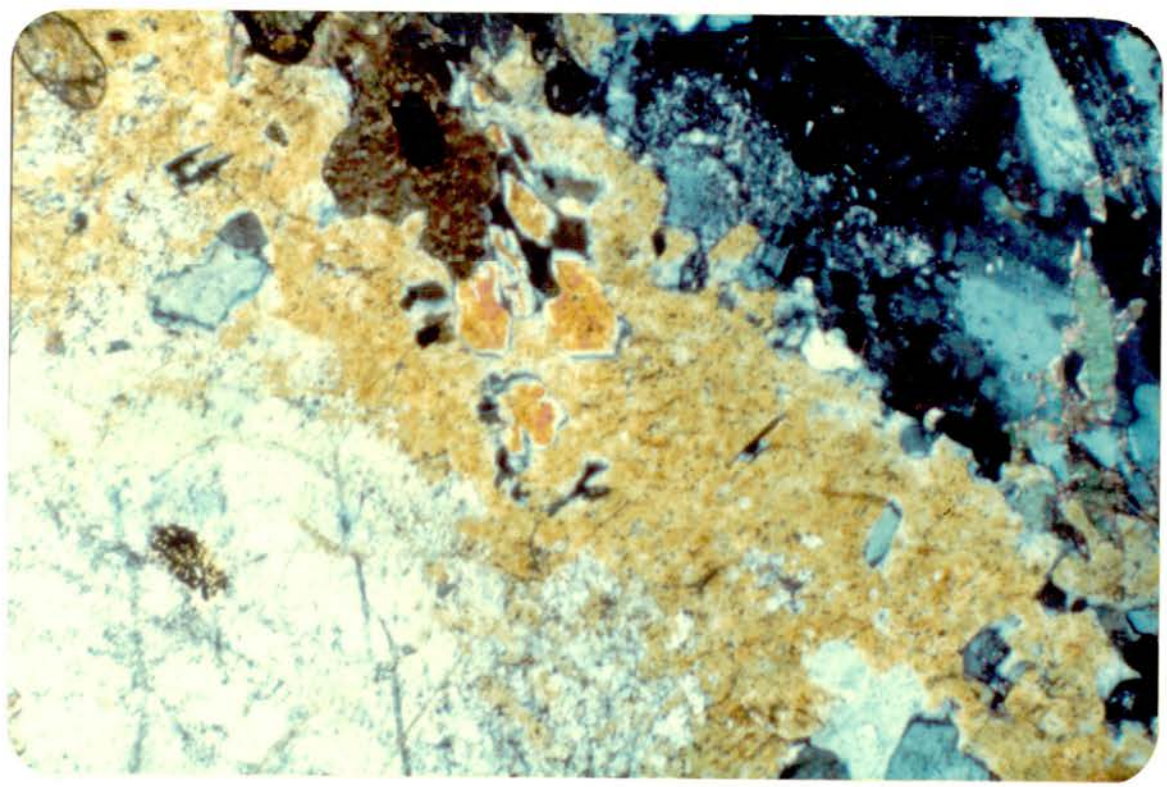

Diorite, Glen Ure (RB048). Detail of a pyroxene phenocryst (5mm) (pale grey) showing alteration to amphibole at the margins (yellow-orange), and the incorporation of biotite (dark brown, upper centre) and fragments of pre-existing amphibole (dark orange, centre field).

ZIRCON was identified as anhedral grains, less than 0.2mm diameter, and associated with the mafic phases.

SPHENE was not positively identified.

APATITE grains <0.1mm are associated with amphibole.

OPAQUE minerals, including magnetite are scarce.

Mafic Minerals

CLINOPYROXENE (Augite) forms irregular shaped cores to euhedral hornblende crystals (5-8mm). The augite varies from pale green to grey in c.p.l. In the groundmass, it forms anhedral grains <2mm.

AMPHIBOLE (Hornblende) is greyish-green in p.p.l. and displays strong pleochroism. It forms euhedral margins to irregular augite cores, which together constitute the phenocrysts phase (5-8mm). Occasionally hornblende makes up the whole phenocryst. Matrix hornblende (<1mm) forms ragged aggregates intergrown with biotite, plagioclase and quartz.

BIOTITE, as lath-shaped crystals, forms clusters of an early greenish-brown variety showing strong foliation. Ragged flakes (<1mm) of an orange-brown biotite occur in the microcrystalline matrix, closely associated with quartz. This latter type also occurs within hornblende crystals, suggesting that there may have

been sub-solidus recrystallisation or hydrothermal alteration.

Felsic Minerals

PLAGIOCLASE forms normally zoned and mostly sericitised phenocrysts, up to 5mm in length, with a composition range of An_{50}-An_{20}. Groundmass crystals (<0.5mm) of An30-20 composition are relatively fresh.

ALKALI FELDSPAR occurs as late stage interstitial assemblages <1mm across. Myrmekitic texture develops at some plagioclase boundaries.

QUARTZ forms a mosaic texture with the other felsic minerals in the groundmass. Grains are generally <0.5mm and exhibit undulose extinction.

3.1.2.2 Sample 6332 (Anderson collection), Quarry Intrusion.

Accessory Minerals

ZIRCON occurs as anhedral grains <0.2mm associated with biotite and the opaque minerals.

APATITE forms euhedral crystals <0.1mm enclosed in biotite.

SPHENE is generally found as anhedral grains 0.5-1.0mm. It shows pale brown - reddish brown pleochroism, and is dark brown in c.p.l. The grains are found enveloping opaque minerals or surrounded by plagioclase.

OPAQUE minerals occur as anhedral and subhedral grains <0.2mm associated with biotite. Magnetite is a major component, and haematite develops from the alteration of hornblende.

Mafic Minerals

CLINOPYROXENE (Augite) occurs as irregular, rounded phenocrysts (1mm) which is light buff colour in p.p.l, and mauve/yellow in c.p.l. It forms cores to the phenocrysts, the outer margins of which are hornblende.

AMPHIBOLE (Hornblende) forms irregular grains about 2mm in diameter and composes some 5% of the rock. Twinning is seen on the [100] plane and all crystals display pale to dark green pleochroism. Quartz forms poikilitic growths within some grains and there is localised alteration to haematite.

BIOTITE occurs as 0.1-2mm irregularly shaped laths, occasionally in aggregates with amphibole. It exhibits pale to dark brown pleochroism and is seen growing interstitial to plagioclase.

Felsic Minerals

Subhedral laths of PLAGIOCLASE up to 5mm long occur in clusters, forming a meshwork in which biotite, alkali feldspar, and quartz are interstitial. Each crystal is zoned with a core of An60-50, and more albitic rim.

ALKALI FELDSPAR occurs as rare irregularly shaped crystals (maximum 5mm) which are interstitial to plagioclase and amphibole. The crystals show perthitic texture.

QUARTZ is a late-stage phase, occurring as anhedral grains (<1mm) which display undulose extinction.

3.1.3 Modal Data

	RB049	6332
Quartz	12	13
K-feldspar	*	7
Plagioclase	46	43
Biotite	12	12
Amphibole	20	12
Pyroxene	9	13
Accessories	*	*
Opaques	*	*

These samples are plotted on Fig 3.7 with symbol D and plot in the quartz-rich sector of the diorite field.

3.1.4 Sequence of Crystallisation

The earliest phases to crystallise were the accessory minerals, clinopyroxene and plagioclase (An_{50}), with the latter two minerals forming phenocryst phases. The pyroxene has been replaced to a variable extent by amphibole. The plagioclase phenocryst cores are sericitised.

Biotite formed later in clusters with amphibole in the groundmass together with more sodic plagioclase. Quartz and alkali feldspar form the latest phases, filling the interstices of the early mineral assemblage.

Inclusions of plagioclase, biotite, and quartz within the amphibole phenocrysts suggest that there has been syn-crystallisation overgrowth. Undulose extinction in quartz is indicative of post-solidification strain.

In the case of the Glen Ure intrusion, the proximity of the later Cruachan monzogranite may have been the cause for the late-stage alteration and foliation.

CRUACHAN MONZODIORITE (CMD)

3.2.1 Rock Description

The rock in hand specimen is grey, equigranular, medium to fine-grained and crystalline. The average grain size is variable (1-5mm) over relatively short distances (10m) and the colour varies from light to dark grey. In the vicinity of a 'pink' granite intrusion in Glen Noe (RB089) amphibole has recrystallised to form 5mm megacrysts. Where the rock is darker it is usually finer grained and is more susceptible to weathering of the 'spheroidal' type reminiscent of dolerite. The distribution of CMD is shown by symbols T and T. (dark variant) on Fig 1.

In the Glen Noe and Glen Liver areas the CMD becomes finer grained and locally dioritic (RB088) as was noted by Anderson (1937). A fine grained dioritic rock (RB108) is net veined by a medium grained grey 'granitic' rock (RB107v).

Up to 2km in from its contact with the PSMG, the CMD exhibits stong foliation parallel to this contact and the feldspars are cloudy (RB077).

3.2.2 Mineralogy

3.2.2.1 Sample RB019 (Plate 3.2.2.1)

Accessories

ZIRCON occurs as anhedral grains <0.1mm in biotite, usually surrounded by pleochroic haloes.

APATITE forms euhedral hexagonal and lath-shaped crystals 0.1-0.2mm long. These generally occur in biotite, though laths also occur in plagioclase.

SPHENE is a common accessory (1.5% modal) varying in size from 0.5-2mm and forms subhedral and fragmented crystals. It is weakly pleochroic, with a brown interference colour. It occurs associated with opaques, biotite and amphibole, and is noted growing interstitially to plagioclase.

OPAQUE minerals (mostly magnetite) occur as individual subhedral crystals (<0.2mm) and in aggregates associated with amphibole (in mafic knots). Amphibole alteration gives rise to the formation of haematite.

3.2.2.1 Cruachan monzodiorite, RB019. (CMD/T). Field shows meshwork of interlocking plagioclase crystals with interstitial quartz and biotite (centre).

Mafic Minerals

Green HORNBLENDE occurs mostly in crystal aggregates up to 1.5mm across with ragged texture. It is often twinned and is strongly pleochroic.

BIOTITE grains range from 0.5-3mm, forming clusters of subhedral laths. It locally contains RUTILE needles (<0.1mm) and occasionally shows flexuring.

Felsic Minerals

PLAGIOCLASE FELDSPAR (An_{35-40}) forms a mesh work of early crystallised subhedral laths up to 5mm long, within which biotite and sphene are interstitial. It is strongly twinned. Some zoned crystals are found with compositions ranging An_{60-25}.

ALKALI FELDSPAR forms large (6-8mm) megacrysts which fill the spaces between the plagioclase network. It is microperthitic and contains fragments of corroded plagioclase, and a rare grain of biotite. It appears to have invaded and replaced the pre-existing plagioclase.

QUARTZ occurs as anhedral, interstitial grains 0.2-1mm across.

3.2.2.2 Sample 083 (Plate 3.2.2.2)

Accessory Minerals

ZIRCON varies in size from <0.1mm to 0.5mm and forms subhedral grains usually in biotite. Strings of zircon grains are found bordering a biotite grain. Some are free-floating in plagioclase feldspar.

APATITE occurs as <0.5mm euhedral crystals, mostly enclosed in biotite.

SPHENE forms anhedral grains 0.3-2mm across, some of which enclose apatite and opaque minerals. It commonly has ragged edges.

OPAQUE minerals are generally <1.5mm and are associated with biotite, amphibole and sphene in mafic knots.

Mafic minerals

HORNBLENDE forms irregular grains in aggregates up to 1mm across. It is frequently twinned and exhibits green pleochroism and second order interference colours.

BIOTITE occurs as laths up to 2mm long with ragged ends. It is sometimes enclosed by hornblende, has bent cleavage and is locally altered to chlorite.

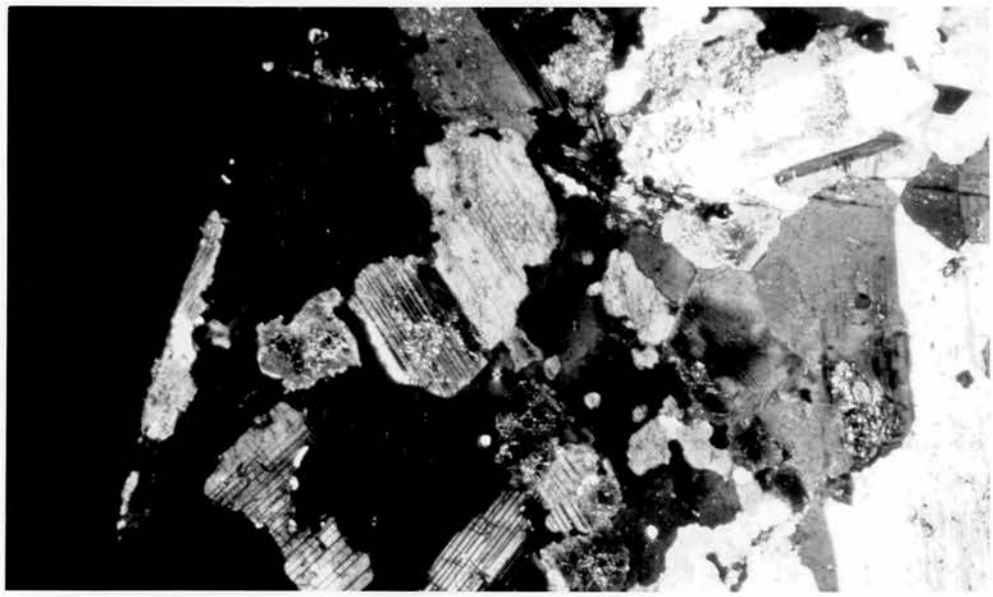

3.2.2.2a Dark Cruachan monzodiorite, RB083 (CMD/T.). Corroded plagioclase crystals are enveloped by a zone of alkali feldspar (at extinction) in the left half of the picture.

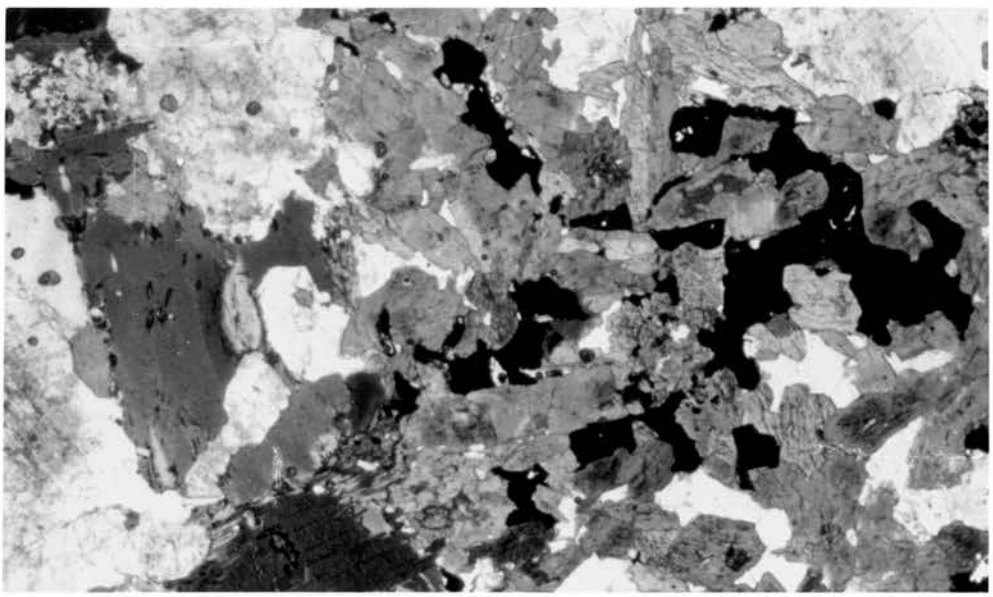

3.2.2.2b Right hand field depicts a mafic knot composed of interlocking subhedral hornblende and magnetite crystals. Large biotite and plagioclase on the left belong to the host rock.

3.2.2.2c A dark stringer of alkali feldspar (at extinction) forms an irregular divide between two plagioclase crystals.

Felsic Minerals

PLAGIOCLASE FELDSPAR varies in size from 0.5-4mm and forms twinned subhedral crystals (An_{30-40}) and some zoned crystals An_{60-30}. The crystals build up an interlocking meshwork in which biotite, alkali feldspar and quartz are interstitial.

ALKALI FELDSPAR forms irregular grains up to 6mm across which invade plagioclase and corrode it. Large areas of interstitial mineral are in optical continuity.

QUARTZ occurs as anhedral interlocking grains <1mm across, forming a late crystallising phase.

3.2.2.3 Sample RB025 (Plate 3.2.2.3)

Accessory Minerals

ZIRCON occurs as euhedral and subhedral grains <0.2mm across mostly in biotite where pleochroic haloes develop. It is rarely found in sphene.

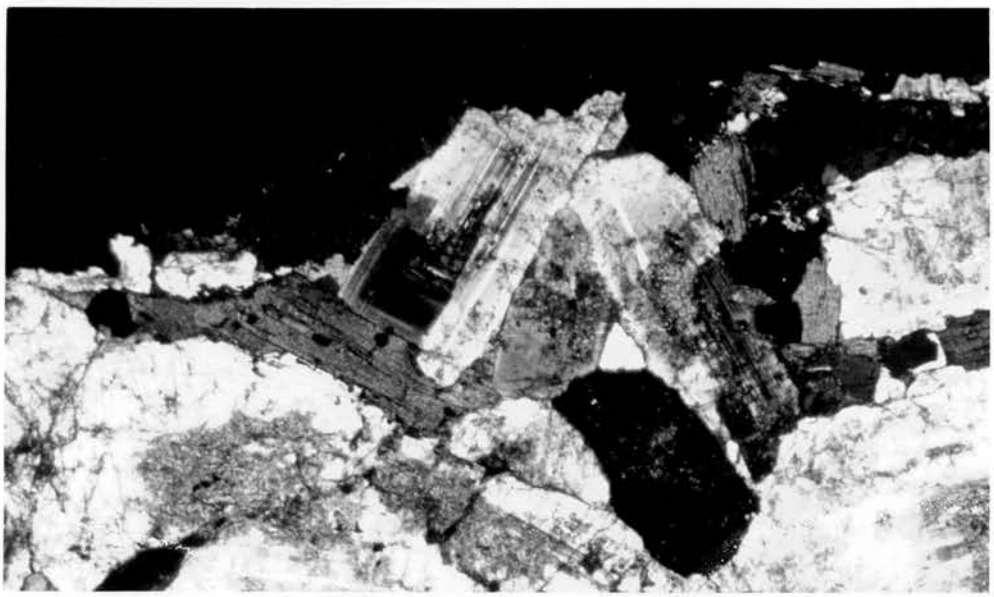

3.2.2.3 Cruachan monzodiorite, RB025 (CMD/T). In the centre of the field a zoned plagioclase crystal is partly enveloped by biotite.

APATITE is found within biotite and on its margins. It is euhedral and does not exceed 0.1mm in size.

SPHENE is frequently fragmented, ranges in size from 0.5-1.5mm and forms subhedral, pleochroic crystals associated with opaques and biotite.

OPAQUE minerals (0.1-0.5mm) often occur in aggregates associated with hornblende and biotite.

Mafic Minerals

HORNBLENDE occurs as subhedral and anhedral crystals 0.5-7mm in length. It exhibits twinning and is strongly pleochroic. The crystals are often broken.

BIOTITE forms subhedral laths up to 3mm long. With hornblende it composes aggregates of mafic knots, and singly it is interstitial to plagioclase feldspar.

Felsic Minerals

PLAGIOCLASE FELDSPAR (An_{30-40}) makes up 58% (modal) of the rock and occurs as subhedral laths up to 5mm long, strongly twinned and occasionally zoned (An_{60-25}) The crystals form a meshwork in which biotite, alkali feldspar and quartz are interstitial phases. The calcic cores are often sericitised.

Late alkali feldspar corrodes some crystals and invades the interstices.

ALKALI FELDSPAR appears to have invaded a crystal mush composed of all the previously described phases. It forms irregular patches up to 4mm across, interstitial to plagioclase and corroding it. It is a microperthite.

QUARTZ is a late phase, forming anhedral grains up to 4mm across which are interstitial to all the other minerals except alkali feldspar. The absence of granophyric texture suggests that quartz may have preceded alkali feldspar crystallisation.

3.2.3 Modal Analysis

	RB012	RB019	RB083	RB025
Quartz	9	5	8	9
Alk. Feldspar	15	18	7	12
Plagioclase	56	56	55	58
Biotite	15	16	21	14
Hornblende	2.5	3	6	2
Sphene	(7)	1.5	2.3	1.3
Apatite	(2)	*	(1)	*
Zircon	(4)	*	*	0.25
Opaques	1.8	0.5	1.3	1.9

These compositions are shown in Fig 3.7 by the symbol T, with the exception of RB083 which is designated 'T.'.

3.2.4 Sequence of Crystallisation

In each sample studied petrographically, the large plagioclase feldspar crystals form a meshwork within which biotite, alkali feldspar and quartz are interstitial phases. This suggests that plagioclase was a relatively early phase and may have formed the solid part of a crystal mush. The strong zonation on some crystals, with development of more albitic rims on the plagioclase crystals indicates that the cores failed to maintain chemical equilibrium as the magma cooled.

Partial corrosion of these plagioclase crystals by alkali feldspar suggests that potassium-rich fluids were active at a late stage in the cooling history of the intrusion. Barium , which is a common constituent of potassium feldspars, is most abundant in the CMD. The whole rock Ba/K ratios are higher than those of the other granitoid members in the Etive Complex and may suggest a local Ba anomaly. (Taylor,1965).

The accessory minerals are early phases. Sphene is the most abundant accessory and is normally associated with the mafic minerals. In one case (RB019) it appears to be interstitial to plagioclase, suggesting that plagioclase formed early in the sequence.

Hornblende is often associated with biotite, forming mafic knots. These features could represent restite material derived from the partial melting of a source rock.

The occurrence of broken plagioclase and biotite crystals, and undulose extinction in quartz, indicate that pressure was exerted on the solidifying pluton. This could have been due to the pluton's own emplacement stress, though there is no evidence of flow textures or preferred orientation within the body of the intrusion. Alternatively the upwelling Starav pluton (as a diapiric structure) could have exerted a deforming stress. Samples of CMD close to the Starav contact show foliation parallel to the contact (RB077).

Textures and mineralogy in the CMD suggest that it was intruded into the Dalradian metasediments as a plagiophyric mush and was subsequently deformed locally by the rising Starav pluton.

CRUACHAN MONZOGRANITE (CMG)

3.3.1 Rock Description

The northern lobe of the Cruachan intrusion (shown on Fig 1 by the symbol 'A') is composed of a medium to coarse grained monzogranite (Streckeisen,1976) containing pink alkali feldspar crystals and minor enclaves of metasediment; the abundance of both increases northwards. Mafic knots also occur, consisting of ragged biotite, amphibole and disseminated opaque minerals. Biotite sometimes pre-dates amphibole.

Plagioclase occurs as early crystals which are zoned and corroded. Alkali feldspar megacrysts are found in the north (RB056) and these show ghost zoning. Modal quartz increases northwards and may be indicative of in-situ fractional crystallisation (Vance 1961).

3.3.2 Mineralogy

3.3.2.1 Sample RB064 (Plate 3.3.2.1)

Accessory Minerals

ZIRCON forms irregular, rounded grains generally less than 0.1mm, though one euhedral crystal 0.2mm across was found. It is sparsely distributed in biotite, and also enclosed by sphene and hornblende.

APATITE occurs as euhedral crystals <0.1mm enclosed in biotite.

SPHENE forms subhedral and fragmented euhedral grains 1-2mm in size. It displays a beige - orange/brown pleochroism, and is an early phase, occurring within hornblende.

OPAQUE minerals, including MAGNETITE, exist as small (<0.1mm) disseminated grains in biotite, hornblende and sphene.

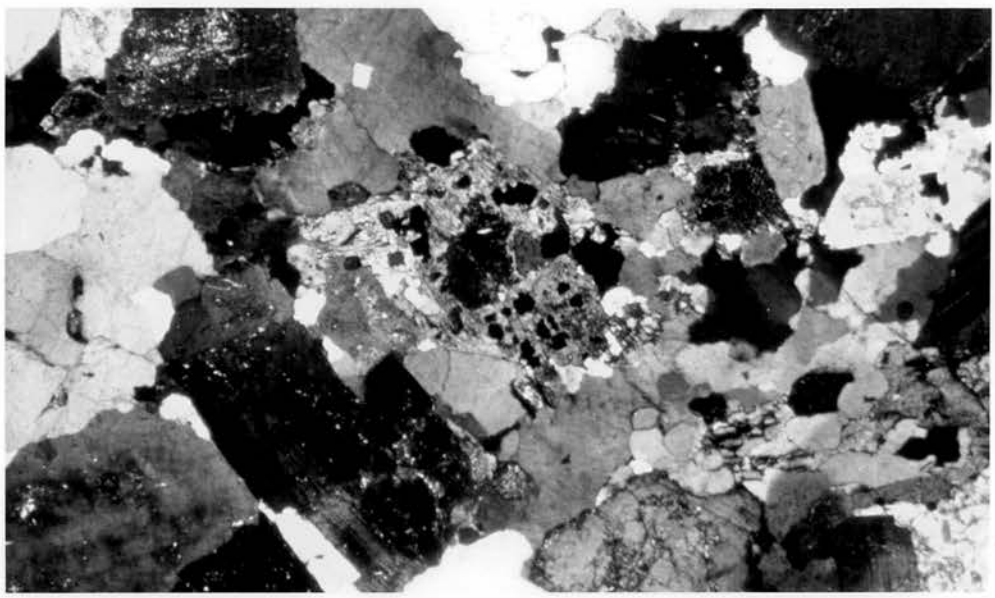

3.3.2.1a Cruachan monzogranite, RB064 (CMG/A). A mafic knot occupies the centre field. A core of clinopyroxene (dark) is surrounded by hornblende containing opaque minerals (including magnetite).

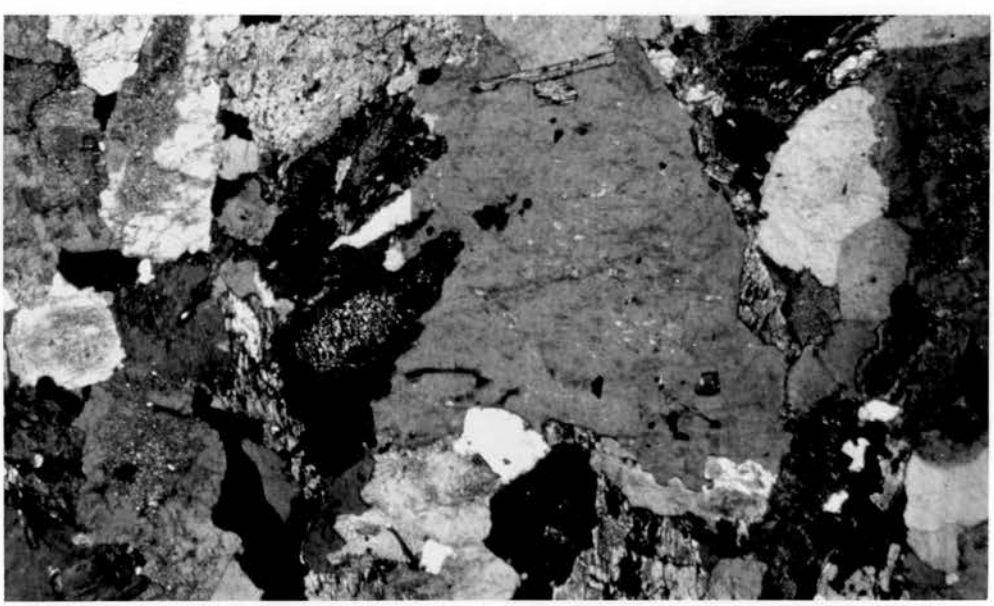

3.2.2.1b A large crystal of alkali feldspar cryptoperthite (grey) sends fingers into a corroded plagioclase crystal.

Mafic Minerals

HORNBLENDE forms part of mafic knots, in association with biotite and opaque minerals, in clusters up to 6mm across. Individual subhedral twinned laths up to 4mm long occur. Hornblende is pleochroic (pale beige to green), and displays orange/brown interference colours.

BIOTITE grains occur up to 2mm across, some forming mafic knots, others as individual subhedral crystals which show flexuring. There is some alteration to CHLORITE.

Felsic Minerals

PLAGIOCLASE FELDSPAR (An_{30-40}) forms 46% (modal) of the rock. The crystals are subhedral laths up to 5mm long, which are twinned. Some are normally zoned (An_{50-25}) with myrmekitic texture developed at their contact with alkali feldspar. The presence of smaller grains may represent a later phase of crystallisation.

ALKALI FELDSPAR is interstitial to plagioclase forming irregular grains up to 5mm across.

QUARTZ is a late interstitial phase. It forms anhedral grains up to 2mm in diameter which exhibit undulose extinction.

3.3.2.2 Sample RB055 (Plate 3.3.2.2)

Accessory Minerals

ZIRCON forms anhedral grains (<0.1mm, occasionally 0.2mm) and occurs most commonly in sphene, but some are "free-floating" within alkali feldspar.

APATITE occurs as subhedral crystals <0.1mm, mostly in biotite.

SPHENE is present as crystals varying from subhedral to euhedral and 0.1-0.5mm in size. It is an early formed mineral by virtue of its association with the mafic minerals. It is pale beige in p.p.l.

OPAQUE minerals form subhedral grains <0.3mm associated with biotite, hornblende, and sphene.

Mafic Minerals

HORNBLENDE forms euhedral crystals, commonly as rhomb [001] end-sections showing good cleavage. It also occurs as subhedral laths. Grain size varies from 0.2-3mm and twinning is common. The mineral is pleochroic (pale beige to green) and exhibits yellow/brown and grey interference colours.

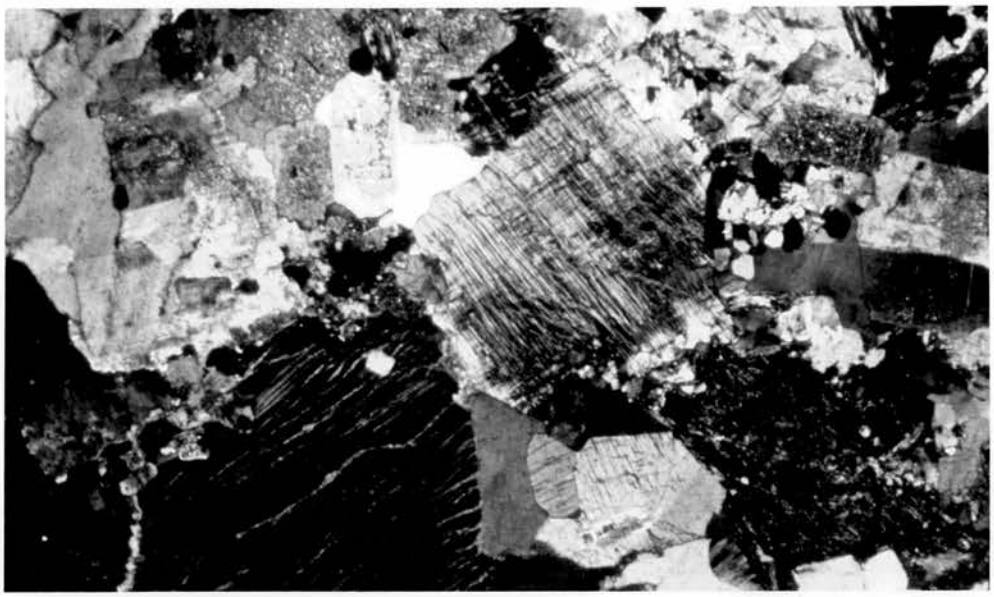

3.3.2.2 Cruachan monzogranite, RB055 (CMG/A). Microcline microperthite fills the centre field, surrounded by sericitised plagioclase feldspar and quartz.

BIOTITE grains may reach 1.5mm across, forming laths with ragged ends. It is beige in p.p.l. exhibiting strong pleochroism.

Felsic Minerals

PLAGIOCLASE FELDSPAR forms subhedral laths up to 6mm long. Synneusis twins were identified, suggesting a second phase of crystallisation. Twinning and zoning is common.

ALKALI FELDSPAR forms an interstitial phase to plagioclase and mafic minerals. Exsolution lamellae and "tartan twinning" indicate the presence of microcline microperthite. Grains are up to 6mm in size.

QUARTZ is a late phase filling the interstitial cavities. Crystals grow up to 2mm and show undulose extinction.

3.3.3 Modal Analysis

	RB064	RB051	RB055
Quartz	16	20	28
Alk.Feldspar	22.5	24	34
Plagioclase	46	39	30
Biotite	5.5	6.5	4.5
Hornblende	9.5	9.5	3
Sphene	0.2	(1)	*
Apatite	*	(1)	*
Zircon	*	*	*
Opaques	0.3	0.3	0.5

These compositions are designated 'A' on Fig 3.7.

3.3.4 Sequence of Crystallisation

The probable existence of two phases of plagioclase feldspar would suggest that the magma was intruded as a plagiophyric mush, in common with the CMD, and that late crystallisation of two feldspars cemented the mush together.

The colour of sphene crystals is notably paler than those in the CMD. This is indicative of a lower titanium content (Deer et al. 1966). Since it crystallised earlier than other titanium bearing phases (biotite) in both Cruachan intrusions, it seems unlikely that it reflects a titanium fractionation effect. The modal distribution of sphene between the southern CMD and the northern CMG is not gradual or consistent (viz. 1.5%, 2.3%, 1.3% to 0.2%, 0.5%). These observations suggest that there exists some discontinuity between the two Cruachan types.

Plagioclase and the mafic minerals are texturally early phases. The alkali feldspar is generally late interstitial, though one sample (RB056) contains a 6mm crystal which exhibits ghost zoning. This may represent a derived crystal which was not in chemical equilibrium with its host melt.

Brown(1975) considered the increase in modal quartz from south to north through the whole of Etive to represent a section through a vertically zoned pluton. The increase in quartz is confirmed in this study, but only within the CMG.

The presence of greisen veins (RB058) are evidence that the northern part of the CMG represents a roof zone, or at least, the upper levels of the intrusion. Metasedimentary xenoliths (RB056) may indicate the proximity of an outer contact zone.

"MEALL ODHAR" GRANITES (MOG)

3.4.1 Rock Description

These members of the Etive suite consist of sheets and dykes of "pink" granitic rock. The colour is attributable to a predominance of alkali feldspar. They are heterogenous over their entire outcrop, comprising saccharoidal (RB026), coarse grained (RB098a, RB084), and fine grained types (RB010). Samples collected by Anderson (1937) but not described by him contain traces of hornfels xenoliths. Schist inclusions are found within the MOG on the east flanks of Beinn Sgulaird (50m NE from RB136). The larger expanses of MOG are designated 'M' on Fig 1. The terms 'depleted' and 'enriched' refer to certain trace element characteristics (see Chapter 4).

3.4.2 Mineralogy

3.4.2.1a Sample RB026 ("Depleted") (Plate 3.4.2.1a)

Accessory Minerals

Two subhedral grains of ZIRCON were identified (0.1-0.2mm) occurring within biotite, and "free-floating" in alkali feldspar. A few anhedral fragments (<0.1mm) were found. No corroded cores could be found. In one case, however, a euhedral crystal within a larger crystal was seen (Plate 3.4.2.1c).

Anhedral APATITE forms grains <0.1mm within chloritised biotite.

One subhedral lath of SPHENE 0.5mm across was found within an opaque, rhomb-shaped grain (? altered amphibole).

OPAQUE minerals are scarce; a few occur as subhedral fragments (<0.2mm) associated with chloritised biotite.

Mafic Minerals

An opaque rhomb-shaped grain (0.5mm) could represent a haematised amphibole.

BIOTITE, which is mostly altered to CHLORITE, occurs as anhedral ragged grains <1mm containing some RUTILE needles. One euhedral [0001] section of unaltered biotite was found.

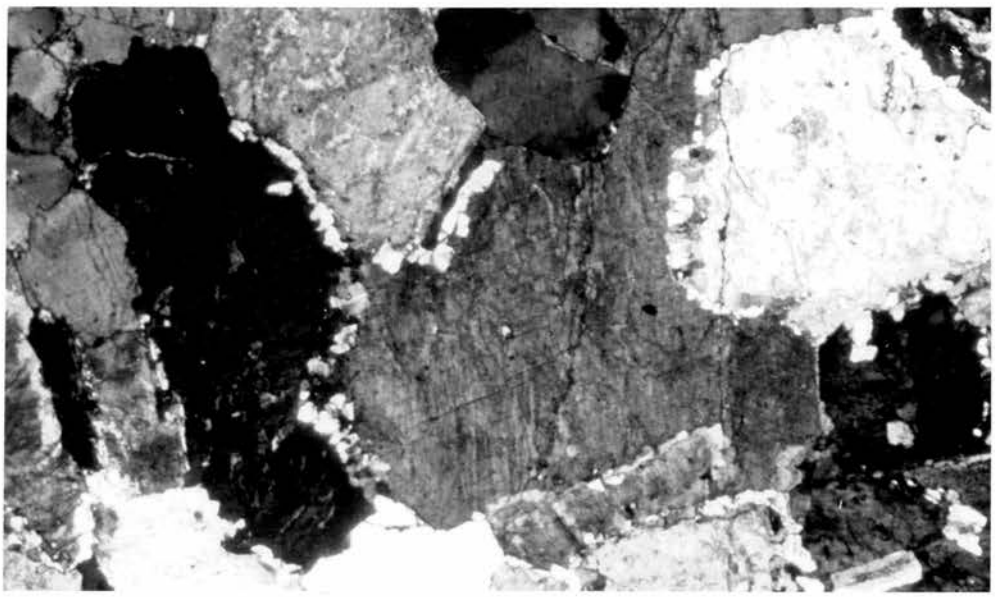

3.4.2.1a Meall Odhar granite 'depleted' type, RB026 (MOG/M.). Small plagioclase feldspar has formed around the periphery of larger alkali feldspar. This is an example of 'necklace' texture believed to be due to extreme perthite unmixing.

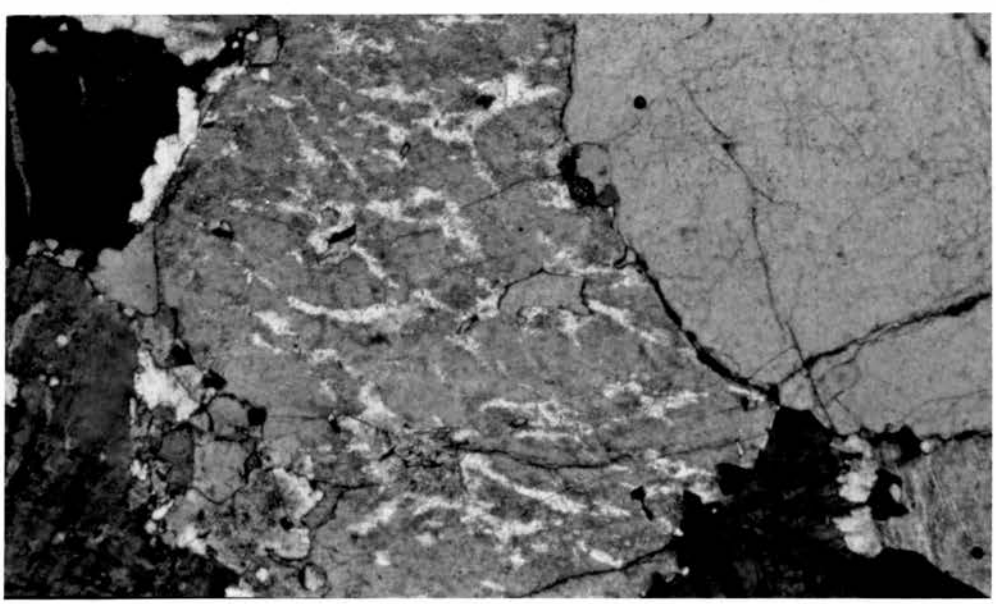

3.4.2.1b Coarse perthitic alkali feldspar with two small zircon crystals (in centre of field) at an inter-grain boundary.

N.B. It is imperative that <u>every</u> reader sign and date this enclosed copyright form. Should more than one reader require access to this thesis a signature is required from each reader in order to protect the candidate's copyright adequately.

We should be most obliged if readers would put their name and initials in <u>block capitals</u> beside their signature.

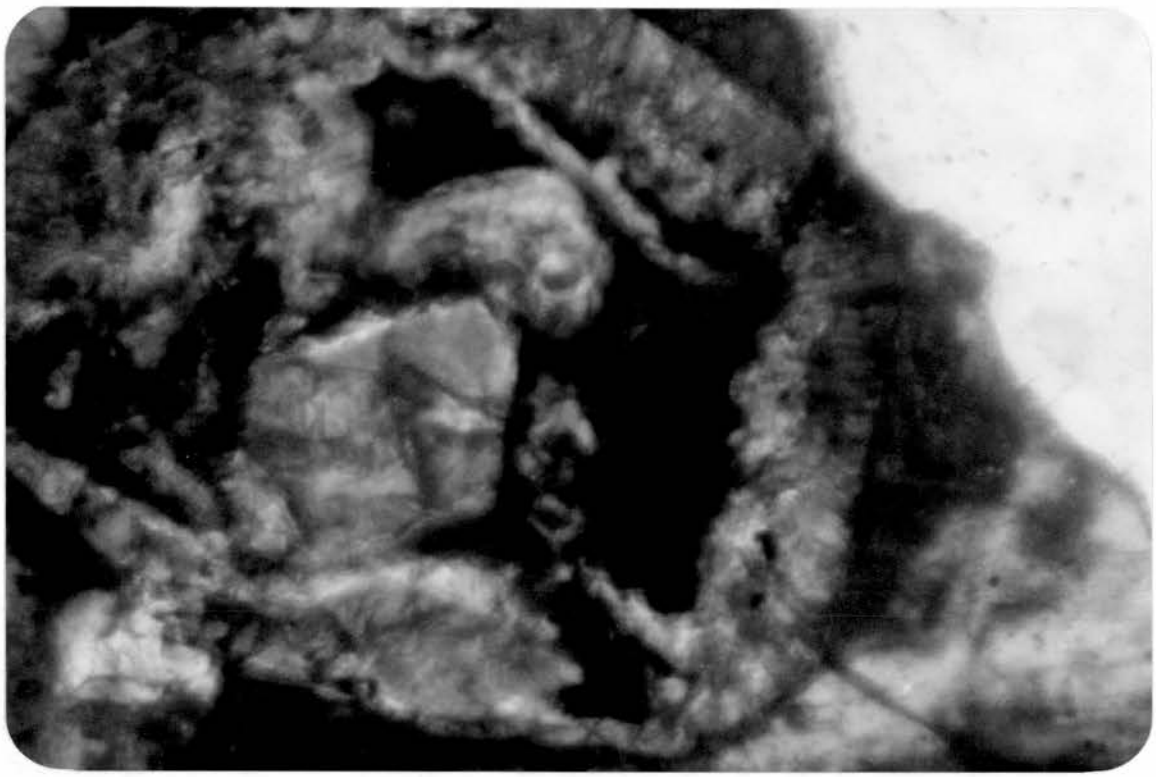

3.4.2.1c Meall Odhar granite, 'depleted' type. RB026 (MOG/M.). Zircon crystal showing two stages of growth. An inner euhedral crystal is surrounded by a subhedral crust of zircon. Magnification x200.

Felsic Minerals

Twinned and zoned PLAGIOCLASE FELDSPAR forms subhedral grains 0.5-1mm long, showing extensive alteration to SERICITE and EPIDOTE. Small laths were seen intergrown with alkali feldspar.

ALKALI FELDSPAR (microcline) is the major component and forms interstitial growths 1-7mm in size, showing perthitic texture. There is an early phase showing resorption which is rimmed by quartz grains (<0.1mm). There is limited graphic intergrowth. A later phase is evident from irregular aggregates with quartz, which cause the localised development of granophyric textures.

QUARTZ is a late phase crystallising interstitially to alkali feldspar and plagioclase. Grain size varies from 1mm to 3mm.

3.4.2.2 Sample RB084 ("Enriched") (Plate 3.4.2.2)

Accessory Minerals

ZIRCON is found as anhedral grains <0.1mm in sphene and chloritised biotite.

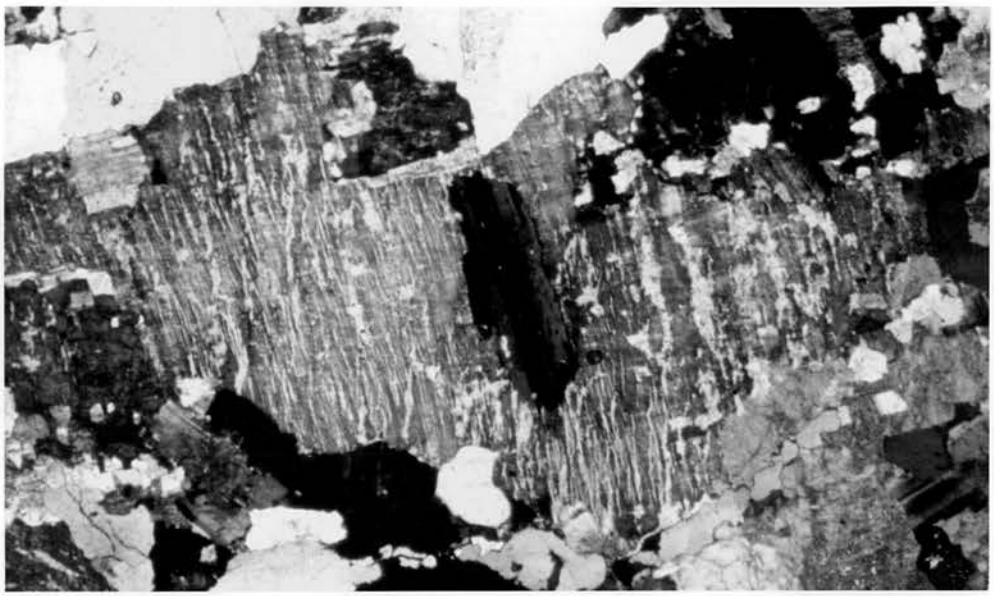

3.4.2.2a Meall Odhar granite 'evolved' type, RB084 (MOG/M). One large crystal of perthitic alkali feldspar encloses a corroded plagioclase crystal (centre). Microcline "tartan twinning" is discernable at the top left of the alkali feldspar crystal.

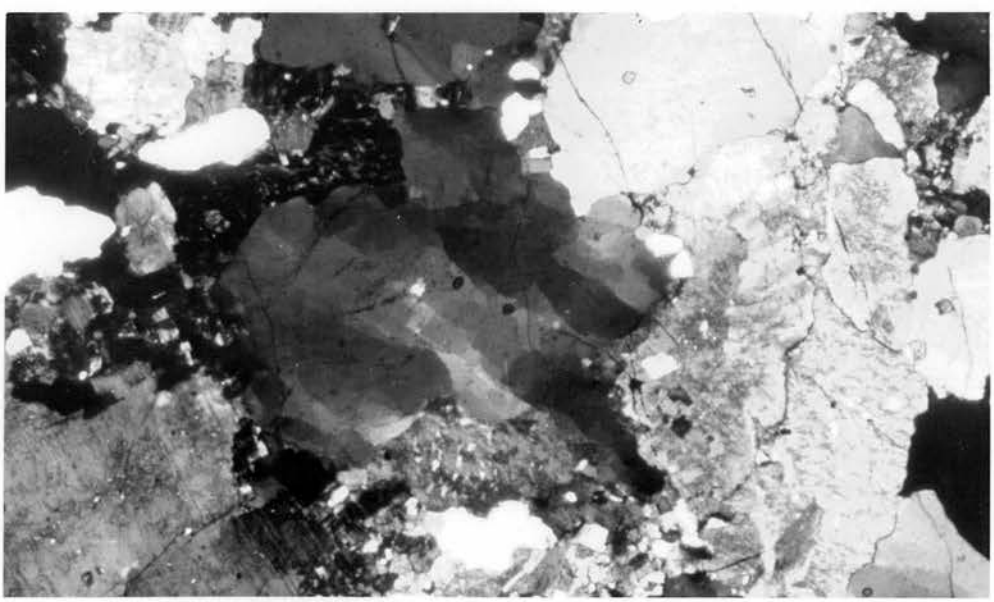

3.4.2.2b The centre field is occupied by a mosaic of quartz, which projects towards the lower right, between alkali feldspar.

Subhedral grains of APATITE average <0.1mm long though one grain 0.5mm long was found. It is a rare phase and occurs in altered biotite.

SPHENE in contrast to apatite is relatively abundant and six euhedral to subhedral crystals occur associated with the opaque phases. It is pleochroic and the colour varies from greyish-beige to pale brown. There is evidence of corrosion at the margins.

Anhedral grains of OPAQUE minerals (<0.2mm) are found within and around sphene grains.

Mafic Minerals

Opaque fragments are ascribed to haematised amphibole/pyroxene.

BIOTITE is mostly altered to CHLORITE which forms ragged laths up to 2mm long.

Felsic Minerals

PLAGIOCLASE FELDSPAR occurs as subhedral laths 0.5-2mm long and as broken fragments within alkali feldspar. It is twinned and zoned.

ALKALI FELDSPAR showing perthitic texture forms irregular shaped grains up to 5mm long. With QUARTZ it grows interstitially.

QUARTZ grains are irregular, 0.1-4mm long, exhibit very ragged junctions between crystals and form an interlocking mosaic.

3.4.3 Modal Analysis

	RB026(Depleted)	RB084(Enriched)
Quartz	27	42
Alk.Feldspar	67	33
Plagioclase	4.5	24
Biotite	1	0.5
Sphene	(3)	(6)
Apatite	*	*
Zircon	(2)	*
Opaques	(4)	(8)

This data is represented on Fig 3.7 by 'M.' and 'M' respectively.

3.4.4 Sequence of Crystallisation

The presence of zircon and apatite in two distinct petrographic environments (bound to mafic minerals in RB084 and "free-floating" in RB026) suggests that there may be two types of Meall Odhar granite. The "free-floating" population may represent either a restite phase or a very early phase in an environment with few or no mafic minerals crystallising in which zircon could be enclosed. The occurrence of an early phase of fragmented alkali feldspar, in RB026, which show resorption features clearly suggests a change in conditions.

The selectively high abundance of sphene in an otherwise highly fractionated system may indicate that it did not crystallise in-situ but was derived from another source. This possibility is strengthened by the fact that sphene often shows corrosion features at the rim. It also exhibits a bimodal distribution, which suggests two types of "Meall Odhar" granite. The two types are here provisionally classified as "Depleted" (RB026) and "Enriched" (RB084) on the basis of sphene content and concomitantly variable concentrations of certain incompatible trace elements (Th,Ce,Hf,La). High fO_2 conditions would favour the formation of sphene plus magnetite over ilmenite (Ishihara 1977).

The "Enriched" type have abundant sphene and a monzogranite composition. This makes them very similar to the PSMG, a fact supported by Anderson(1937) who considered the Meall Odhar 'granite' to have been an acid fractionate of the PSMG. It is tentatively suggested that this variant represents a ring dyke emplaced just prior to the intrusion of the Starav plutons.

The "Depleted" types have little or no sphene and a high alkali feldspar content. They plot within the alkali granite field (Fig.3.7) and may represent partial melts (Lameyre and Bowden,1982) under low P_{H2O} and high temperature conditions (Carmichael et al. 1974). This could explain the "free-floating" zircons, the zircon showing a two-stage growth (?inherited), and fragments of corroded alkali feldspar.

PORPHYRITIC STARAV MONZOGRANITE (PSMG)

3.5.1 Rock Description

This rock type is characterised by the presence of abundant subhedral 'pink' alkali feldspar phenocrysts of variable size up to 30mm long. The groundmass is coarse-grained (1-10mm) and comprises approximately equal proportions of plagioclase and alkali feldspar, with subordinate quartz, and a relatively high abundance of amphibole and sphene. Mafic knots (comprising amphibole, biotite and opaques) are common; pyroxene fragments are rare. In samples RB014, RB075 and RB080, biotite and amphibole are locally altered to epidote.

3.5.2 Mineralogy

3.5.2.1 Sample RB013 (Plate 3.5.2.1)

Accessory Minerals

Euhedral ZIRCON crystals (0.1-0.2mm) occur in association with opaque minerals.

APATITE forms euhedral laths and hexagonal shaped crystals <0.1mm across which are totally enclosed within biotite.

SPHENE occurs as subhedral and euhedral grains 0.2-1.5mm across and is normally associated with biotite and opaque minerals. It is pale brown and pleochroic.

The OPAQUE phases form anhedral grains up to 0.1mm in size.

Mafic Minerals

HORNBLENDE is a relatively abundant phase (4.9% modal) and occurs as euhedral rhombs and laths which vary in size from 0.5-2mm. It exhibits twinning and has pale green-beige pleochroism. It constitutes the bulk of mafic knots (4mm across) in which it takes on a very ragged shape and is 'peppered' with minute (<0.1m) grains of opaque minerals.

BIOTITE is locally altered to CHLORITE and RUTILE. The majority, however, forms unaltered laths 1-1.5mm long which display a cream-brown pleochroism.

3.5.2.1 Porphyritic Starav monzogranite, RB013 (PSMG/P). One crystal of alkali feldspar (microperthite) encloses fragments of plagioclase, biotite, sphene and amphibole.

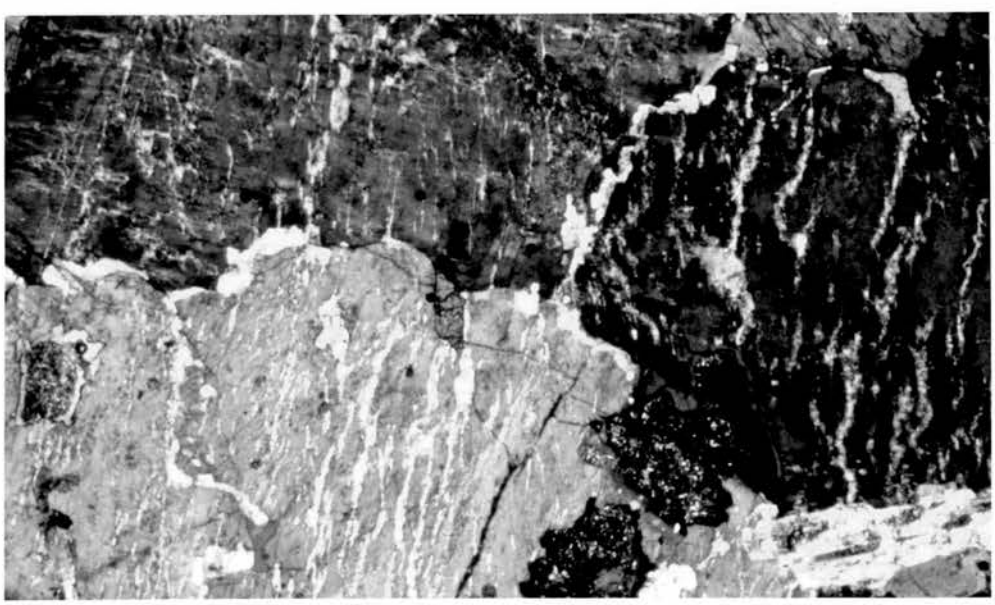

3.5.2.1.1 Porphyritic Starav monzogranite, RB080 (PSMG/P). A triple junction between perthite alkali feldspar. The pale grey crystal encloses some sericitised plagioclase feldspar and a euhedral crystal of sphene (centre).

Felsic Minerals

PLAGIOCLASE FELDSPAR occurs as subhedral grains 2-7mm long which are zoned and twinned, sometimes showing synneusis twinning. Myrmekite develops at its contacts with alkali feldspar.

ALKALI FELDSPAR forms the phenocryst phase, as subhedral crystals up to 30mm long, and occurs in the groundmass as subhedral grains 6-11mm across. There is no visible perthite development in the phenocryst phases and some show faint normal concentric zoning. Biotite, amphibole and plagiclase fragments occur sporadically within the phenocrysts.

QUARTZ occurs as irregular interstitial grains (<0.1-4mm).

3.5.2.2 Sample RB017 (Plate 3.5.2.2)

Accessory Minerals

ZIRCON (<0.1mm) forms anhedral grains associated with opaque minerals.

APATITE (0.1-0.2mm) grows as euhedral crystals in biotite.

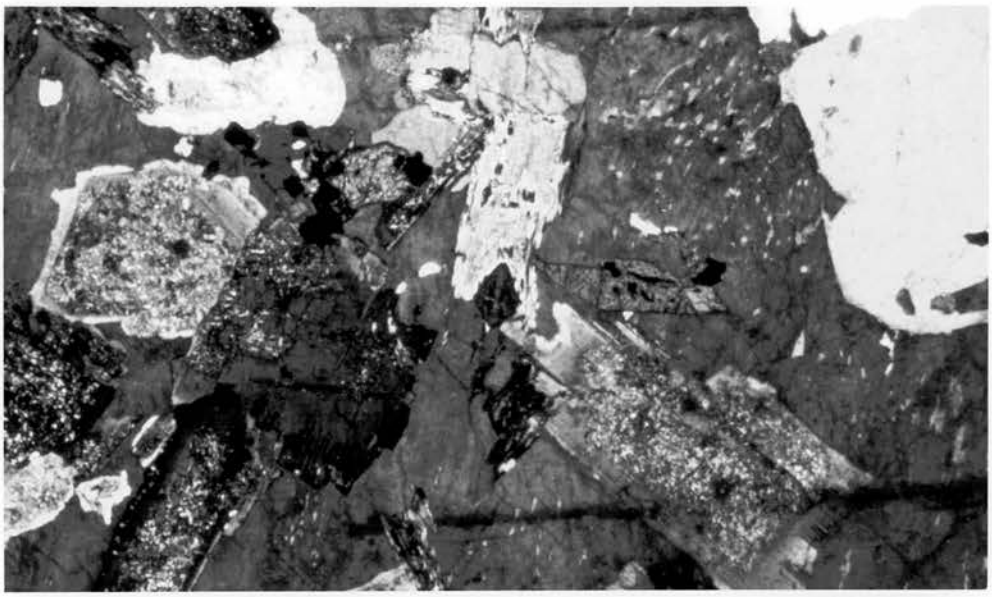

3.5.2.2a Porphyritic Starav monzogranite, RB017 (PSMG/P). Almost the whole field is occupied by alkali feldspar in optical continuity (grey) which encloses sphene, biotite, plagioclase and opaques. The lozenge- shaped dark crystal partly enclosed by biotite (centre) is attributed to chloritised clinopyroxene. The fragment of sericitised plagioclase in the left field shows a pale reaction rim of albite.

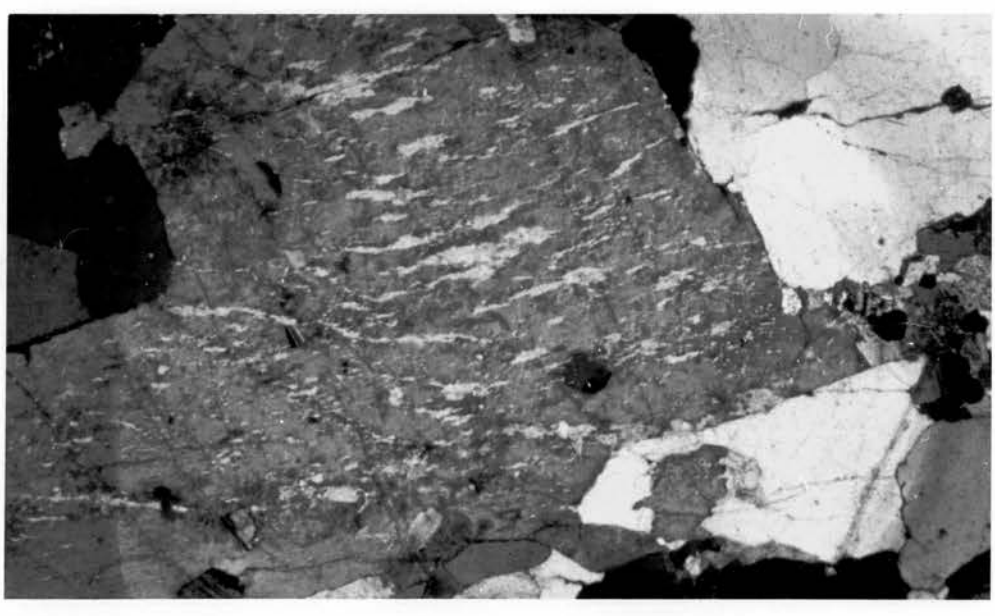

3.5.2.2b Coarse perthitic alkali feldspar.

SPHENE is the most abundant accessory phase (0.4% modal). It forms euhedral crystals 0.5-1.5mm across which are always associated with hornblende and biotite.

The OPAQUE minerals occur as subhedral grains <0.2mm across and are found intimately associated with hornblende and biotite.

Mafic Minerals

A rhomb-shaped grain (0.3mm) showing 1st. order grey interference colours and with fibrous texture was interpreted as a pseudomorph after PYROXENE, now altered to CHLORITE.

HORNBLENDE occurs both as isolated euhedral rhombic sections, and as aggregates with biotite and opaque minerals. It displays twinning and greyish-green pleochroism. Grains vary in size from 0.5 to 2mm.

BIOTITE forms laths and subhedral [0001] sections, 0.5-2mm across. Most has been partially or totally altered to CHLORITE.

Felsic Minerals

PLAGIOCLASE FELDSPAR forms subhedral laths and irregular grains, 6-10mm long which often show some alteration to sericite. It is twinned and zoned. A composite megacryst was found.

ALKALI FELDSPAR forms the phenocryst and groundmass phases. The latter population is composed of subhedral perthitic grains 4-12mm in size. Some has crystallised interstitially to quartz. The larger grains occasionally enclose fragments of biotite and plagioclase feldspar.

QUARTZ is a late phase growing as irregular grains in the interstices of the earlier phases. Grains vary in size from <0.2 to 4mm.

3.5.2.3 Sample RB015 (Plate 3.5.2.3)

Accessory Minerals

ZIRCON forms subhedral grains 0.1-0.3mm in size and is associated with the opaque minerals.

APATITE is found in biotite as subhedral grains approximately 0.1mm long.

SPHENE occurs in a variety of sizes, from fragmented euhedral grains , (<0.1mm) to subhedral grains 0.5-2mm long. Some of the latter have brown patches which may indicate post-magmatic alteration. The grains often occur in clusters, together with biotite.

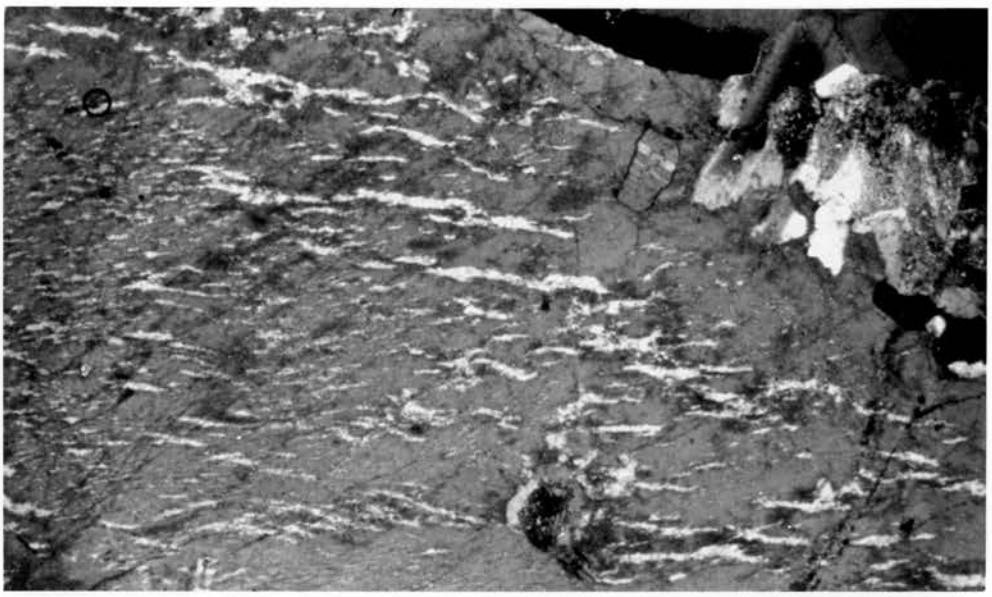

3.5.2.3 Porphyritic Starav monzogranite, RB015 (PSMG/P). Coarse perthitic alkali feldspar encloses a small twinned plagioclase feldspar.

OPAQUE minerals have an irregular or subhedral form and sizes range from 0.1 to 0.5mm.

Mafic Minerals

HORNBLENDE shows green pleochroism and is occasionally altered to an opaque mineral. The grains are anhedral and vary in size from 0.5-2mm.

BIOTITE occurs as subhedral laths 0.2-2mm long which are mostly altered to CHLORITE, and occasionally to EPIDOTE.

Felsic Minerals

PLAGIOCLASE FELDSPAR exhibits normal zoning and the calcic cores usually show extensive sericitisation. The grains are subhedral and range in size from 1.5-5mm.

ALKALI FELDSPAR occurs as a phenocryst phase with crystals 4-8mm across and a groundmass phase (1-3mm). The phenocrysts enclose small fragments of plagioclase randomly distributed, and plagioclase and biotite grow around the periphery. One megacryst has a euhedral core with microperthite texture and small

plagioclase fragments around its margin. This core is surrounded by a subhedral growth of coarse perthite. The groundmass phase grows interstitially and is less perthitic than the phenocrysts, but has more inclusions.

QUARTZ grains vary in size from 2-5mm and form an interstitial phase. Some grains form euhedral hexagonal [0001] sections.

3.5.2.4 Sample RB014 (Plate 3.5.2.4)

Accessory Minerals

ZIRCON is scarce and only occurs as anhedral grains <0.1mm across within biotite flakes.

APATITE occurs as euhedral crystals <0.1-0.2mm in size within biotite.

Only one crystal of SPHENE was found which was euhedral and 0.3mm across. It is pleochroic and occurs in alkali feldspar.

OPAQUE MINERALS are euhedral and form isolated crystals approximately 0.2mm in size. Some may represent altered mafic minerals.

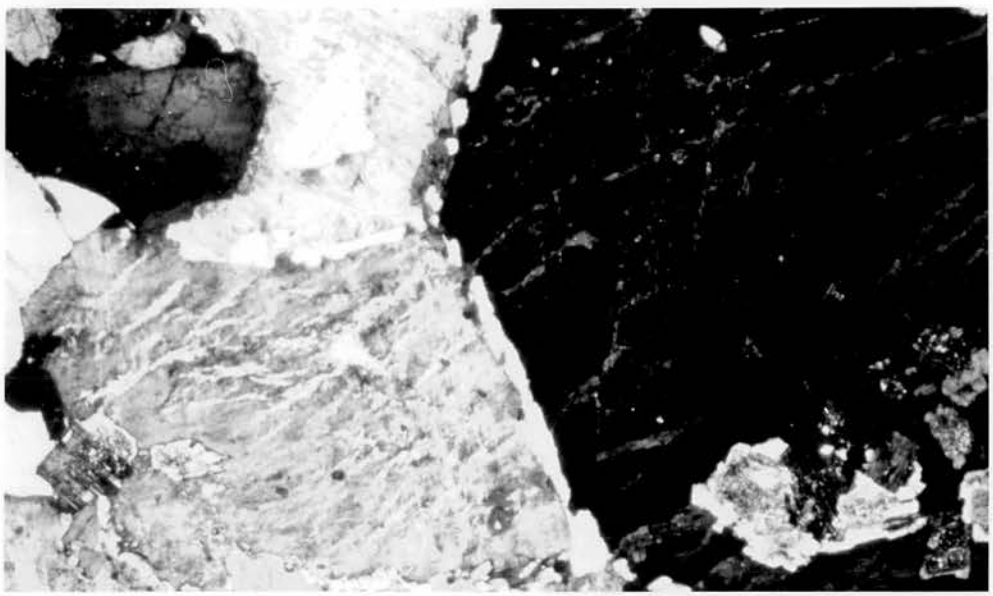

3.5.2.4 Starav monzogranite, RB014 (PSMG/P.). Triple junction between perthitic alkali feldspar, with enclosed fragments of plagioclase feldspar and intergranular 'necklace' texture, indicating extreme perthite exsolution.

Mafic Minerals

HORNBLENDE has been mostly altered to EPIDOTE and can be identified by its basal section form. The anhedral grains are about 0.5mm across.

BIOTITE forms euhedral hexagonal [0001] sections and subhedral laths up to 1mm long. Some has been altered to CHLORITE, EPIDOTE and RUTILE.

Felsic Minerals

PLAGIOCLASE FELDSPAR forms subhedral laths which vary in size from 1mm to 4mm in length. It is twinned and zoned and slightly sericitised.

ALKALI FELDSPAR occurs in two forms. An earlier phase consists of very coarse perthitic subhedral grains 4-7mm across which show twinning. The later phase grows interstitially to plagioclase and the larger early alkali felspar, shows no twinning and has microperthitic texture. The grains reach 4mm across and enclose quartz.

QUARTZ grains occur as both euhedral and irregular shaped grains 1-4mm across. They form the groundmass in conjunction with the late alkali feldspar. There is no granophyric texture.

3.5.3 Modal Analysis

	RB013	RB017	RB015	RB080	RB014
Quartz	21	22	27	32	28
Alk.Feldspar	46	28	31	27	48
Plagioclase	23	41	36	37	22
Biotite	3	3	6	3	2
Hornblende	6	5	0.2	0.6	*
Zircon	*	*	*	*	*
Apatite	(1)	*	*	*	*
Sphene	0.3	0.5	0.3	0.4	(1)
Opaques	0.7	0.5	(1)	0.7	(4)

These samples are represented on Fig 3.7 by the symbols 'P' and 'P.'(RB014).

3.5.4 Sequence of Crystallisation

The identification of the alkali feldspar phenocryst phase as orthoclase using X-ray Diffraction techniques (Hutchison, 1974; Borg & Smith, 1969) suggests that these crystals formed as an early magmatic phase. They are contemporaneous with hornblende crystallisation as evidenced by the growth of an elongate hornblende crystal alongside an orthoclase phenocryst (RB013). The occurrence of large (20mm) phenocrysts adjacent to the PSMG - Cruachan intrusion contact increases the likelihood that this phase formed an early solid component to the upwelling Starav pluton. Work by Whitney(1975) and Kawachi & Sato(1978) shows that orthoclase can crystallise as the sole early phase from a granitic melt under high P_{H2O} viz. 7-8% H_2O at 5-10kb. The presence of hornblende and biotite could indicate that water levels were initially high, but much would have vented off during the final cooling stages, forming aplite veins (RB016, RB031), and the pegmatite at RB094. The occurrence of epidote confirms the presence of post-magmatic hydrothermal fluids. The fact that orthoclase has not ordered to microcline suggests that water levels must have fallen after consolidation, to slow the ordering process down to imperceptible levels. The presence of water is believed to accelerate the ordering process in alkali feldspars (Martin 1974).

The orthoclase phenocrysts decrease in number inwards to the geographical centre of the intrusion, and their size contrast with the groundmass feldspar decreases, as the later alkali feldspar grains increase in size. Plagioclase and biotite

crystals are more noticeably altered near the inner margins of the intrusion. Another feature of the alkali feldspar is the increased development of perthite texture inwards to the centre of the pluton. This is consistent with an increase in water content and cooling time from the outer margins to the inner core of the intrusion.

Mafic knots may represent restitic material after partial melting of crustal rocks. Isotope evidence indicates that most of the Etive rocks were derived from crustal rocks of Lewisian (Grenville) age (Clayburn et al. 1983).

CENTRAL STARAV MONZOGRANITE (CSMG)

3.6.1 Rock Description

The innermost member of the Etive complex is a coarse to medium (5-2mm) equigranular leucocratic granite. It is locally fine grained (<1mm) near the summit of Ben Starav (RB106). Coarse quartz-microcline pegmatite has developed on the NE flanks of Ben Starav (RB101a) and at the SW contact with the PSMG (RB137) where the alkali feldspar has been haematised to an intense brick-red colour. Mafic and accessory minerals are rare.

3.6.2 Mineralogy

3.6.2.1 Sample RB093

Accessory Minerals

ZIRCON occurs in biotite, associated with opaque minerals, as anhedral grains <0.1mm.

APATITE also occurs within biotite and varies in size from 0.1-0.6mm as subhedral and euhedral crystals.

SPHENE is found as pale beige pleochroic grains 0.2-0.7mm long which occur in biotite, attached to opaque minerals and also 'free' within plagioclase crystals.

OPAQUE phases are both euhedral and irregular in shape, usually 0.1mm in size and mostly occur in biotite.

Mafic Minerals

BIOTITE is the only recognisable mafic mineral and it is mostly altered to CHLORITE. It varies from 1-1.5mm subhedral laths.

Felsic Minerals

PLAGIOCLASE FELDSPAR forms subhedral laths 1-5mm long. It is zoned (An30-20) and twinned. Some occurs as fragmented crystals within alkali feldspar, and some laths cluster into aggregates.

ALKALI FELDSPAR occurs as fragments of twinned coarse perthite (2-4mm) and as a late interstitial microperthite (1.5-2mm) phase. The larger perthitic grains enclose fragments of plagioclase feldspar and quartz.

QUARTZ varies in size from 0.2-7mm. It is anhedral and forms a late interstitial phase.

3.6.2.2 Sample RB034 (Plate 3.6.2.1)

Accessory Minerals

ZIRCON occurs as subhedral grains 0.1mm across within alkali feldspar.

APATITE forms euhedral crystals <0.1-0.2mm long which have grown within biotite.

SPHENE occurs as rare anhedral fragments up to 0.2mm in size associated with subhedral OPAQUE MINERALS (0.1-0.2mm).

Mafic Minerals

BIOTITE is the only mafic phase and it forms anhedral laths 0.5-1mm long which have been mostly altered to CHLORITE with a development of RUTILE needles.

Felsic Minerals

PLAGIOCLASE FELDSPAR forms anhedral grains 0.5-3mm across which are zoned (An30-20), twinned and slightly sericitised. The fragments appear to be enclosed or 'cemented' by late alkali feldspar, with the development of myrmekitic texture. There is local development of secondary MUSCOVITE.

3.6.2.1a Central Starav monzogranite, RB034 (CSMG/C). Perthitic alkali feldspar fills the field of view, and encloses fragments of twinned plagioclase and subhedral quartz.

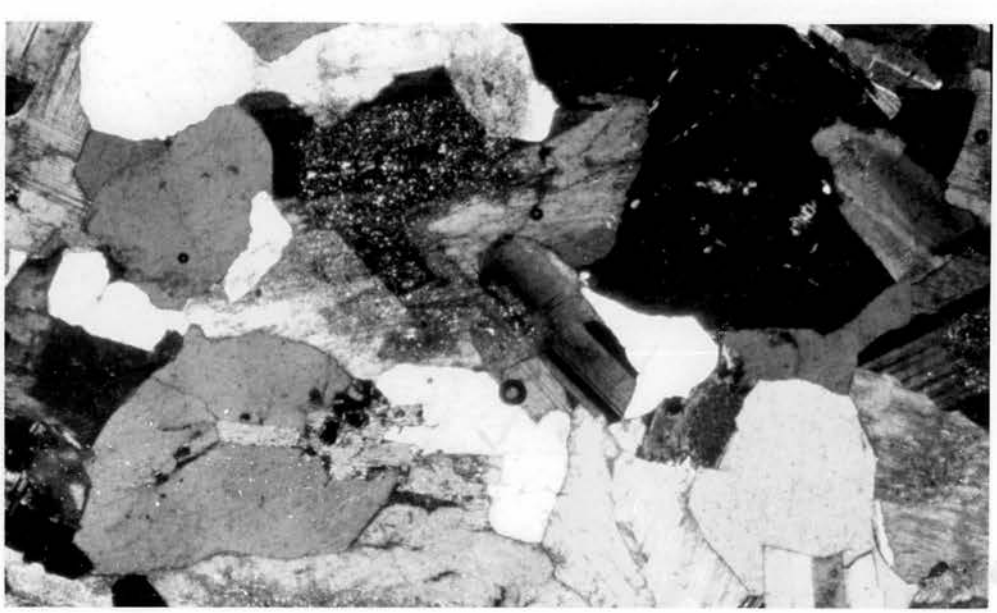

3.6.2.1b Subhedral quartz showing late, interstitial growth; it overgrows plagioclase and alkali feldspars, biotite, and opaques.

ALKALI FELDSPAR occurs in two distinct modes. One is represented by large (2-7mm) irregular perthitic grains, and the other is an interstitial anhedral microperthite. The former phase contains inclusions of plagioclase feldspar fragments.

QUARTZ is a late stage mineral by virtue of its interstitial form of growth and triple junction grain boundaries. Grain size varies from 0.5-2mm with a mean diameter of about 1mm.

3.6.2.3 Sample RB099

Accessory Minerals

ZIRCON occurs as 0.1-0.2mm euhedral crystals set in biotite, in association with opaque minerals.

APATITE also occurs in biotite and forms euhedral crystals <0.1mm long.

SPHENE was not found.

OPAQUE MINERALS form subhedral grains 0.2-1.5mm. The smaller ones tend to be pseudo-cubic, whereas the larger ones have an elongated hexagonal outline which suggests they may be haematised pyroxene or amphibole.

Mafic Minerals

BIOTITE forms subhedral laths and euhedral hexagonal crystals 0.2-1.5mm across. It is mostly altered to CHLORITE which contains RUTILE needles.

Felsic Minerals

PLAGIOCLASE FELDSPAR occurs as irregularly-shaped laths and fragments 0.3-4mm in size which show zoning and twinning. There is some sericite alteration.

ALKALI FELDSPAR forms both large (2-4mm) perthite fragments which contain plagioclase fragments and smaller (<2mm) twinned microperthite phase which grows interstitially. Microcline has developed in both forms.

QUARTZ has grown with a wide range of grain sizes, from 0.1-2mm across. They form subhedral or irregular interstitial grains.

3.6.3 Modal Analysis

	RB093	RB034	RB099
Quartz	40	29	36
Alk.Feldspar	27	33	29
Plagioclase	29	36	34
Biotite	3	2	1
Amphibole	-	-	-
Zircon	*	(1)	0.5
Apatite	(3)	*	*
Sphene	(1)	*	*
Opaques	0.7	(6)	*

The values listed above are shown by the symbol 'C' on Fig 3.7.

3.6.4 Sequence of Crystallisation

A notable feature of the CSMG is the almost complete absence of sphene in sharp contrast to its abundance in the PSMG. Modal quartz shows a significant greater rate of increase in the CSMG (28-41%) than it does in the PSMG (21-28%). If the two intrusions were co-magmatic, this change in abundance could be expected to be regular.

The similarity in texture and major mineralogy of the inner PSMG and the outer CSMG led most workers to consider the two Starav types to be one zoned intrusion (Anderson 1937; Kynaston & Hill 1908; Bailey & Maufe 1960).

The presence of fragments of perthitic alkali feldspar within a matrix of secondary microperthitic alkali feldspar suggests that the former phase was derived from a source reservoir and did not crystallise in-situ. This postulated reservoir may have been common to the PSMG magma. The CSMG magma represents compositions close to the felsic ternary eutectic (Tuttle & Bowen 1958) (See Page 4-77) and may reflect a late fractionate from an inferred Starav magma reservoir.

The petrographic and field evidence (see Section 2.6) lead to the conclusion that the CSMG is related to the PSMG but is separated from it in time. They may share a common source but are probably not part of one continuously fractionated pluton. From the petrographic textures and the existence of coarse pegmatite it can be concluded that the CSMG crystallised from a melt or at least a crystal mush.

3.7 STRECKEISEN CLASSIFICATION

On the basis of the Streckeisen (1976) modal classification system for plutonic rocks, the rock types represented in the Etive complex (Fig 3.7) are given the new names shown below. The new names have been adopted in this study.

LOCALITY NAME	OLD NAME	NEW NAME
Quarry Intrusion & satellites	Diorite, Quartz Diorite	Diorite, Quartz Diorite
Cruachan(south)	Tonalite	Monzodiorite
Cruachan(north)	Adamellite	Monzogranite
Starav	Adamellite	Monzogranite
Meall Odhar	Granite	Monzogranite Alkali granite

Of particular note is the alkali feldspar-dominated trend in P, in contrast to the quartz-dominated trend in C. The A trend lies between these two.

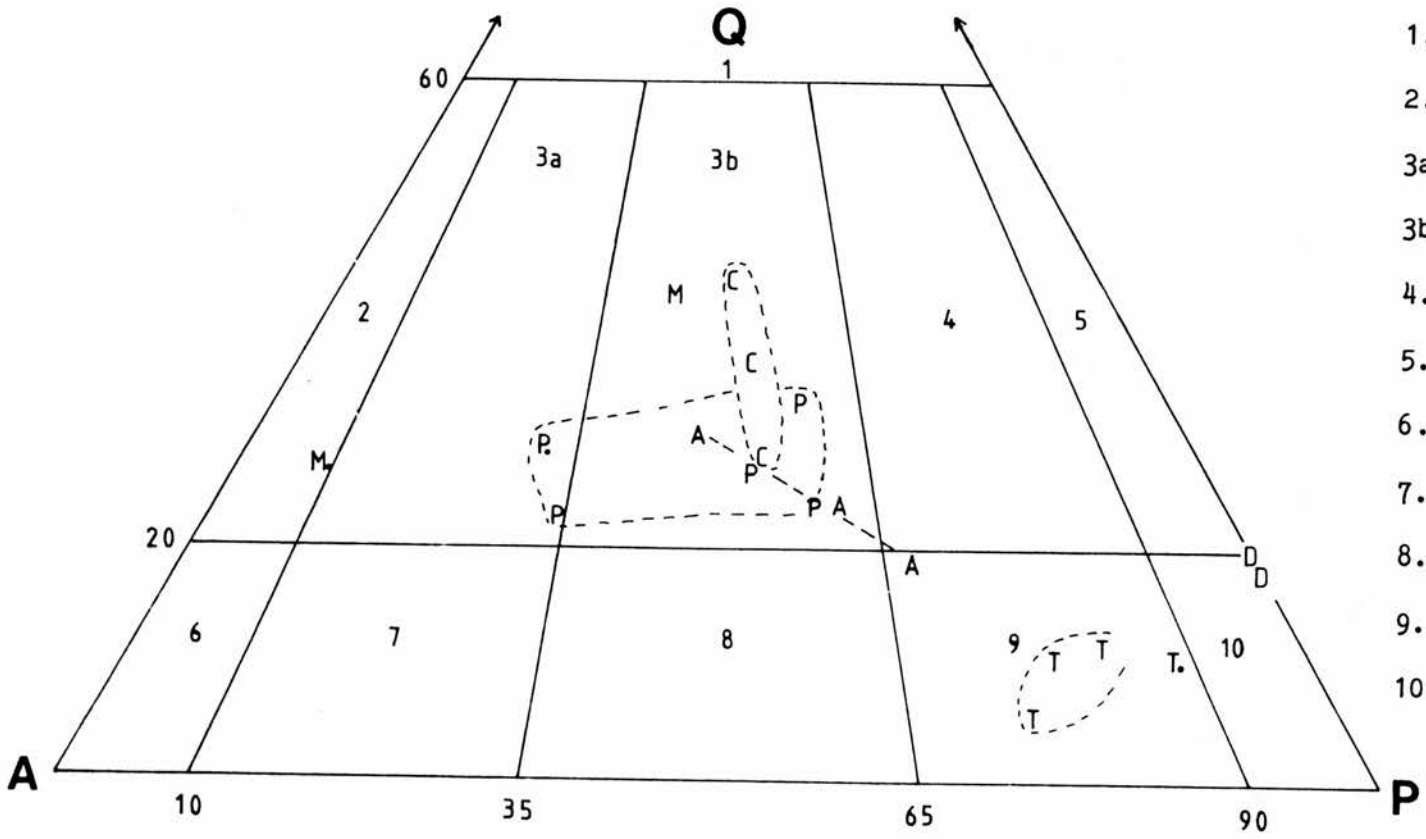

(After Streckeisen, 1976)

Key to diagram.

1. Quartz-rich granitoid
2. Alkali granite
3a. Syenogranite
3b. Monzogranite
4. Granodiorite
5. Tonalite
6. Alkali granite
7. Syenite
8. Monzonite
9. Monzodiorite
10. Diorite/Gabbro

fig 3.7 Modal Quartz - Alkali Feldspar - Plagioclase

3.8 ALKALI FELDSPAR STRUCTURAL STATES

Fractions of alkali feldspar were physically separated from selected samples using magnetic and heavy liquid techniques (see Appendix A.1.1). Each clean fraction was finely powdered and subjected to X-ray diffraction investigation. (See Appendix A.1.2 for instrumental conditions).

A slow scan over 29 - 31° 2θ was made to identify the 131 and $1\bar{3}1$ peaks. Potassium bromate was then added as internal standard and a scan made over 20 - 52° 2θ to identify the $[\bar{2}01]$, [060], and $[\bar{2}04]$ peaks. The angular positions were indexed according to Borg and Smith (1969). This information is summarised in Fig 3.8 using the diagram after Wright(1968). MM (Maximum Microcline), IM (Intermediate Microcline) and Or(Orthoclase) represent type mineralogies according to Borg and Smith (1969). The data is listed in Table 3.8

In all but a few cases the [060] and $[\bar{2}04]$ peaks split into two components. This may reflect the co-existence of orthoclase and its partially ordered product, microcline. It is assumed that all alkali feldspar crystallised as an homogenous phase but which has subsequently undergone exsolution to form perthitic texture. (Bowen and Tuttle, 1950). Such a transition involves a change in symmetry from monoclinic (disordered) to triclinic (ordered).

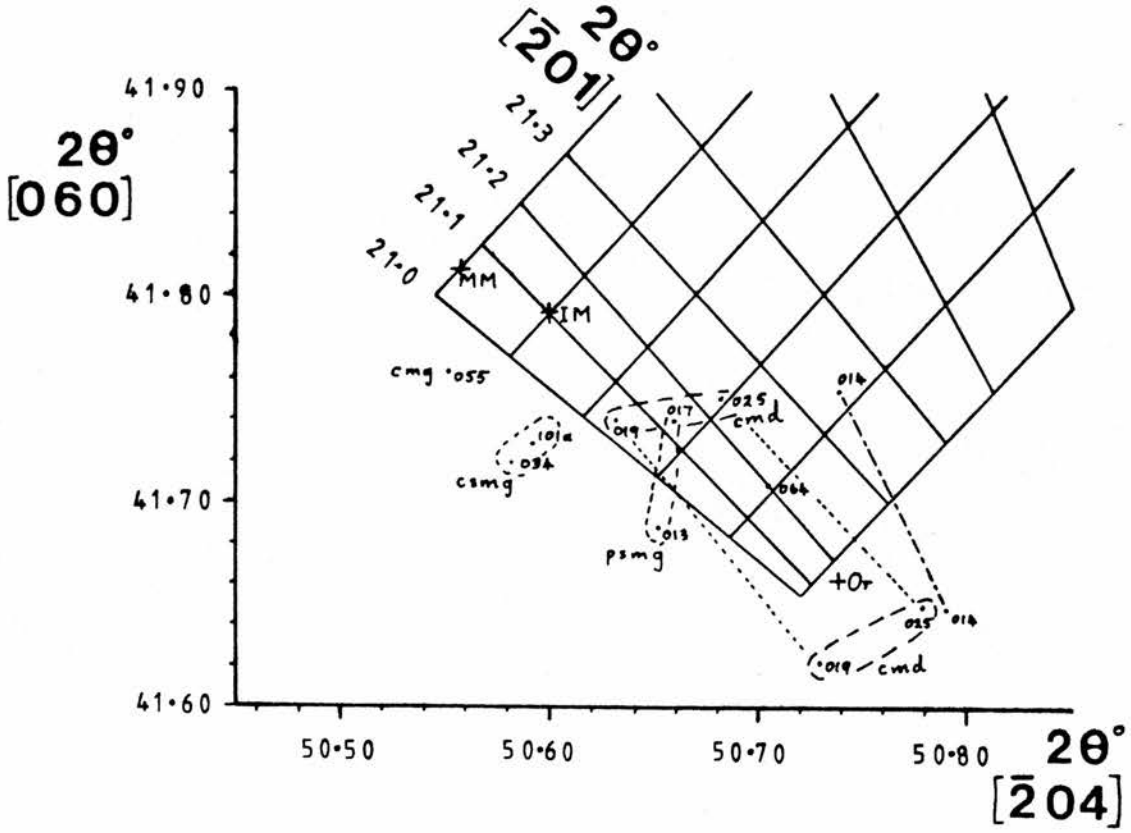

Fig 3.8 Alkali feldspar structural states (after Wright 1968). Maximum microcline (MM), Intermediate Microcline (IM) and Orthoclase(Or) compositions from Borg and Smith (1969).

Table 3.8

Sample	[131]	[1$\bar{3}$1]	J.r.	T.	[$\bar{2}$01]	[060]	[$\bar{2}$04]	Ab/Or
RB019	29.70	29.83	5.2	0	20.86	41.62	50.63	48%
	29.76				21.03	41.74	50.73	
RB025	29.78	-	8.1	0	20.99	41.66	50.68	44%
						41.75	50.78	
RB064	29.78	-	7.0	0	21.01	41.71	50.71	340%
RB055	29.45	30.15	-	0.87	20.99	41.76	50.55	35%
RB026	29.85	-	6.2	0	21.00	41.69	50.60	35%
							50.75	
RB013	29.80	-	10.5	0	21.02	41.69	50.65	28%
RB017	29.78	-	9.5	0	21.02	41.74	50.66	19%
RB014	29.76	-	10.0	0	20.98	41.65	50.74	31%
	29.5	30.0	-			41.77	50.79	
RB034	29.78	-	2.4	0	20.97	41.72	50.58	20%
	29.5	30.0	-				50.68	
RB101a	29.77	30.07	1.7	0.36	20.99	41.73	50.59	31%

Reflections [hkl] in $2\theta^{o}$; J.r= Jiranek (1982) ratio; T= Triclinicity index (Goldsmith and Laves (1954); Ab/Or= ratio of albite to orthoclase [$\bar{2}$01] peaks.

Texturally, alkali feldspars from the Etive rocks vary from cryptoperthitic to perthitic. The sodic feldspar contribution is in evidence and the Ab [$\bar{2}$01] (22° 2θ) peak is ratioed to the Or [$\bar{2}$01] (21° 2θ) peak to estimate its relative abundance.

In some cases the raw value of [$\bar{2}$01] does not coincide with the diagram value. This indicates that the cell dimensions are abnormal for the CMD samples (RB019 and RB025) and the marginal PSMG sample RB014. Such abnormality may reflect a non-equilibrium situation. In contrast, the cell dimensions are normal for CMG RB055 maximum microcline, the PSMG orthoclase phenocrysts, and the CSMG intermediate microcline. The basic member of the CMG (RB064) gives an ambiguous result. For samples with normal cell dimensions, it is possible to assess the Or content of the potassic phase using the following equation (after Wright 1968):

Or% = 2031.77 - 92.19 x [$\bar{2}$01] 2θ

RB055, RB101a (20.99°) = 96.70% Or

RB013, RB017 (21.02°) = 93.94% Or

RB034 (20.97°) = 98.50% Or

The triclinicity index (Goldsmith and Laves, 1954) was

calculated, where possible from the [131] (29.4°2θ) and [1$\bar{3}$1] (30.2°2θ) peak positions. However, where the Or [131] peak broadens but does not divide into the two microcline peaks, this index is not applicable. Jiranek (1982) proposed an alternative index which ratios the peak height to half-peak width of an undivided Or [131] reflection. This value is sensitive to peak broadening, a feature which reflects the increase in ordering of the alkali feldspar lattice. The lower the value of this index, the broader is the peak and indicates an increase in triclinic character.

The most chemically evolved member of the CMG (RB055) contains well-ordered maximum microcline (triclinicity = 0.87). The presence of water is thought to accelerate the ordering of alkali feldspar (Ragland, 1970; Martin, 1974). This is consistent with the fact that this sample represents the upper levels of the pluton, where residual fluids had longer to interact with the rock, and also gave rise to greisen veins (RB058).

The phenocrysts of alkali feldspar in the PSMG intrusion show clear evidence that they are orthoclase (viz. single [131] peak at 29.80° 2θ; highest Jiranek ratio of 10.5). Petrographic examination shows an increase in perthite development towards the inner margins of this intrusion (RB013-RB017-RB015-RB014)(See plates 3.5.2.1 to 3.5.2.4) . The later inner intrusion of CSMG contains intermediate microcline perthite with a Jiranek ratio of 2.4. This increased ordering and perthite development inwards is

consistent with increasing concentration of water in the magma, which is thought to facilitate the ordering process (Ragland; Martin; op.cit.).

Whitney (1975), and Kawachi and Sato (1978) have shown that orthoclase can form as a sole phenocryst phase at high P_{H2O} (7-8% H_2O at 5-10kb). There is no doubt that it crystallised early. In contrast, the CSMG has more ordered alkali feldspar and this fact indicates it was a wetter magma.

The evidence for mixed assemblages (Or + Int. Microcline) within some samples may reflect domains of triclinic feldspar within the primary monoclinic (orthoclase) phase. (Smith, 1974).

The rate of ordering within an alkali feldspar is dependent upon the relative diffusion rates of Na and K ions. Na ions are more mobile in a feldspar lattice than are K ions (Lin and Yund, 1972). Senderov et al.(1975) found that potassium feldspars order more slowly than albites.

It may be concluded that the alkali feldspars in the Etive rocks crystallised from a magma and have since undergone selective ordering, to greater or lesser degrees, from primary orthoclase to microcline, aided by the presence of water.

GEOCHEMISTRY

Major and trace element data were obtained for 56 samples, selected for their freshness, which are representative of the different rock types found in Etive. The analytical methods are described in Appendix 1, and the data is listed in Appendix 4.

Traditional Harker-type diagrams and combinations of elements have been plotted on bivariate diagrams which achieve good discrimination between rock types and individual samples. Chondrite-normalised displays have also been used as these help to give an overall picture of the regional variation in chemistry.

Superimposed on most diagrams are vectors which were generated by computer programmes (listed in Appendix 3) to calculate changes in liquid compositions during fractional crystallisation. In the case of linear-linear plots the vectors are only meant to give a general sense of direction and not quantitative information. The Rayleigh law ($Cl/Co=F^{(D-1)}$) was applied to trace element behaviour. Major element modelling was based on a subtractive procedure using a high-alumina basalt (de la Roche et al. 1980) as a starting composition. This choice was arbitrary and does not necessarily have any petrogenetic implications. Recent work by Mann (1983) has studied the role

of fractional crystallisation in a calc-alkaline volcanic sequence starting from a high-alumina basalt. The major element mineral compositions were selected from the literature (see Appendix 3). The initial trace element assemblage was a theoretical one and the mineral-melt distribution coefficients were compiled from numerous sources (see Appendix 3).

In the diagrams each intrusion is identified by a symbol which reflects the petrography. Identifiable trends are marked by pecked lines, with an arrow to indicate the direction of liquid evolution.

It has been pointed out by Meighan (1979) that some granites may be intruded as mushes, and as such, whole rock analyses cannot represent liquid compositions. From petrographic evidence in Chapter 3 it was suggested that the CMD may have been intruded as a plagiophyric mush. Any interpretations of its petrogenesis in terms of a melt must take this fact into consideration.

'Harker' diagrams
(after Harker 1909)

This series of plots summarise the variation of each trace element and major element oxide against SiO_2. All symbols used are as listed at the beginning of the chapter with the exception of Tx which for clarity is represented as +.

The overall impression is one of a general co-linear trend which encompasses most rock types from diorite (D) to evolved granites (M). However groups T, M and M. deviate from this trend in a number of plots and it is these groups which are considered in greater detail.

The overall decreasing trends shown by MgO, CaO, TiO_2, FeO, Sr and V suggest that the Etive magmas may all be related to a parental mafic magma which has fractionated out olivine (Mg), pyroxene (Ca, Mg, Fe), amphibole (V, Fe, Ca), plagioclase (Ca, Sr) and iron/titanium oxides (Fe, Ti, V).

In spite of some wide scatter on selected trace element diagrams, there is a general coherence of sample points within groups. Field evidence clearly separates A from P, M from C, and D from T, so that a more detailed appraisal of the chemistry may be attempted using these constraints.

Considering the T group first, with reference to an inferred general trend (D-Q,T.-A-P-C) the following deviations are noted:

T compositions: Low in CaO, MgO, FeO, MnO, Y, (V).

: High in Al_2O_3, Ba, Zr, Hf, La, Ce, Na_2O, TiO_2, (K_2O).

The depleted components could be explained by pyroxene, amphibole ± iron/titanium oxide fractionation. Removal of Al-poor amphibole could cause an aluminium enhancement. However, the quantity of pyroxene which needs to be removed from Q compositions to generate the observed Ba enhancement is in the order of 60 to 80%. This amount cannot be produced from the elemental components available in Q. Sodium and aluminium may reside in an alkali feldspar phase though the levels of potassium are not exceptionally high. Plagioclase (An_{30-40}) at levels up to 58% (in RB019) is not compatible with the relative depletion in calcium, though some cores of An_{60} may reflect remnants of an earlier generation causing loss of calcium. Zr will reside in zircon and La and Ce will be concentrated in sphene and apatite.

The concentrations of these elements relative to other rocks with similar SiO_2 values is greater than those found in any of the other Etive rocks and cannot be explained in terms of a normal consanguinous fractionated series. If increased lanthanum and cerium values were to reflect selective HREE depletion due to amphibole fractionation, then yttrium values in T should be correspondingly depleted, but they are not excessively low. Zirconium in calc-alkaline or high-potassic calc-alkaline rocks

behaves as a compatible element, forming zircon. It is therefore depleted in the melt during fractionation. The higher zirconium levels found in T are likely to indicate the existence of an independent magma.

The very high barium levels are difficult to explain in terms of a fractionation model, and its affinity for potassium minerals means it must be associated with either biotite or alkali feldspar.

The combination of high Zr, Ba, La, Ce and Al_2O_3 in T relative to other rocks with similar major chemistry indicates that T samples had a different origin, either in terms of source, or in terms of petrogenetic mechanism.

A distinction can be made between M and M. compositions with respect to yttrium, cerium, thorium and rubidium. As these elements belong to the incompatible group (with the exception of Y and Th which could be taken out of a melt by early accessory minerals) whose concentrations normally increase in the melt with increased fractionation, M samples have been termed 'evolved'. M. samples are termed 'depleted' in the sense that for such high SiO_2 and K_2O values, M. are relatively depleted in these elements. This difference has been attributed to differences in origin, the former (M) being closely linked to C (Starav magmas) whereas M. does not fit in with any fractionation model. The combination of high K_2O and low Rb strongly suggests an origin by partial melting of Rb- (and Th-) depleted material (Shaw 1968).

Barium is enriched in M. samples. A concomitant depletion in yttrium supports the notion of partial melting from a garnet and/or amphibole-rich source.

A separation is seen between P and C compositions with reference to lead, thorium and lithium. These elements are strongly associated with biotite (Li), oxides or zircon (Th) and alkali feldspar (Pb), and in view of the non-linear relationship with P, indicates either a change in crystallising conditions or a fresh influx of magma. The lower values of K_2O in C relative to the most evolved P point to an influx of fresh magma.

Compositions marked +, which represent a paler version of T, generally appear to be silica-rich variants of T.. In some diagrams (FeO, Al_2O_3, V) and from field evidence certain of these rocks appear to be related to A (CMG). Since + share the idiosyncracies of T, which have been discussed earlier as probably being due to a separate magma, the + - A connection appears tenuous. The fact that these + samples are mostly marginal to the Dalradian country rocks allows for localised fluid interaction to have changed the chemistry.

In general terms, fractional crystallisation appears to have controlled the chemical variations found within A, P and C, and in the trends D to Q to A. Compositions T. have an affinity for Q and may lie on the D to Q trend, and they may also be precursors for T samples which lie off the main trend. There is overlap between A and P though field evidence clearly separates

these two groups. There is also some field evidence for a discontinuity between P and C. M. and M compositions are clearly not homogenous and cannot be fitted directly into a simple petrogenetic model.

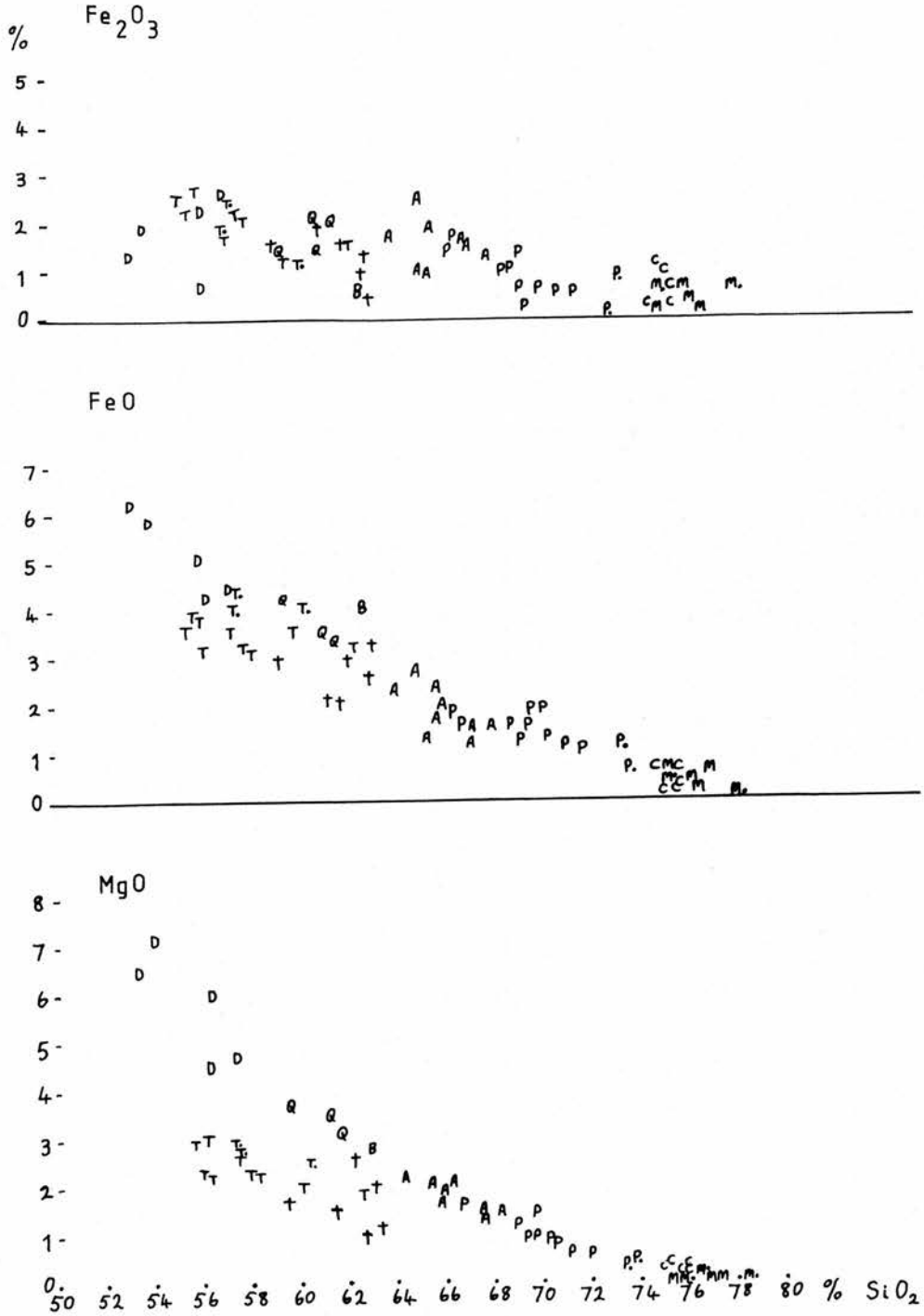
Fe2O3
%
5
4
3
2
1
0
FeO
7
6
5
4
3
2
1
0
MgO
8
7
6
5
4
3
2
1
0
50 52 54 56 58 60 62 64 66 68 70 72 74 76 78 80 % SiO2

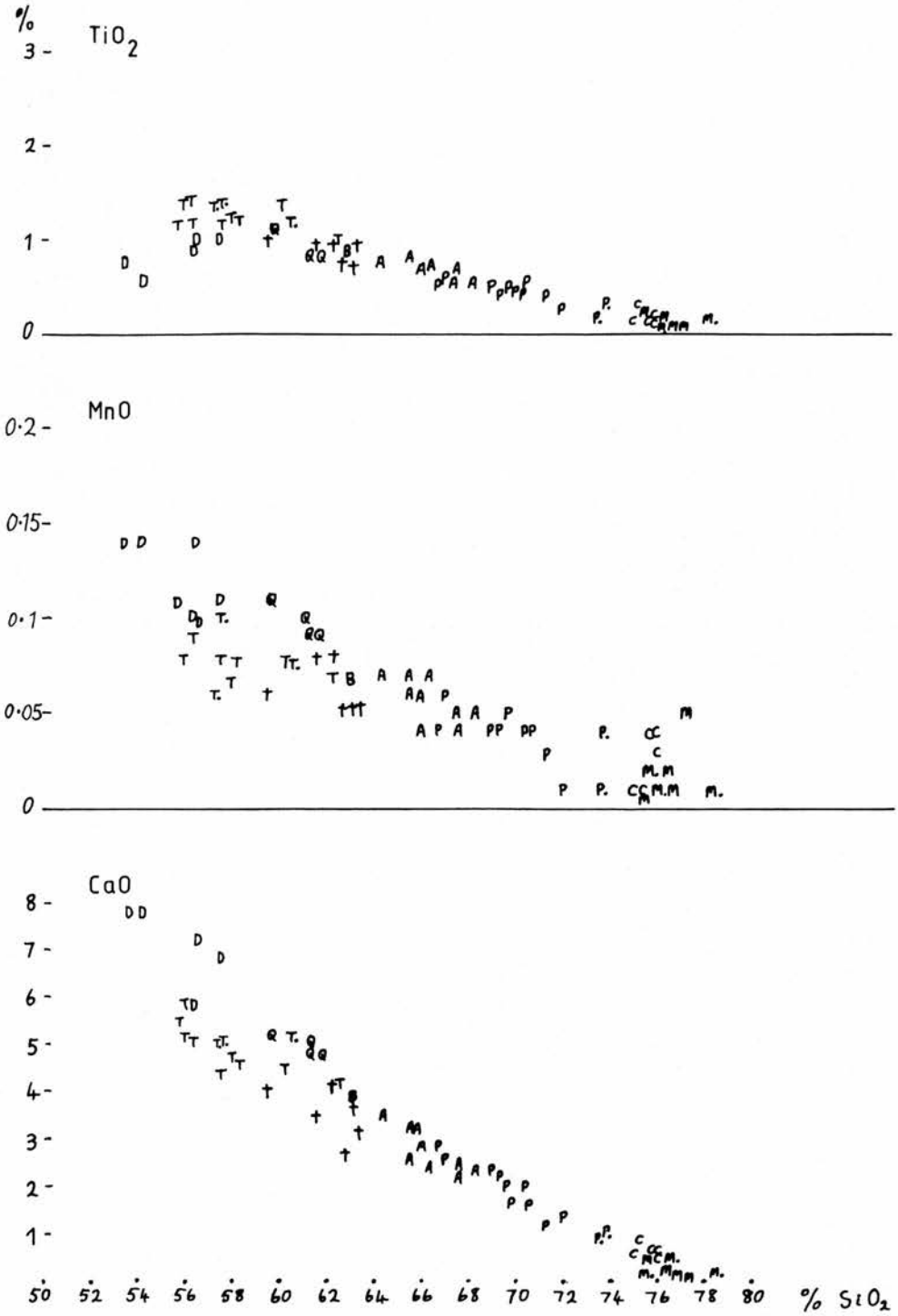
%
TiO2
3
2
1
0
MnO
0·2
0·15
0·1
0·05
0
CaO
8
7
6
5
4
3
2
1
50 52 54 56 58 60 62 64 66 68 70 72 74 76 78 80
% SiO2

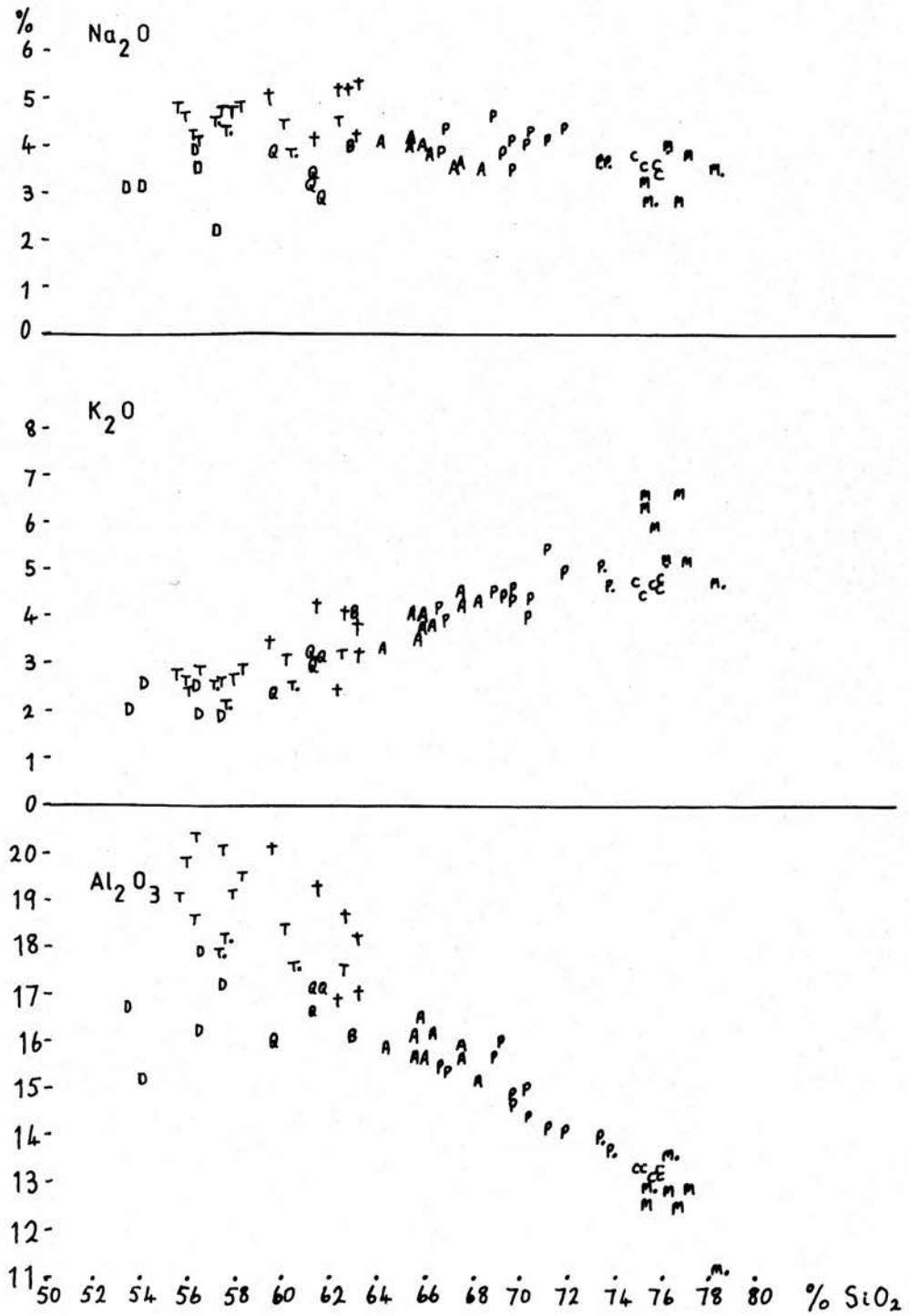
%
Na2O
6
5
4
3
2
1
0
K2O
8
7
6
5
4
3
2
1
0
Al2O3
20
19
18
17
16
15
14
13
12
11
50 52 54 56 58 60 62 64 66 68 70 72 74 76 78 80 % SiO2

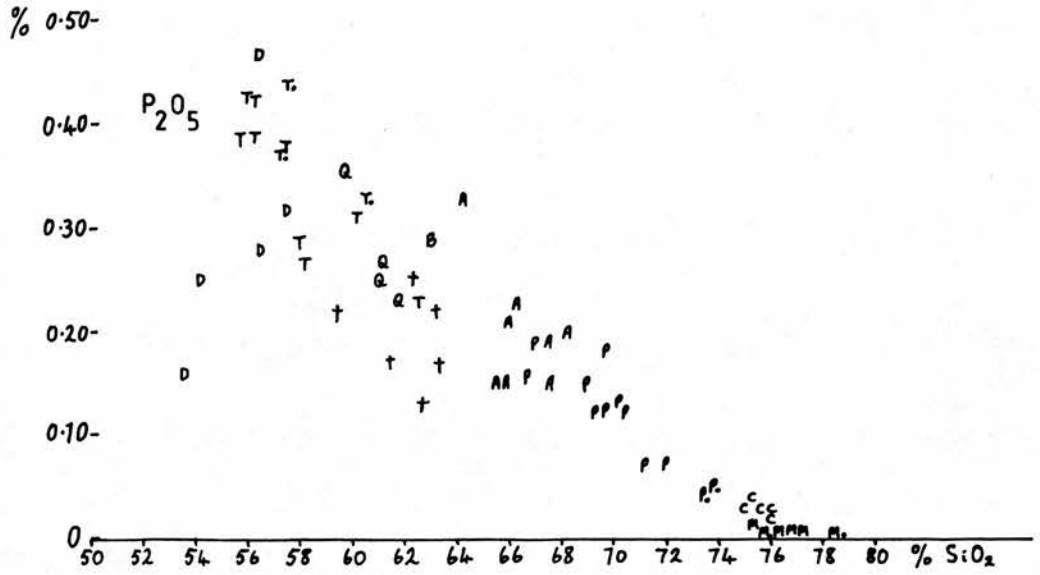
% 0·50-
P_2O_5
0·40-
0·30-
0·20-
0·10-
0
50 52 54 56 58 60 62 64 66 68 70 72 74 76 78 80 % SiO_2

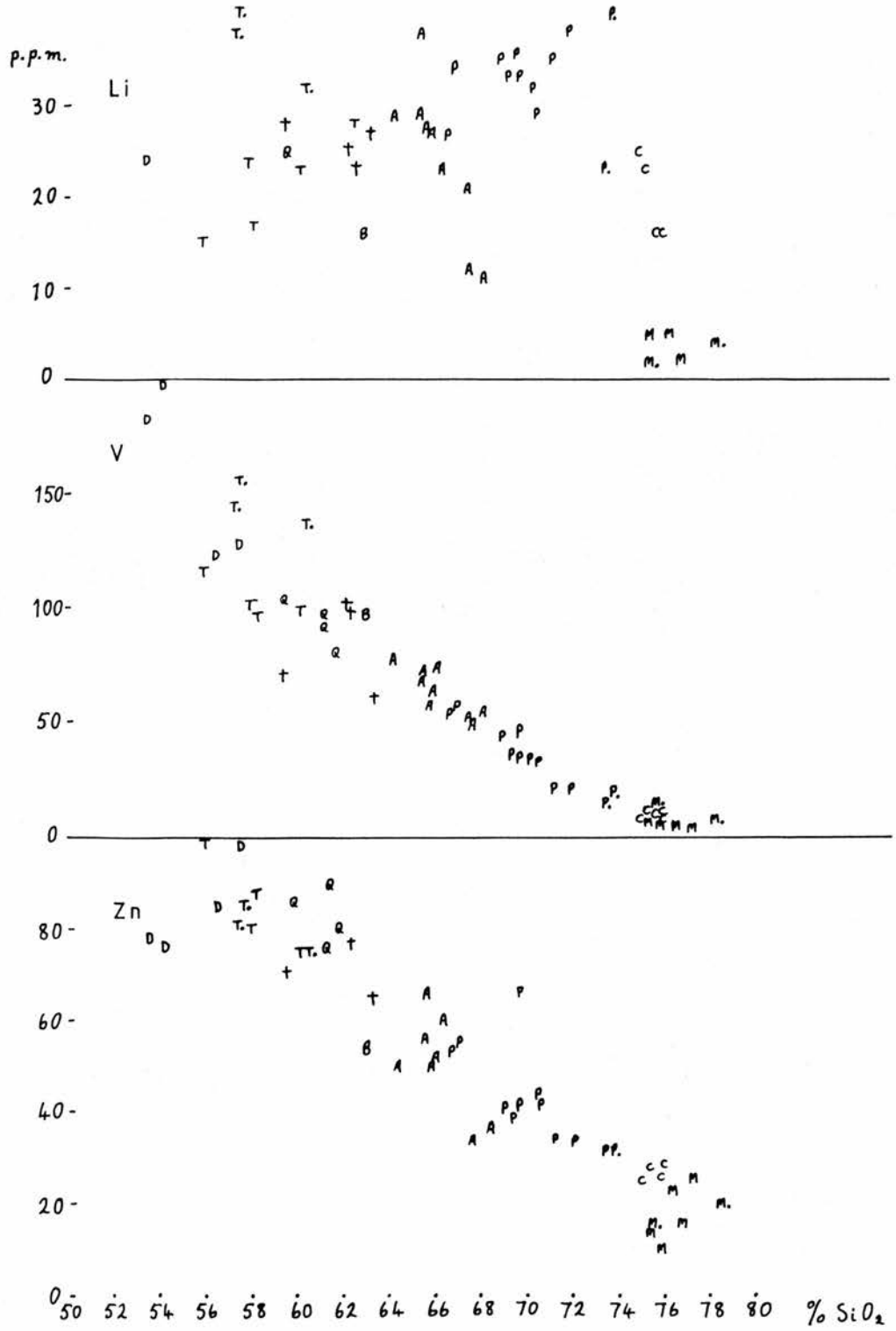
p.p.m.
Li
30
20
10
0
V
150
100
50
0
Zn
80
60
40
20
0
50 52 54 56 58 60 62 64 66 68 70 72 74 76 78 80
% SiO2

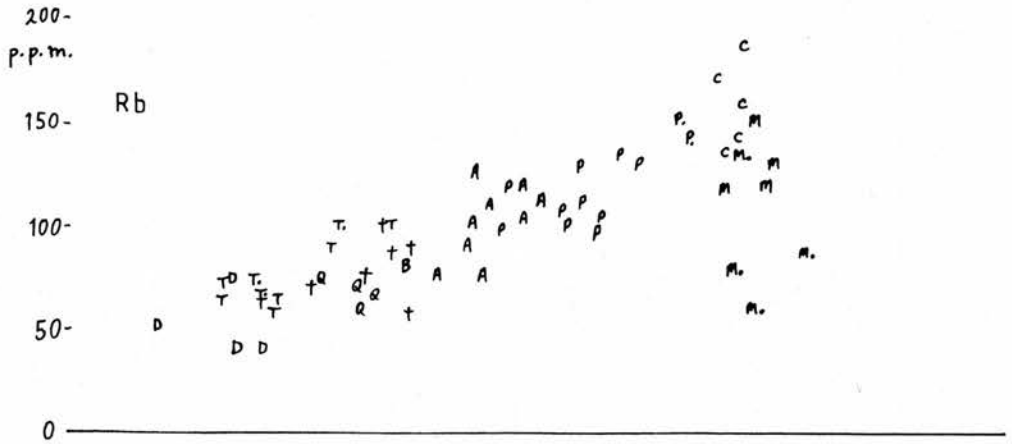
200-
p.p.m.
Rb
150-
100-
50-
0

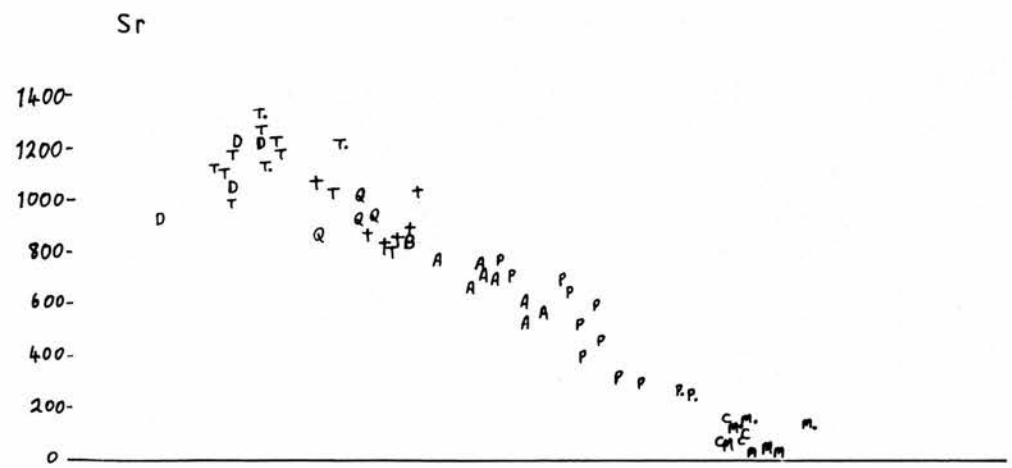
Sr
1400-
1200-
1000-
800-
600-
400-
200-
0

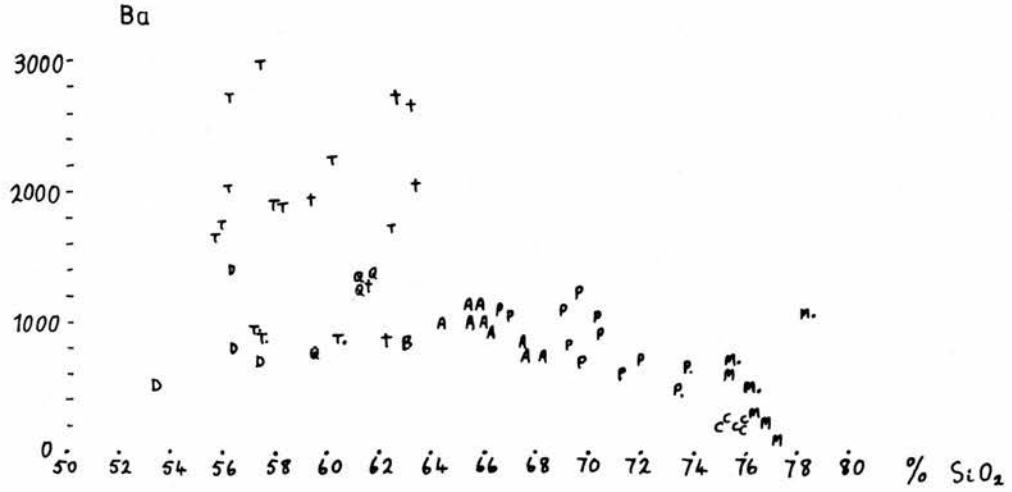
Ba
3000-
2000-
1000-
0
50 52 54 56 58 60 62 64 66 68 70 72 74 76 78 80 % SiO2

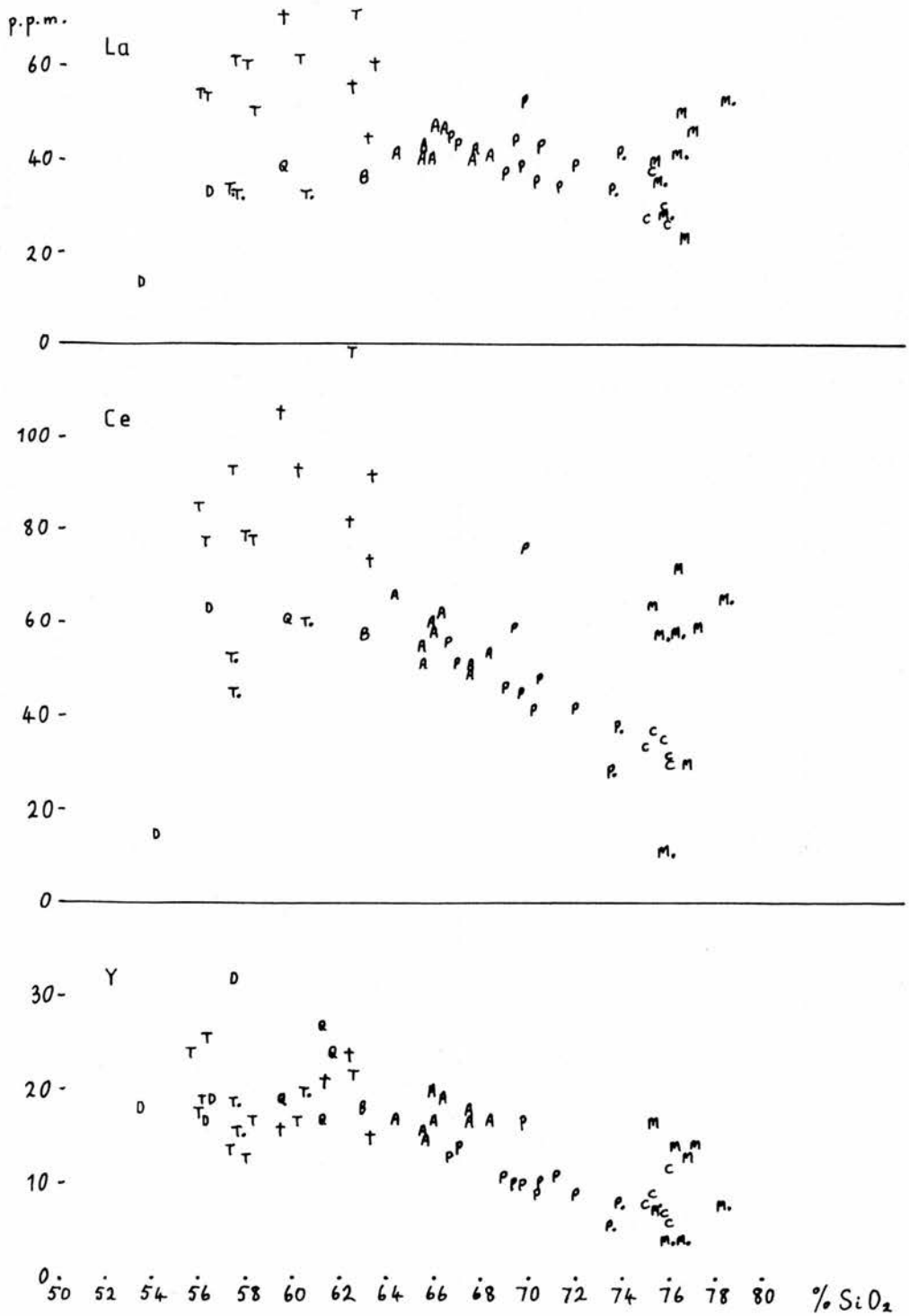
p.p.m.
La
60
40
20
0
Ce
100
80
60
40
20
0
Y
30
20
10
0
50 52 54 56 58 60 62 64 66 68 70 72 74 76 78 80
% SiO2

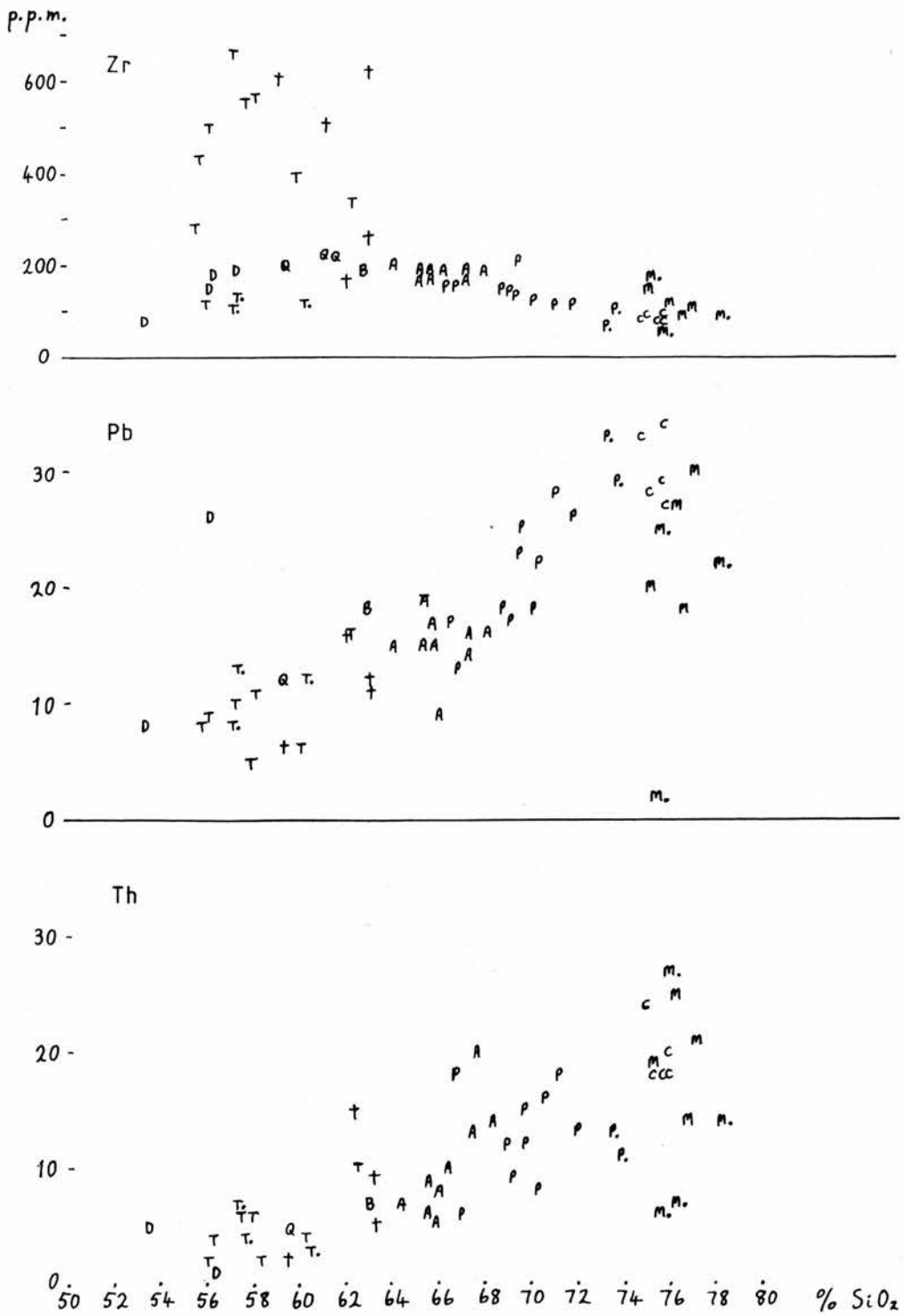
p.p.m.
Zr
600
400
200
0
Pb
30
20
10
0
Th
30
20
10
0
50 52 54 56 58 60 62 64 66 68 70 72 74 76 78 80
% SiO2

$CaO - Al_2O_3$

Mineral vectors portraying melt compositions during fractional crystallisation show good separation and makes this diagram useful in determining the major controls in any fractionation sequence. The sense of the hornblende vector is less certain due to the wide range of possible compositions.

Clinopyroxene ± orthopyroxene ± hornblende are likely to control the D trend, while a combination of clinopyroxene + calcic plagioclase feldspar controls D to T. to Q. The T. to T field vector could be explained by sphene fractionation. While both rock types contain sphene (T=1.4%, T.=2.3%) this situation would require the removal of nearly 50% sphene. Alternatively removal of aluminous hornblende could produce the variable (T) compositions. A third possibility is that T compositions are not related to T..

The trends T. or Q to A, and within P can be attributed to removal of plagioclase and hornblende ± clinopyroxene in a ratio approximately 1:2.

The trends within A and P are ambiguous, though hornblende and plagioclase probably dominated these compositions. Within the A group modal hornblende varies from 9.5% to 3%, with a corresponding decrease in plagioclase from 46% to 30%. However

sphene increases from 0.2% to 0.5% and this cannot be considered in the variations found in CaO.

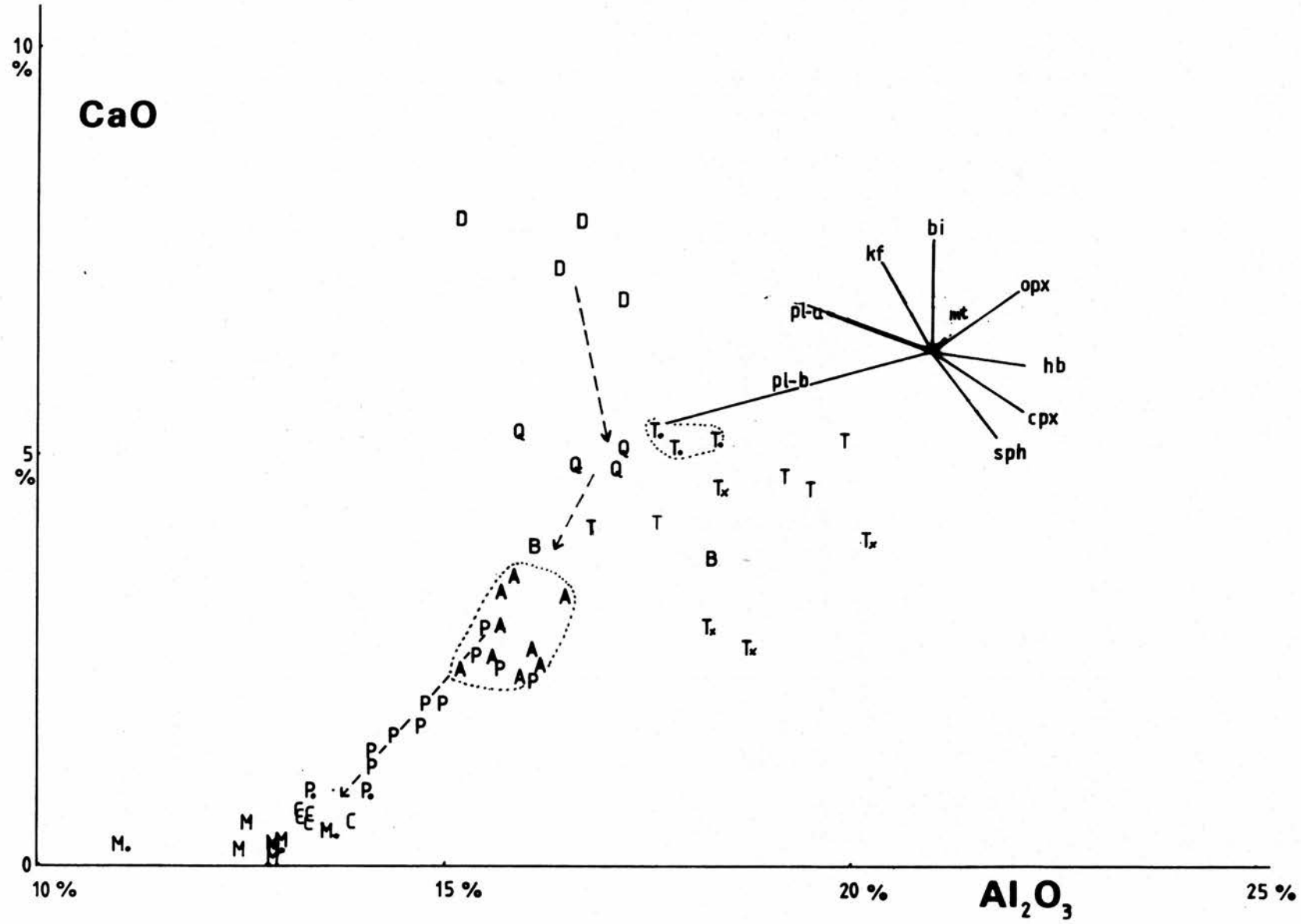
CaO
10 %
5 %
0
10 %
15 %
20 %
25 %
Al_2O_3
bi
kf
opx
pl-a
mt
hb
pl-b
cpx
sph

CaO - MgO

With a good spatial spread of the calculated fractionation vectors, this diagram is potentially useful in identifying petrogenetic mechanisms, particularly for the more mafic compositions.

The overall trend reflects depletion in both elements as the magmas evolved to more silicic compositions.

The trend within D appears to be related to the fractionation of hornblende ± clinopyroxene ± orthopyroxene, which then leads to the Q to A trend by predominantly clinopyroxene removal, though some calcic plagioclase could also be involved. Contrary to prevous opinion that all the Cruachan rocks were part of one differentiated pluton (Anderson 1937; Bailey & Maufe 1960; Brown 1975; Kynaston & Hill 1908) the evidence here suggests that T. (dark CMD) and their related T(CMD) are not consanguinous with A(CMG) rocks, but are an offshoot from Q compositions.

Assuming the Q samples represent compositions at the end of a clinopyroxene fractionation trend from D, then T. reflects the result of predominantly hornblende ± biotite removal from Q (orthopyroxene is not found in Q), whereas A reflects mainly clinopyroxene removal from Q.

The linear association of Tx (marginal silicic southern Cruachan) may indicate a genetic link with A compositions. Geographically they could represent an outer ring fault intrusion.

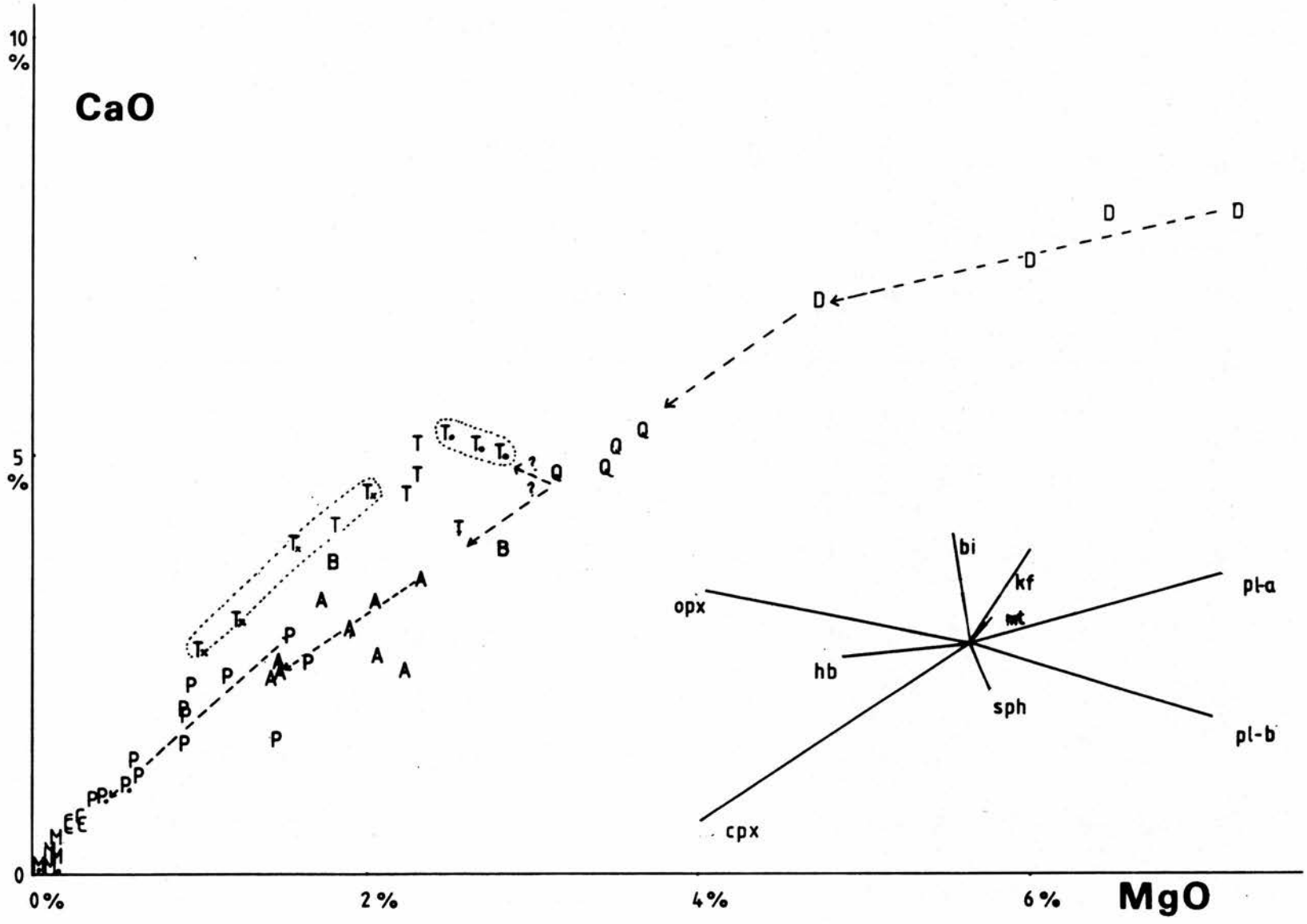
10 %
CaO
5 %
0
0 %
2 %
4 %
6 %
MgO
D
Q
T
B
A
P
E
bi
kf
mt
pl-a
opx
hb
sph
pl-b
cpx

log MgO - log K_2O

This diagram is based on work by Masuda etal.(1979) who plotted a compatible element (Kd>1) against an incompatible one (Kd<<0.1). In this version, an early mineral-forming element (Mg) is plotted against a late mineral-forming element (K). If fractional crystallisation involving common mafic minerals dominates the magmatic process then the trend is a sub-vertical straight line. Successive partial melts from eclogite or ocean basalt produce sub-horizontal trends (Gill 1981) since potassium is enriched in early melts relative to magnesium.

The general trend for the Etive suite suggests that the parental magma for each of the granitoid intrusions was generated by fractionation of clinopyroxene $\pm$ olivine $\pm$ orthopyroxene from a mafic parent. Plagioclase may also be involved as its effect would be to attenuate the mafic vector without changing its sense of direction. Little can be said about trends within individual groups.

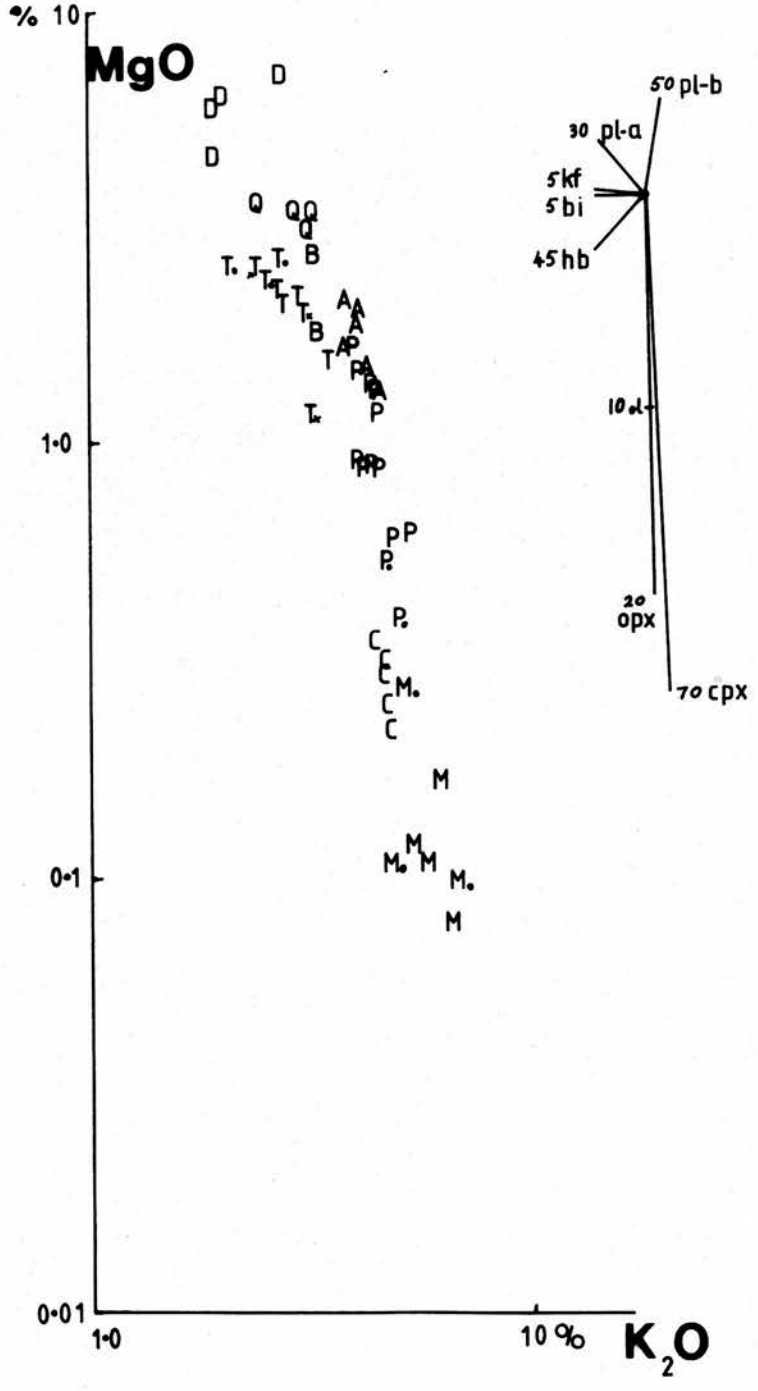
% 10
MgO
1·0
0·1
0·01
1·0
10 %
K2O
50 pl-b
30 pl-a
5 kf
5 bi
45 hb
10 ol
20 opx
70 cpx

Alkalis - Iron - Magnesium (AFM)

The general trend displayed by the Etive rocks follows the traditional 'calc-alkaline' trend as defined by Nockolds & Allen (1953). Petrographically the Etive suite consist of monzodiorites and monzogranites (Streckeisen 1976)(see Section 3.7) and as such deserve the term high-K calc alkaline (Peccerillo & Taylor 1976) or calc alkaline potassic (Lameyre & Bowden 1982). A plot of CaO and (Na_2O + K_2O) against SiO_2 produces convergence at 55% SiO_2, justifying the term alkali-calcic (Peacock 1931).

Notably, T compositions lie off the main trend, reflecting a higher relative abundance of alkalis and iron. This shift may be due to derivation from a different parental magma, pyroxene fractionation or an alteration effect.

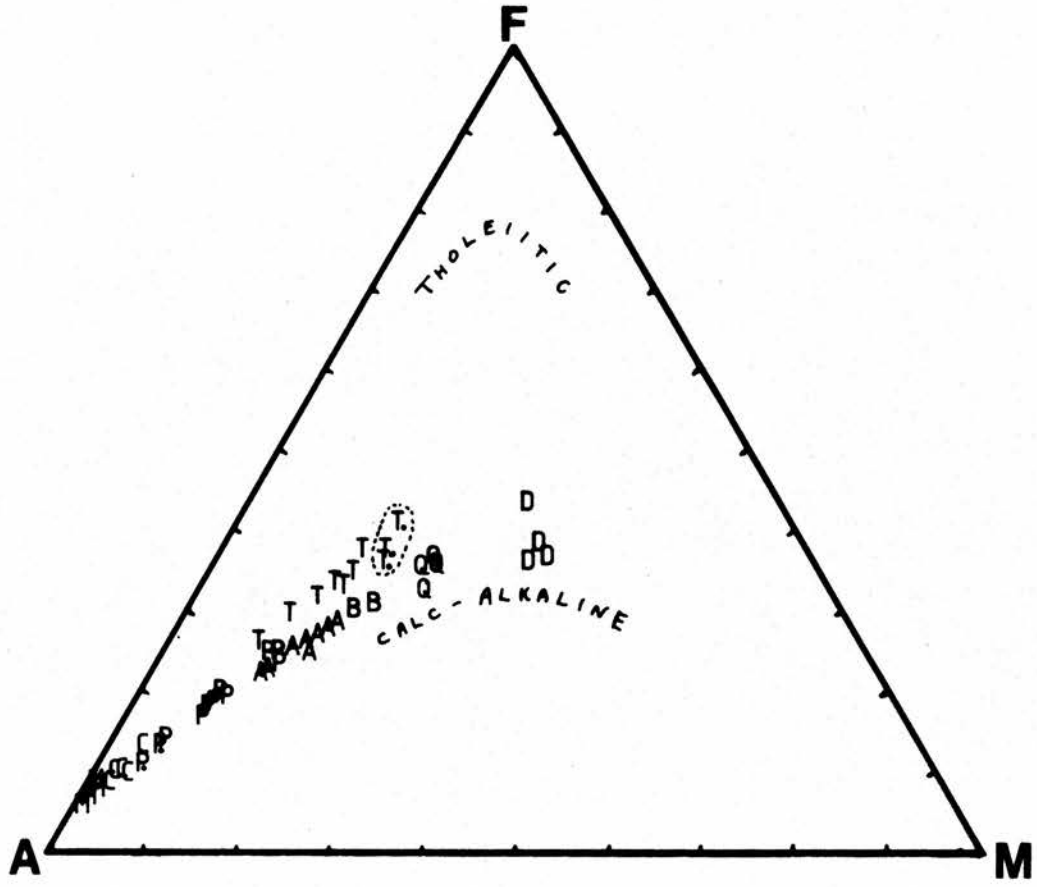
F
THOLEIITIC
CALC - ALKALINE
A
M

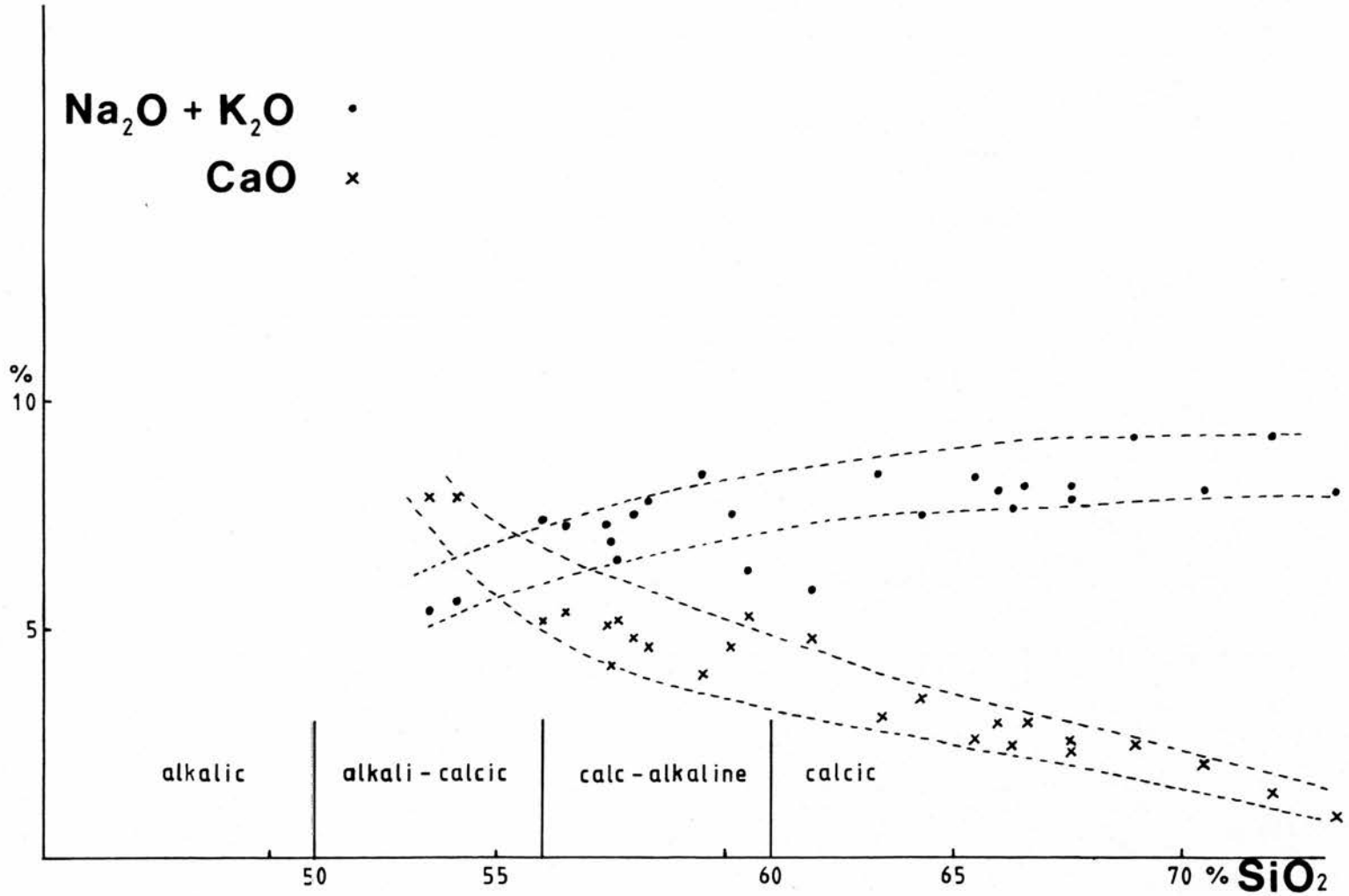
Na2O + K2O •
CaO ×
%
10
5
alkalic
alkali - calcic
calc - alkaline
calcic
50
55
60
65
70 % SiO2

R1 - R2 'de la Roche' Diagram

This diagram was developed by de la Roche and his co-workers (1980) to display and classify igneous rocks. It is based on a form of factor analysis which expresses each apex of the Yoder and Tilley (1964) tetrahedron in terms of each major element. An expression is derived to define the plane of silica saturation which is then expressed in terms of two orthogonal vectors, R1 and R2. The apportioning of cations to each vector was arbitrary and was based on empirical tests to find which combination gave the best discrimination for any given set of plutonic rock data. The elements are expressed as millications/100g rock.

$$R1 = 4Si - 11(Na + K) - 2(Fe + Ti)$$

$$R2 = 6Ca + 2Mg + Al$$

In addition, mineral compositions can be represented on the diagram and natural trends related to them. Fractional crystallisation vectors are included which show the change in liquid composition starting from a high-alumina basalt. Orientation of the vectors will vary in different parts of the diagram depending on the position of the mineral poles. Also superimposed on the diagram are compositions for amphibolite (am), charnockite (ck) and granite gneiss (gg) taken from Mason (1978). 'zpm' represents 'zone of partial melting' - the

feldspar ternary minimum (Tuttle and Bowen 1958) where the first melts from a quartzo-feldspathic source would be expected to occur. The gradual decrease in angular orientation of the granitoid trends relative to the R1 axis during magma evolution is a feature of this diagram. It reflects an increase in silica and alkalis.

A good spatial separation is achieved for most Etive rocks, in particular between A, P and C trends. D and Q are well separated and could be related by clinopyroxene ± plagioclase fractionation. The complexity within the T./T field could be a function of variability in modal alkali feldspar, (T.=7%; T=18%). If T. represents the parental, or earlier, rock type in this group, then the scatter in T compositions is difficult to explain in terms of fractional crystallisation. A combination of orthopyroxene and clinopyroxene fractionation could drive T. to T but neither of these minerals is found in T. rocks. The alternative is that they were separate magmas.

The proximity of T. to Q suggests the possibility of a genetic link and they could share a common, more mafic source which may have fractionated at depth to generate two types.

Within the P group three sub-parallel trends can be identified which relate to definite geographic zones. The uppermost trend represents an outer, presumably earlier, zone (Cadderlie zone), the middle one is an intermediate zone (Glenkinglass zone) and the lowest trend represents an inner zone

(Barrs) adjacent to, but separate from the CSMG (C) intrusion. This evidence strongly suggests that the PSMG was intruded as three pulses, each one intruding with a more mafic composition than the previous one had evolved to. This three-fold zonation is also highlighted in the Ce/Y - SiO_2 diagram.

If, as suggested by Clayburn et al. (1983) some rocks in Etive could have been produced by mixing 'enriched' mantle with juvenile crust, then from this diagram T., Q, A or P starting compositions, or the Q - A trend, could be derived by mixing only if the crustal component had a bulk composition approximating to an alkali granite. It is further suggested that the heterogenous T and Tx compositions could be the products of mixing Q (or T.) with a source which lies somewhere in the syenite field.

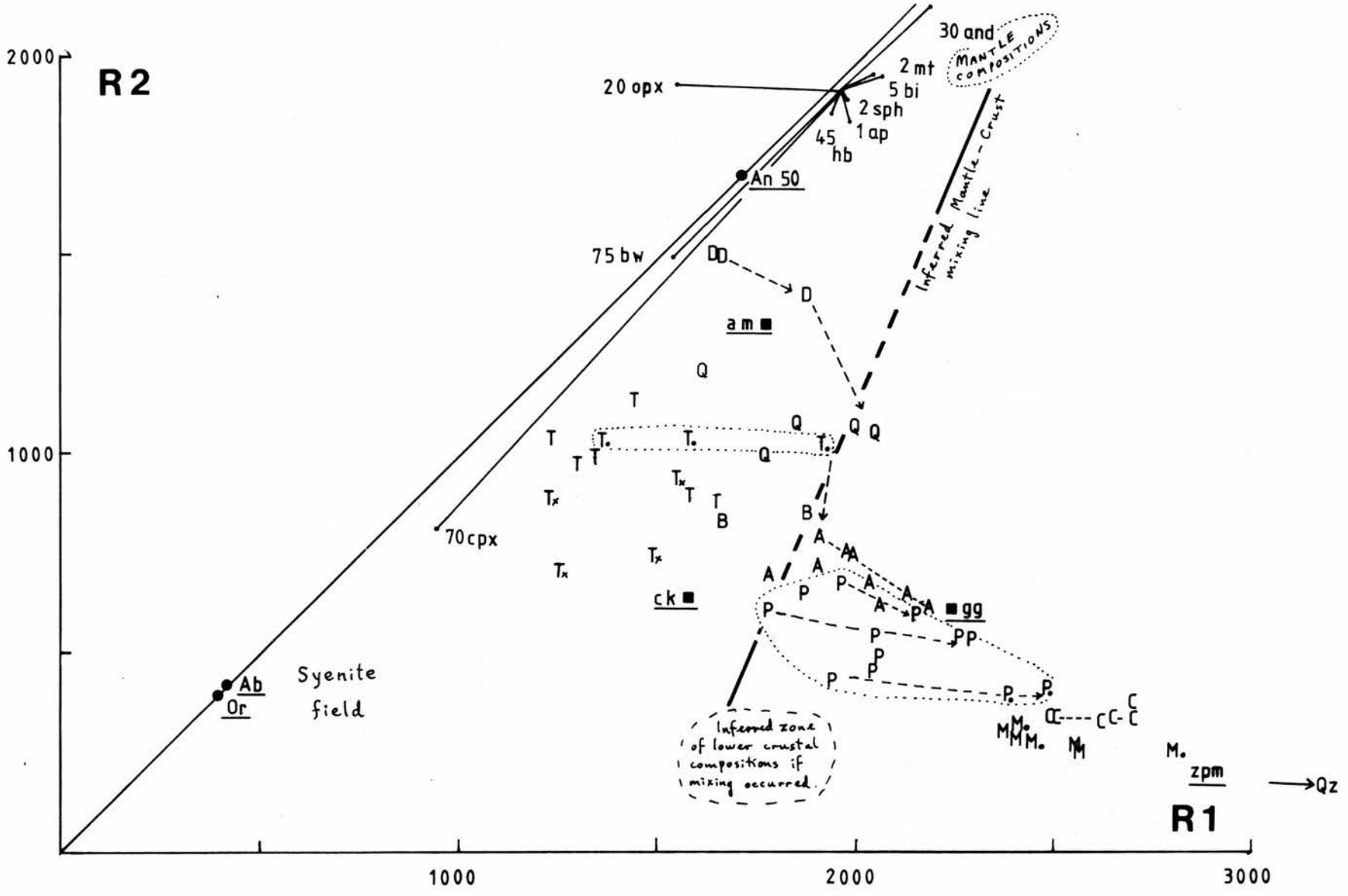
R2
2000
1000
1000
2000
3000
20 opx
2 mt
5 bi
2 sph
1 ap
45 hb
30 and MANTLE COMPOSITIONS
An 50
Inferred Mantle-Crust mixing line
75 bw
70 cpx
am
ck
gg
Ab
Or
Syenite field
Inferred zone of lower crustal compositions if mixing occurred
zpm
R1
Qz

MgO - Rb

This diagram belongs to the type used by Treuil and Varet (1973) and Masuda and Aoki (1979) whereby an incompatible trace element (one with low crystal to melt distribution coefficient, <<0.1 eg Rb) is plotted against a compatible trace element. In this case MgO is used instead since it, too, is depleted from a mafic melt by early-crystallising mafic phases. A linear-linear plot commonly yields a hyperbolic curve (as defined by the Rayleigh fractionation equation: $Cl/Co=F^{(D-1)}$) (see Cox et al. 1979) if two trace elements are used, when crystal fractionation is the operative mechanism. The use of MgO will cause the graph to deviate from true hyperbolic status. Mixing of two magmas will give rise to a straight line.

The overall trend would suggest that fractionation has occurred in the Etive parental magma.

It is possible to separate the two Meall Odhar types (M. from M) and to reinforce their respective chemical affinities with respect to Rb, namely M. with the T group, and M with Starav (P and C). It is also clear that the C field overlaps the end of the P group and therefore cannot be considered as a continuation of it.

If all the Etive rocks originated from one source then the overall trend can be attributed to fractionation of clinopyroxene ± hornblende ± orthopyroxene from an inferred parental magma. The exception to this trend are MOG samples which lie off this trend and show distinct MgO depletion.

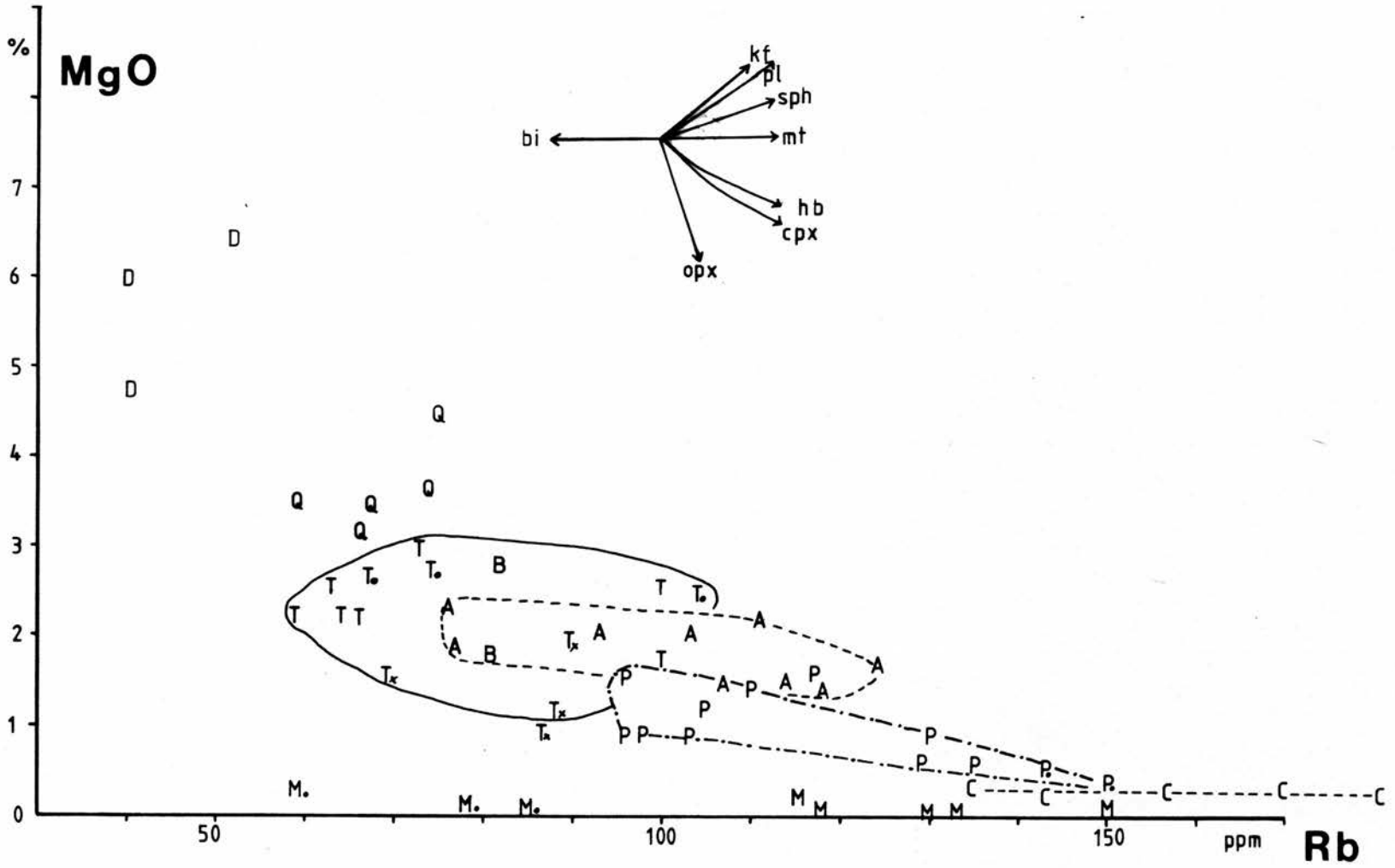
%
MgO
kf
pl
sph
bi
mt
hb
cpx
opx
0
1
2
3
4
5
6
7
50
100
150
ppm
Rb

Rb - K_2O

Rubidium is only appreciably removed from a melt by biotite (Kd 2-3). In general, it behaves as an incompatible element (Kd<<0.01) which concentrates in residual melts. This gradual increase is highlighted in this diagram which tends to confirm that fractional crystallisation was the overall mechanism in the generation of the Etive rocks, both within intrusions and in the parental magmas.

A reasonable separation is achieved between M and M.. The former lies close to the Starav compositions (P and C) with respect to their Rb content.

There is scatter in Rb within T. and T compositions which may be related to late hydrothermal activity, perhaps related to the intrusion of the CMG and related Fualt Intrusion or perhaps to separate origins. The C trend starts at Rb values which are lower than those of the most evolved P. samples. This feature confirms field evidence of contact phenomena (RB137) that P and C represent two separate pulses of magma.

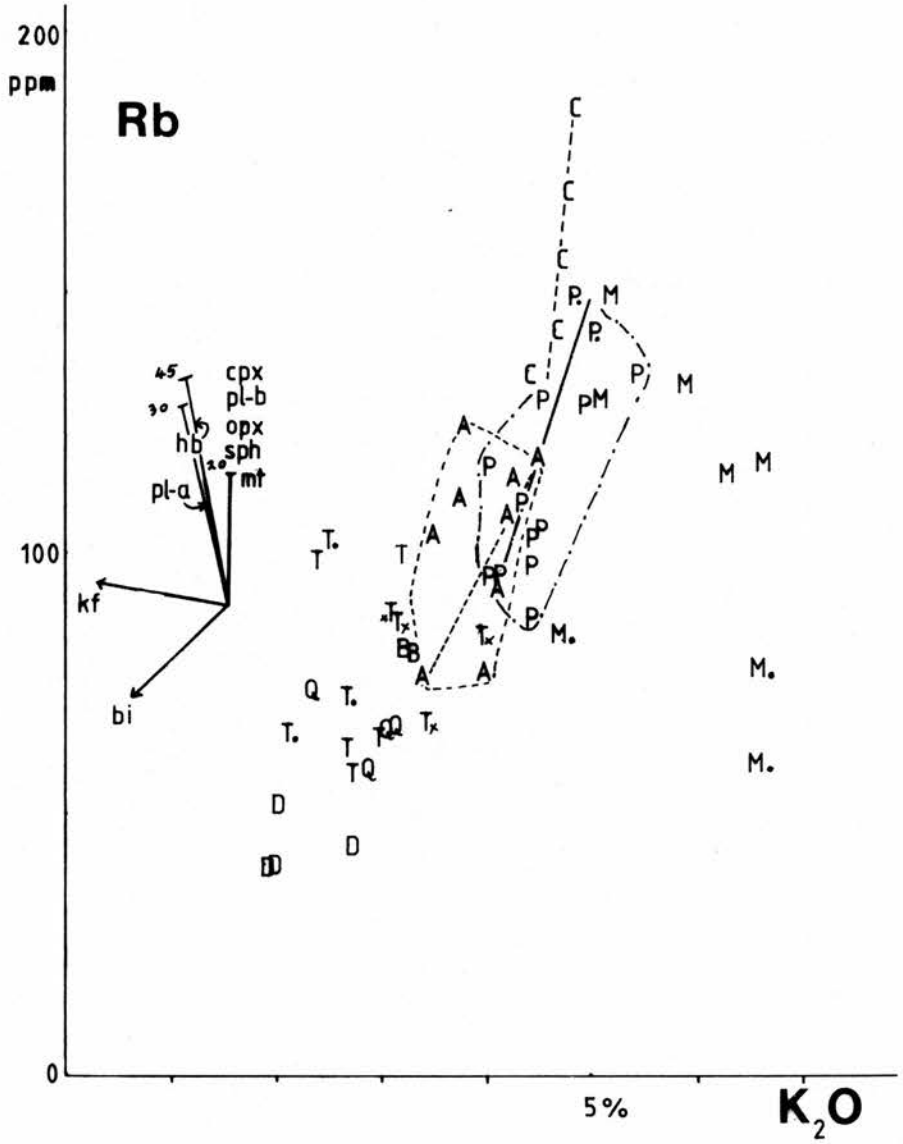
200
ppm
Rb
100
0
cpx
pl-b
opx
sph
mt
hb
pl-a
kf
bi
45
30
20
5%
K2O

Ba - K_2O

Barium is concentrated in early-formed potassium minerals (Taylor 1965) (Kd:Ba/biotite=10, Kd:Ba/alkali feldspar=6, from Cox et al. 1979). It will therefore concentrate in the melt during early stages of fractionation when mafic minerals and calcic plagioclase dominate the process, but will be depleted from the melt once biotite and alkali feldspar crystallise. This general pattern is seen here. Ba is enriched from D through T. to Q, and then is depleted in A, P and C.

This diagram shows well the separation of T from T., the latter lying on the main trend. It suggests that T. represents a primary magma and T is an altered version of it. The data indicate an enhancement in Ba and to a lesser extent, in potassium. This difference cannot be due to extreme fractionation of mafic minerals (60-80% clinopyroxene) from T. since this proportion cannot be extracted from the components present in T. or Q. Also evidence from Harker diagrams suggest that fractionation is not a feasible mechanism since silica values do not change appreciably between Q, T and T. an effect which would be expected if augite or hornblende were removed from Q compositions.

From discussion on the log Sr - log Ba diagram, it is assumed that Kd:Ba/alkali feldspar is >6, as recommended by Cox et al (1979) and therefore the 'kf' vector will steepen. (It should be noted that the negative slope on the 'plag-a' vector is caused by a high K_2O content in the original analysis. Potassium-poor plagioclase would generate a vector with slope close to +1).

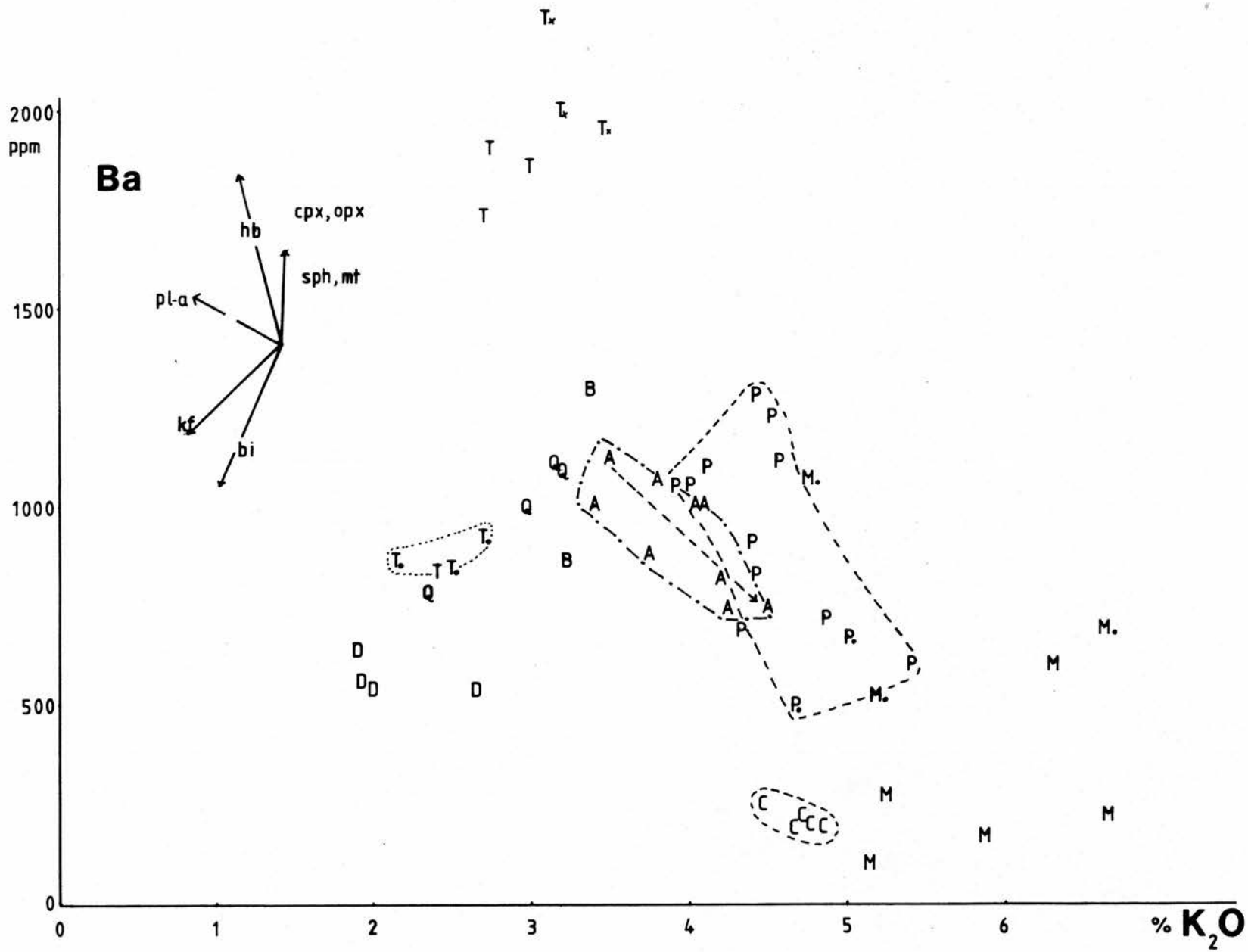
Ba
ppm
2000
1500
1000
500
0
hb
cpx, opx
sph, mt
pl-a
kf
bi
0
1
2
3
4
5
6
% K2O

Element ratios - Geographical distribution

This plot was used to gain an idea of the spatial distribution of sample compositions. The sample points are grouped according to rock type. Within one division the points are arranged in approximately sequential order of increasing distance normal to the outer margin in towards the centre. A few points lie off an imaginary traverse as they are difficult to place in exact juxtaposition. For the A(CMG), P(PSMG) and C(CSMG) groups, chemistry generally changes progressively across the intrusion.

Rb/Sr ratio

The combined (2 std. dev.) error for an average ratio of 0.1 is $\pm$0.003. At Rb/Sr=1.6 the error is $\pm$0.15. Such small combined errors allow interpretations of chemical trends to be made with confidence.

Little change is seen in D,Q,B,T and T.. This suggests that neither plagioclase (Kd Sr:2-4) nor biotite (Kd Rb:2-3) singly played a significant role in the formation of these rocks, though together, these minerals would maintain a constant Rb/Sr ratio. An increase in the ratio, consistent with Sr depletion and concomitant Rb increase is seen in the CMG(A) intrusion. This effect is pronounced within the PSMG, indicating a high degree of

plagioclase fractionation. Some biotite fractionation would attenuate the rate of increase in the ratio.

The rate of increase in this ratio is even higher for the CSMG. There is uncertainty whether sample RB093 which occurs within the inferred CSMG boundary represents a mafic variant of CSMG or is a part of PSMG. Central Starav magma has fractionated to a high degree relative to the dioritic compositions, and its normative composition of felsic minerals places it close to the ternary minimum at 1kb in the feldspar system of Tuttle & Bowen (1958).(See page 4-77)

The bimodal distribution of MOG types is highlighted here. Sample A108 represents the typical MOG type as defined by Bailey & Maufe (1916) and is one of a group enriched in Rb. It is described in this work as "evolved". The low Rb group is called "primitive".

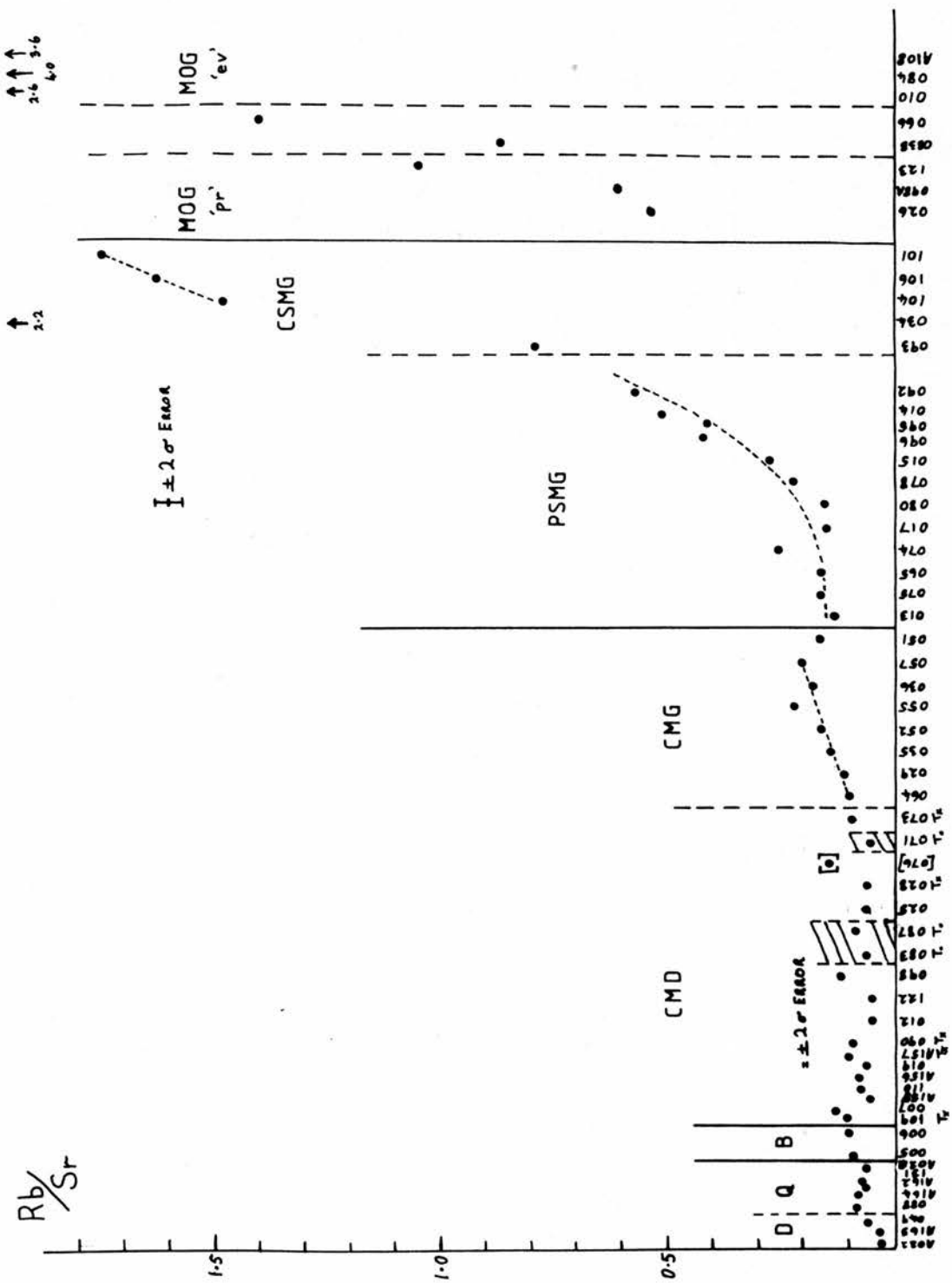
Rb/Sr
1·5
1·0
0·5
D
Q
B
CMD
CMG
PSMG
CSMG
MOG 'pr'
MOG 'ev'
± 2 σ Error
± 2 σ Error
2·2
2·6
3·6
4·0

Ba/Rb ratio

The compounded error (2 std. dev.) is ±0.3 at a ratio of 10. As Ba is removed by early crystallising potassium minerals (eg biotite) and Rb is concentrated in residual melts (Taylor 1965) the ratio will decrease with fractionation in a silica saturated system. This trend is exhibited by both the CMG and PSMG. It is less obvious in the other groups.

The difference between CMD(T) and dark CMD(T.) is highlighted here. The ratio for CMG(A) and PSMG(P) show a downward trend in both cases, indicating that fractional crystallisation (of biotite and feldspar) was the operative mechanism. The PSMG intrusion is later than the Cruachan types and the change in chemistry is shown as a new trend.

There may be a genetic link between T. and the mafic CMG(A) though no field evidence was found to confirm this connection. Samples RB076, RB107v, RB109 and JFB157 all occur on the outer margin of the southern lobe of the Cruachan intrusion, but their chemical and petrographic characteristics place them with the CMG. There is little change within the CMSG intrusion suggesting it underwent little or no fractionation of biotite or feldspar during cooling.

The MOG types are well separated into two fields. RB066 cannot be assigned to either group (it occurs close to the Cruachan-Starav contact) and RB083B relates to the low ratio group but in other respects shows anomalous behaviour.

Ba/Rb
30
20
10
0
47.4
CMD
CMG
PSMG
CSMG
MOG
'pr'
MOG
'ev'
ERROR
± 2σ
D
Q
B

V - Ti/1000

This diagram is based on work by Shervais (1982) and is particularly sensitive to variations in fO_2 which influence the behaviour of opaque oxide minerals, specifically ilmenite and magnetite.

At low fO_2 (-13) V exists as the V^{3+} ion and behaves like Fe^{3+} and Cr^{3+}. It has a high Kd for magnetite (23-190) and clinopyroxene (5). The size of the magnetite vector indicates the large effect on V concentrations after removal of approximately 1% magnetite from a basaltic melt.

At high fO_2 (-6 to -4) it exists as V^{4+} or V^{5+} and behaves as an incompatible element (Kd<0.1).

At low fO_2 values the Ti/V ratio increases rapidly with fractionation of amphibole, clinopyroxene and magnetite, though this trend would be reversed if ilmenite crystallises. At high fO_2 V is enriched into the melt and the Ti/V ratio falls (Shervais 1982) enhanced by the crystallisation of sphene. For most Etive rocks the ratio rises slowly from 50 to over 200 and would indicate an intermediate fO_2 regime (between -6 and -13)

The vectors shown on the diagram were calculated for low fO_2 conditions. This diagram isolates T from T.. If these rocks are related the connection could be hornblende ± biotite ± magnetite fractionation from T. (T. contains 21% biotite, T contains 14%). However since magnetite, amphibole and clinopyroxene vectors will shift clockwise as fO_2 increases from low to intermediate levels (and V removal diminishes), this makes it less likely that fractionation of these minerals can explain the T. to T variation. The D to T. trend is difficult to explain by either vectors or fO_2 changes. Magnetite is probably partly responsible for the A and P variations since its strong influence at 1% removal will dominate over other minerals.

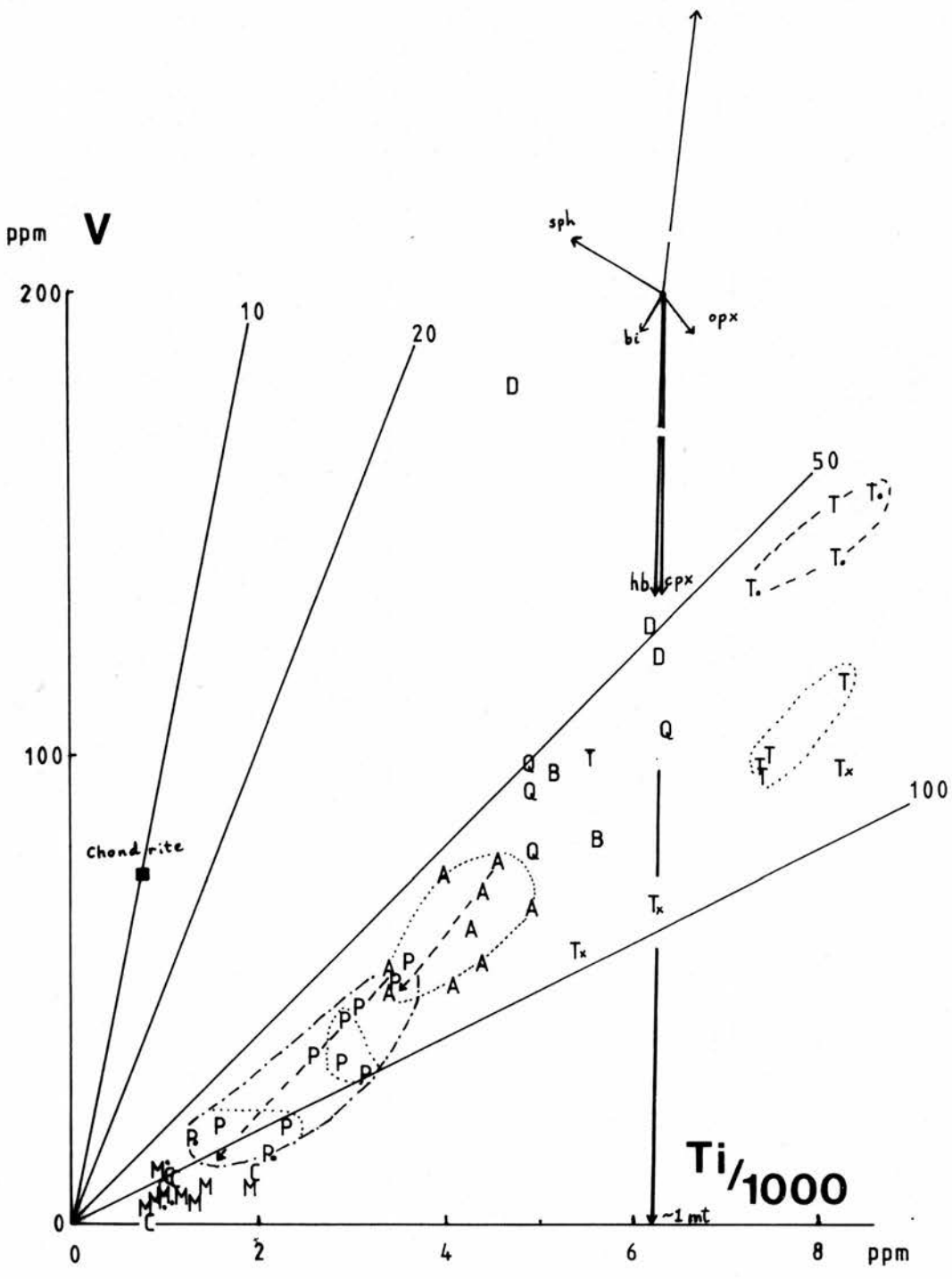
Plag-a
Kf
ppm V
200
100
0
0
2
4
6
8
ppm
10
20
50
100
sph
bi
opx
hb
cpx
Chondrite
Ti/1000
~1 mt

Rb/Sr - D.I.

Rb is removed from a melt primarily by biotite, otherwise it tends to concentrate in residual melts, whereas Sr is removed early from a melt crystallising plagioclase feldspar. Therefore the ratio will increase as fractionation in silica saturated environments proceeds. This is shown by A, P and C trends. 'A' and P trends can be explained by removal of plagioclase together with either clinopyroxene or hornblende. The rate of change in the ratio between P and C changes and may indicate an increase in the proportion of plagioclase crystallising.

Rb and Sr do not discriminate T, T. or Q. The separation between M and M. appears to be related to plagioclase with a small contribution from a mafic mineral. This is confirmed petrographically. M. are alkali granites with 67% alkali feldspar whereas M are monzogranites with roughly equal alkali feldspar, plagioclase and quartz. These two types lie noticeably off the main trend. The proximity of Tx to A is notable and may indicate consanguinity.

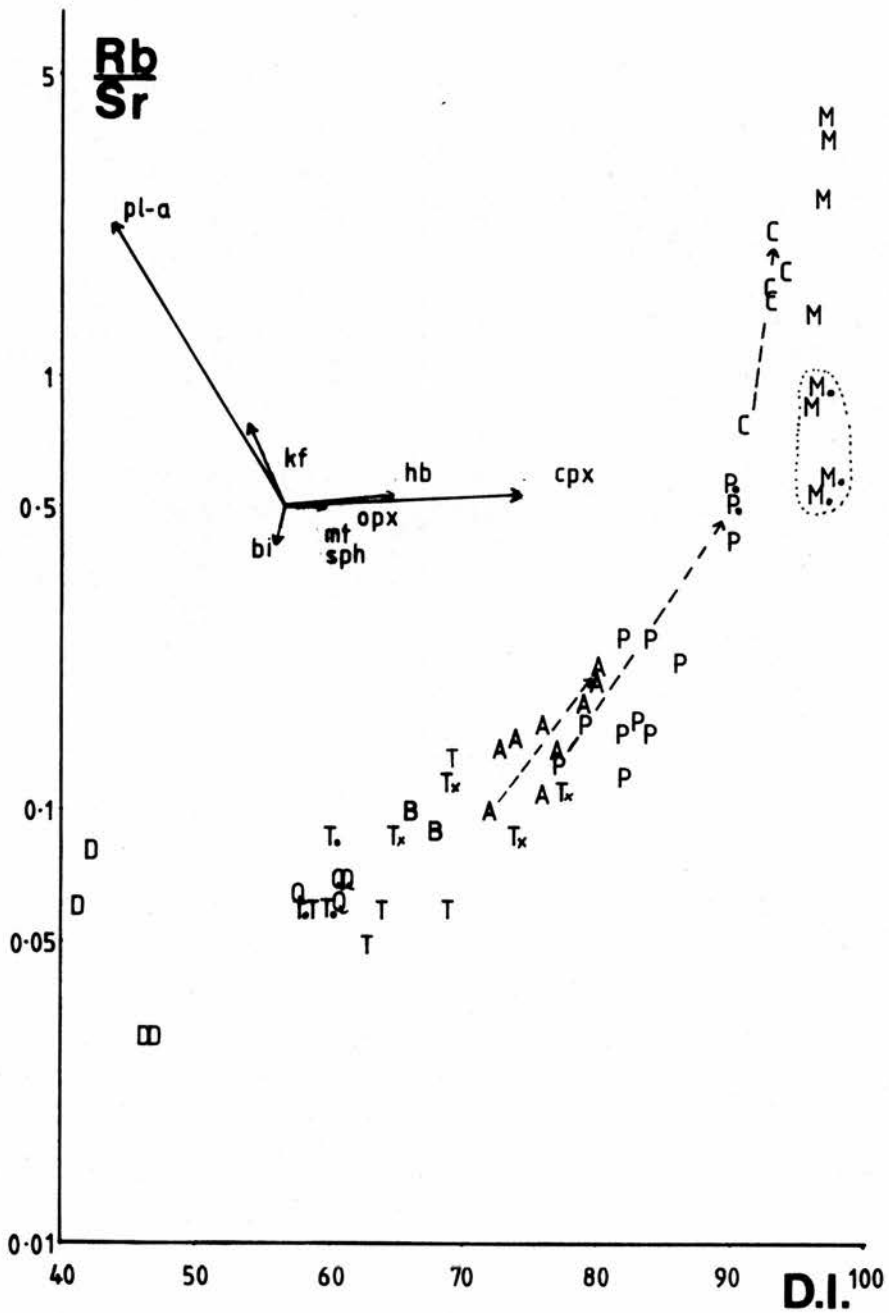
Rb/Sr
5
1
0·5
0·1
0·05
0·01
pl-a
kf
hb
cpx
opx
bi
mt
sph
40
50
60
70
80
90
100
D.I.

K/Rb - D.I.

During fractional crystallisation the ratio K/Rb falls, as Rb is progressively enriched in the melt and potassium is taken by biotite (with some Rb) and feldspar (Taylor 1965). D.I increases with fractionation as the normative felsic components (Q+Or+Ab) increase.

The wide spread in data may reflect heterogeneity in either element. The point subscripted 'm' represents a sample collected close to the margin of the intrusion, where red veining of haematised alkali feldspar is common.

The difference between T. and T compositions can be ascribed to a slight increase in potassium relative to Rb in T.

The wide range in K/Rb ratio for the M samples is difficult to explain in terms of fractionation processes (Shaw 1968) in view of their vertical array. The high ratios (450-700) for M. samples suggest a derivation by partial melting from a Rb-depleted source such as a basic meta-igneous rock or psammite (Wedepohl 1969). Another explanation is offered by Culbert (1972) who invokes degassing and eruption, with attendant alkaline metasomatism to explain high K/Rb ratios. Rubidium, it is argued, being more mobile than potassium, would be preferentially lost. The lower ratios for M (300-450) are close

to the normal igneous range (Shaw 1968).

Also highlighted is the three-fold division of the PSMG discriminated by D.I. according to geographic distribution. This feature is ascribed to multiple-pulse intrusion.

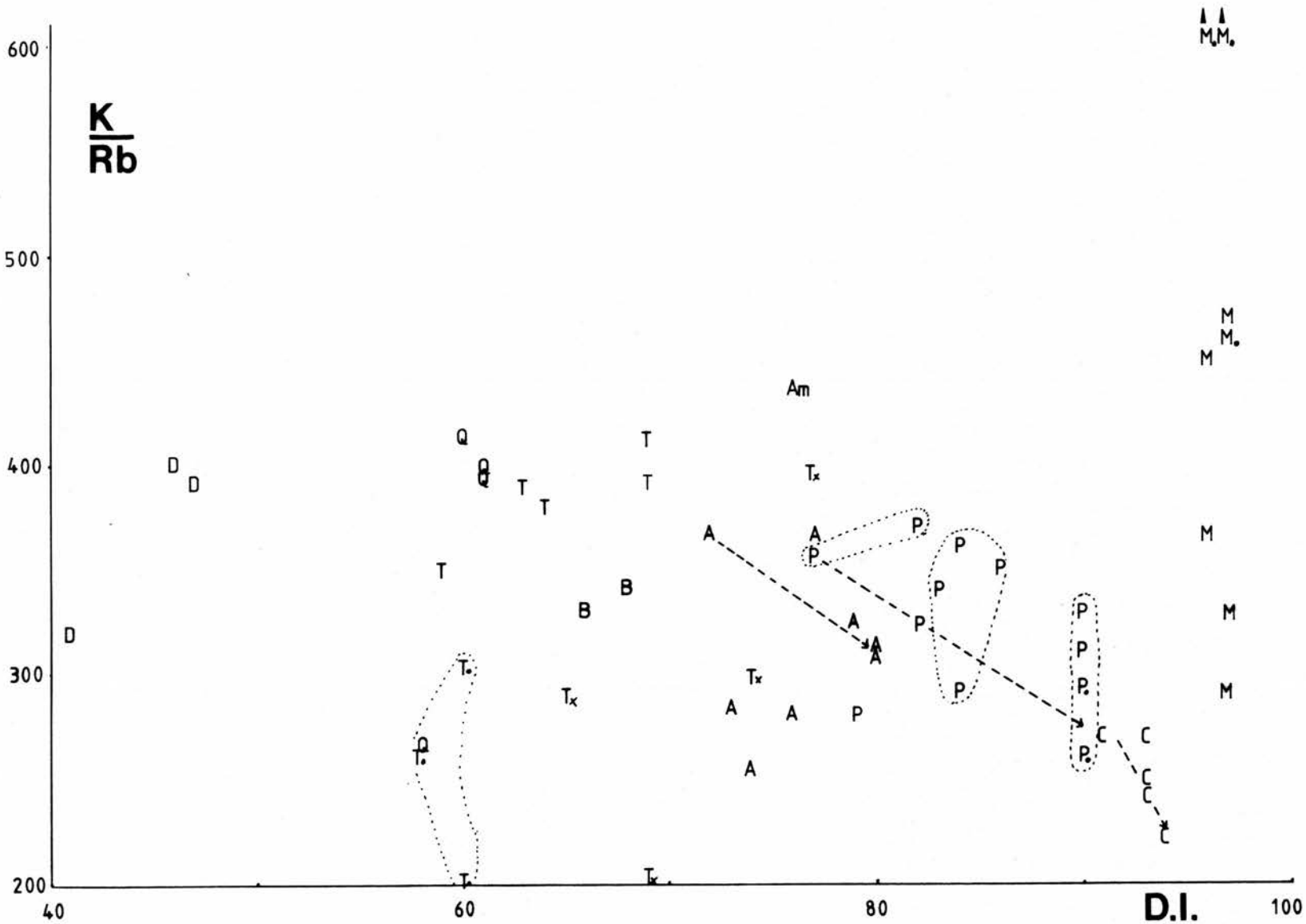
K/Rb
600
500
400
300
200
40
60
80
100
D.I.

Ba/Rb - D.I.

Barium is removed by early-formed potassium minerals while rubidium is mostly rejected into residual melts (Taylor 1965). The ratio will tend to fall during normal fractional crystallisation and the D.I. will rise. Tauson and Koslov (1973) used this ratio with some success in discriminating between granitoid types. (Ultrametamorphic granites=11.5; calc-alkalinegranites=5.3; high-K leucogranites=0.5). The actual values quoted are not comparable to those in Etive (which show consistently higher ratios - from 1 to 47). This suggests the existence of a regional barium anomaly.

Within groups A and P the general falling trend seems to suggest that fractionation is operating, involving one or more mafic minerals. The D to Q trend is independent of biotite though some may explain the D to T. trend.

The isolation of T from T. compositions could be either dueto an increase in Ba or a reduction in Rb. Information from Harker diagrams indicates that the effect can be attributed mainly to an enhancement in Ba. There is no single vector or combination of vectors which can relate T to T. by fractional crystallisation.

A good separation is achieved between M. and M samples which confirms petrographic evidence that there are two separate types. Chemically, M. is higher in Ba and lower in Rb relative to M.

The two circled sample points T. (RB071) and Tx (RB073) are geographically 0.8km apart. The change in chemistry is very rapid and may reflect a chemical boundary with respect to Ba and Rb.

Three groups within the PSMG (P) intrusion can be related to their geographic association. This three-fold division is highlighted in the Ce/Y - SiO_2 and R1-R2 'de la Roche' diagrams. Its identification here reinforces the notion that the PSMG was emplaced as at least three magma pulses, each one varying slightly in chemistry from its predecessor.

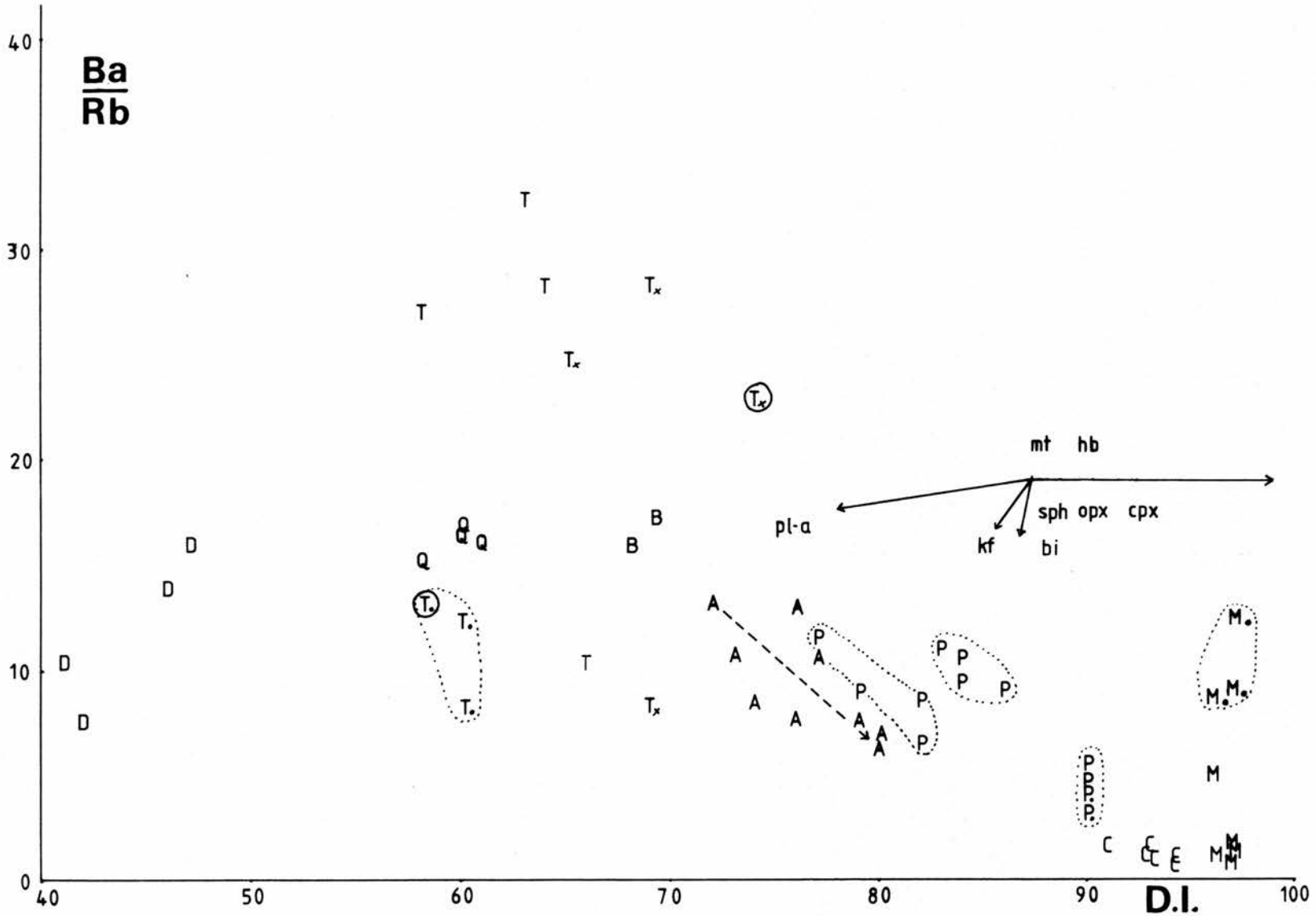
Ba/Rb
D.I.
mt hb
sph opx cpx
pl-a
kf
bi

log Sr - log Rb

Strontium is particularly sensitive to feldspar behaviour whereas rubidium is primarily controlled by biotite.

The gradual fall in Sr through the suites is consistent with fractionation of plagioclase feldspar. The trend D-Q-T. is more dependent on mafic minerals. In particular it is worth noting that T. and T compositions lie off the inferred main trend D-Q-A. This feature is noted elsewhere and implies the lack of a genetic link between T/T.(CMD) and A(CMG), rocks which are geographically connected. The change in slope between the D to Q trend and A to P to C trend can be attributed to crystallisation of alkali feldspar (McCarthy and Robb 1978).

No interpretation can be made on the distribution of M except that they appear more chemically evolved (ie richer in Rb, poorer in Sr) than M..

The overall plagioclase-dependent trend may be a feature of the parental magma common to each of the individual intrusions. The fact that the separate intrusions represented by A and P overlap suggests that the parental magma either had an influx of fresh, more mafic material, or it originated from a different region of the crust.

According to McCarthy and Groves (1979) two sub-parallel en echelon trends on this diagram represent liquid(L) and solid(S) compositions (ie pseudo-cumulate compositions). The liquid line of descent is continuous whereas the solid trends 'back-track' when crystallising conditions change (see below). Their experience is that whole rock trends show more 'solid' trend character, although in reality, some crystallised interstitial material will cause compositions to fall between the two trends.

(see Fig 4.1)

It is not clear from the distribution of the Etive data whether this two -fold process is operating. The distinction between A and P petrographically and geographically is sufficient to discriminate between them without recourse to geochemical parameters. Where the process could be applied is in relating C and M, since they are chemically similar. However, to invoke this model requires that M represent the 'solid' pseudocumulate phase of CSMG, yet its pervasive injection as an inferred ring dyke of Starav would mitigate against this hypothesis. The reverse situation would be more feasible, ie that CSMG is the solid phase and M the liquid, but this is not in keeping with the McCarthy and Groves (op cit) diagram.

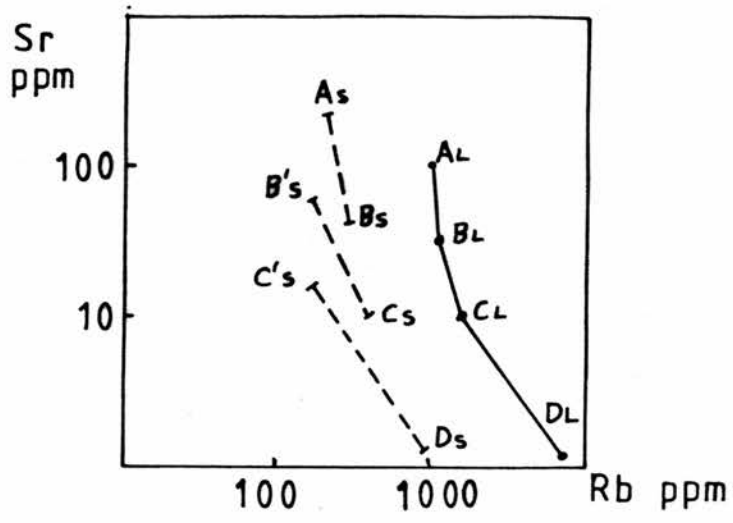

Fig 4.1

The initial magma, AL, undergoes fractional crystallisation of hornblende + biotite + plagioclase + quartz (this assemblage is represented by AS). The liquid composition moves to BL while the solid changes to BS. At BL, hornblende crystallisation ceases and alkali feldspar appears. This solid composition is shown as B'S, and fractional crystallisation changes this to CS, while the liquid moves to CL. At CL muscovite appears and the first solid has a composition C'S. Further fractionation moves the liquid to DL while the solid changes to DS. The liquid line of descent is continuous whereas the composition of the solid is discontinuous at points where new minerals appear.

The sub-parallel attitude of the P and C trends is evidence that these magmas were either separate melts (Fourçade and Allègre 1981) or that C represents a pseudo-cumulate phase of the P magma (McCarthy and Groves (1979). If the latter hypothesis is true then it infers that the P (liquid) trend extended to more evolved compositions (higher Rb, lower Sr) but these compositions are not found.

D and Q are both early intrusions though not visibly related in the field. T/T. and A have long been considered part of one Cruachan intrusion, but the chemical variations seen in this study indicate the existence of two magmas.

From field evidence (chapter 2) A and P are clearly two separate intrusions. A contact is inferred between P and C.

This diagram suggests that the independent pulses of magma which form each rock type within Etive may have shared a common parental magma, in which plagioclase fractionation changed the Rb/Sr signature.

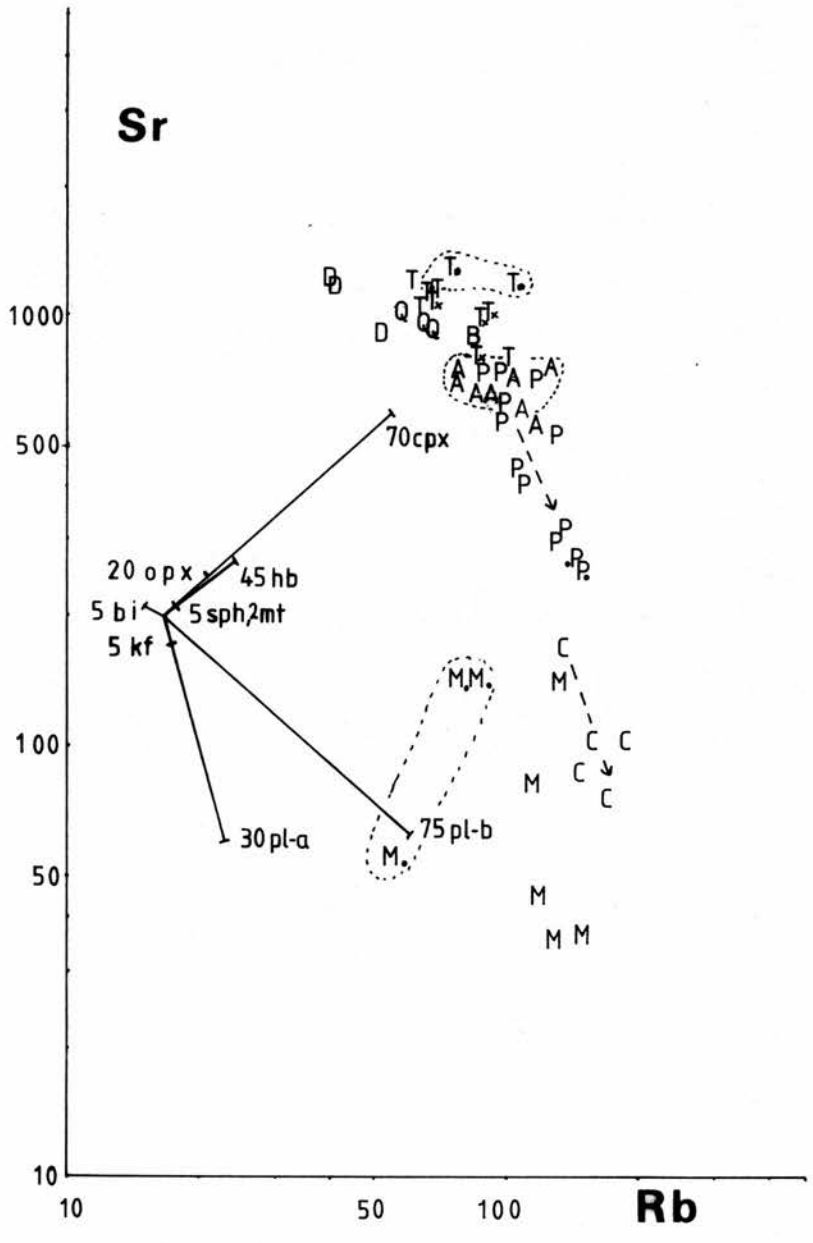
Sr
1000
500
100
50
10
10
50
100
Rb
70cpx
20 opx
45 hb
5 bi
5 sph, 2mt
5 kf
30 pl-a
75 pl-b

log Sr - log Ba

Barium is sensitive to biotite and alkali feldspar behaviour while strontium reflects plagioclase feldspar behaviour.

The overall trend appears to be controlled by a combination of mafic minerals and plagioclase fractionation in the early stages (D to Q), followed by plagioclase and alkali feldspar ± biotite, (A to P to C) (McCarthy and Robb 1978). Fourçade and Allègre (1981) pointed out that if separate sub-parallel trends show up on this diagram, they can be taken to represent independent intrusions of magma. This feature is clearly shown by A and P, P and C, M. and M compositions. The gap between P. and C is notable, especially since they are virtually adjacent to each other in the field (RB014 and RB093 respectively). The comments made for the log Sr - log Rb diagram with reference to the McCarthy and Groves (1979) hypothesis apply to this diagram too. While C could just conceivably be considered a pseudocumulate of PSMG, the same problem arises over the place of M compositions with respect to C.

A clear separation is obtained between T. and T/Tx samples, the latter being enriched in Ba. Assuming that all the barium is contained within biotite and alkali feldspar then consideration of the relative modal proportions of these minerals in

T. (7% alk.feld.+ 21% biot.contain 900ppm Ba) and

T (18% alk.feld.+ 14% biot.contain 1900ppm Ba)

leads to the conclusion that most barium in T must be contained in alkali feldspar. This assumes that both phases are consanguinous.

The Kd:Ba/alkali feldspar = 6 quoted by Cox et al. (1979) is considered low and should be realistically higher for the Cruachan rocks.

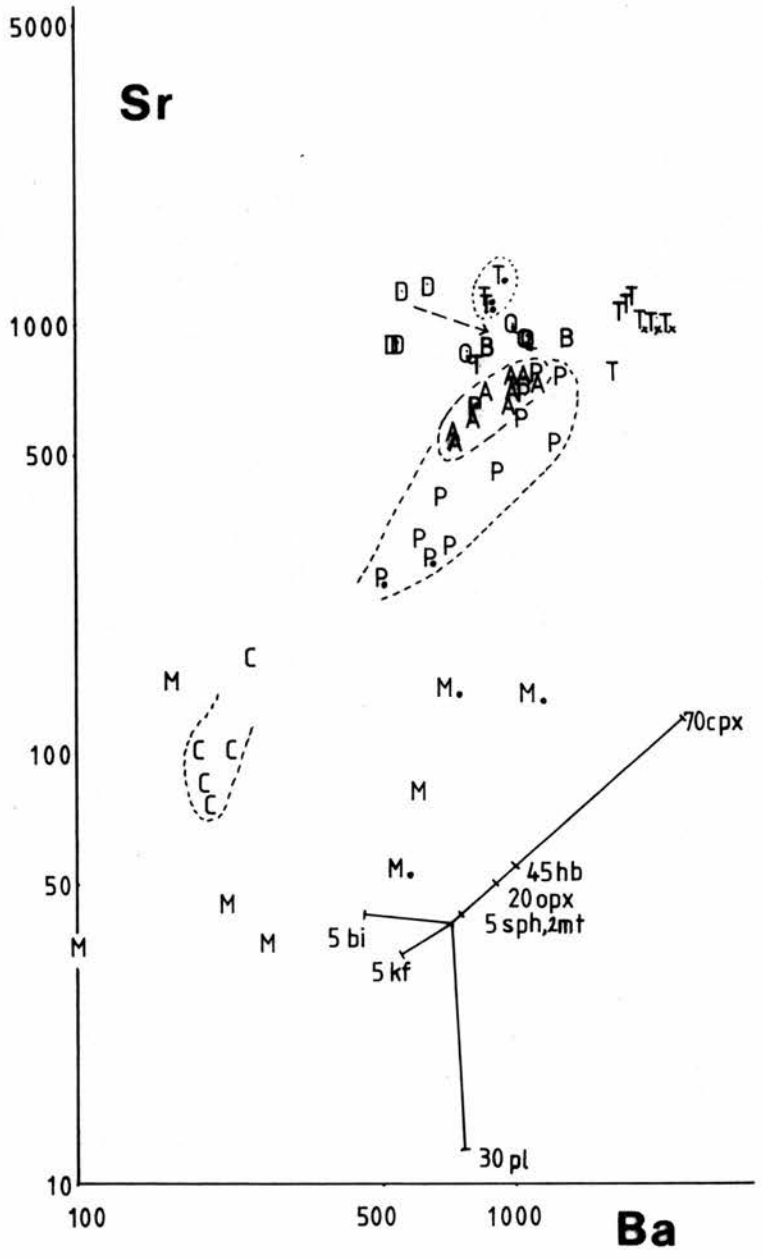
5000
Sr
1000
500
100
50
10
100
500
1000
Ba
70cpx
45hb
20opx
5 sph,2mt
5 bi
5 kf
30 pl

Ce/Y - SiO_2

Cerium reflects light rare earth element (LREE) behaviour and Y can be considered as a heavy REE. As Y is preferentially removed by clinopyroxene and amphibole, as well as by apatite, fractionation of these phases will cause the Ce/Y ratio to increase.

This positive trend is seen in D to Q/T., within T, P and C. A feature of the PSMG is revealed in this diagram which is not very clear in other plots, namely the presence of at least three en-echelon trends within P samples. Each trend reflects a geographic zone in the PSMG; an outer (Cadderlie) zone (left), an intermediate (Glen Kinglass) zone (centre) and an inner (Barrs) zone (right). Two sample points, P. from the inner zone are underlined and superscripted with an arrow to indicate that they have a high La/Ce ratio, ie >1. All the other samples have La/Ce ratios which lie between 0.6 and 0.9, which is similar to the global average for acid igneous rocks (0.7) (Wedepohl 1970). During weathering or hydrothermal alteration Ce^{3+} will oxidise to Ce^{4+} and as such becomes more mobile (Masuda and Nagasawa 1975). This loss in Ce will therefore cause the ratio to fall and affect petrogenetic interpretations based on its use as a LREE (Hellman 1979). Hence the La/Ce ratio is used here as a monitor of Ce loss. The two labelled samples, P., coincidentally lie closest to the CSMG intrusion, postulated to be a later intrusion, which has associated pegmatite and vein formation (RB094, RB137,

RB138), fluids from which could mobilise Ce.

Contrary to the positive, mafic mineral-controlled fractionation trend, is the A array which generates a negative trend. This can only be explained if biotite and/or apatite or sphene dominated a fractionating system.

The CSMG (C) stands alone at the end of the overall Starav trend as a late, independent pulse of magma, reinforcing the hypothesis that it is related to P at depth but was intruded later after some chemical modification. There is a close affinity between C and M compositions.

A strong Y depletion in M. is highlighted in this diagram. Since the La/Ce ratio is within the normal range (0.6-0.8) it is assumed that Y has been removed in order to generate high Ce/Y ratios. Low Y could be due to extreme fractionation of mafic minerals or partial melting of a garnet- or amphibole- rich crust. Extreme fractionation would also result in a high concentration of incompatible elements eg Th, Nb and Rb, but this is not the case for M.. The alternative theory of partial melting seems more consistent with the data.

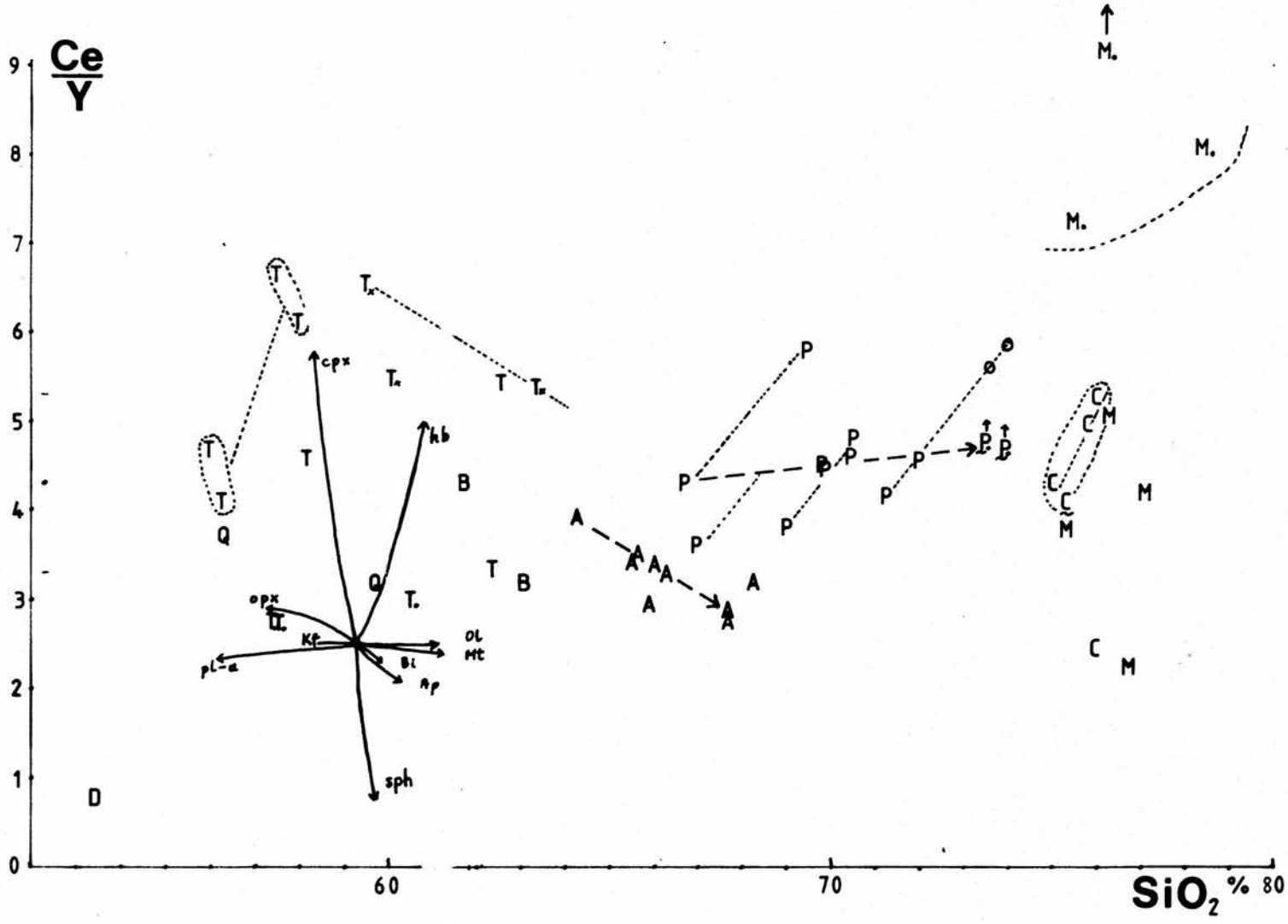
Ce/Y
SiO2 %
60
70
80
0
1
2
3
4
5
6
7
8
9
cpx
hb
opx
Kf
pl-a
Ol
Mt
Bi
Ap
sph
T
B
A
P
C
M
Q
D

Chondrite-normalised elements

Normalising trace element data to chondrite abundances has been used for a long time to display rare earth element variations. Recently this technique has been applied to other elements of interest in petrogenesis (Thompson 1982).

The source of chondrite abundances is a compilation taken from Sun et al. (1979) and Thompson(op cit).

The compositions used here are of samples which are representative of each group. A number of features are highlighted in this diagram.

1. M. is enriched in Ba relative to M, and T is similarly enriched relative to T.. Alkali feldspar ± biotite could explain these differences. M and C are depleted in Ba.
2. The order of relative abundances for the P-P.-C trend changes for Th. The content of Th in the later, more differentiated CSMG would be expected to be lower than for P.. Therefore there is a positive Th anomaly in CSMG which suggests it is a separate intrusion. Values for Th in M are higher than C and point to a high crustal component in M. Although the relative error in the Th determination is relatively high (24±4.2ppm), there is clearly a Th enrichment relative to T and D.
3. With the exception of D and T., all rock groups show depletion in Sr which is consistent with plagioclase feldspar fractionation from a common source magma.

4. The variation in T compositions with respect to T. changes significantly between elements. T samples are enriched in Ba, La, Ce, Zr and Hf, and depleted in Th and Y relative to T.. There is a very slight depletion in Rb, Sr and Nb. The former association is compatible with an enhancement of alkali feldspar, and/or biotite (Ba), zircon (Zr,Hf), or sphene (La,Ce). Alternatively fractionation of apatite could account for a relative increase in the light REE (La,Ce). The strongly depleted elements Th and Y could be accounted for by removal of apatite (Y) and ilmenite (Th) fractionation. Alternatively T and T. could represent two separate magmas.

5. All rock types show depletion in Y relative to D. This data is consistent with either a source magma which separated as a partial melt from garnet- or amphibole-rich material (eclogite, granulite, amphibolite) or a source magma which fractionated amphibole $\pm$ clinopyroxene and apatite.

6. There is a regional enrichment in Rb and Th.

The following observations can be made:

The source magma for most of the Etive rocks could have been derived from a garnet- or amphibole-rich crustal rock by partial melting, followed by plagioclase fractionation. Alternatively an original mafic source fractionating amphibole $\pm$ clinopyroxene and apatite could produce the required Y depletion. The enrichment in Rb and Th favours the involvement of an evolved crustal source, a finding which is compatible with the Proterozoic (Grenvillian age) source advocated by Clayburn et al. (1983) on the basis of Nd and Sr isotope data. He advocated rocks of Grenvillian age

based on the fact that this period of the Proterozoic was one of major crustal addition, and that other Lewisian rocks are generally low in radioactive elements ie U and Th (Blaxland et al. 1979).

Differences in the normalised values for dioritic rocks suggest they were formed from a separate source. In particular, the lack of a negative Sr anomaly, high Y and low Nb,Rb,Th are consistent with an origin from a primitive mafic igneous magma.

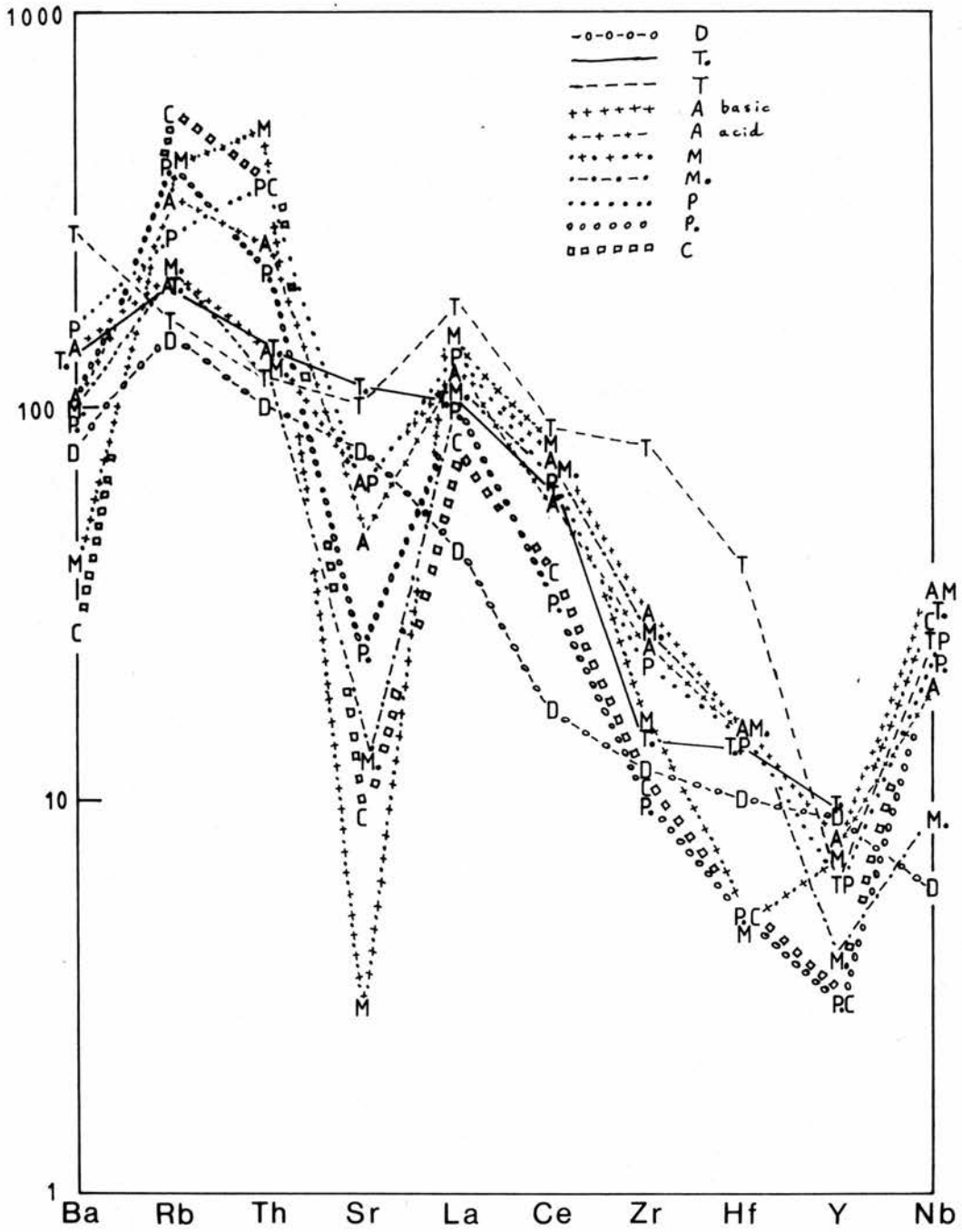
1000
100
10
1
Ba
Rb
Th
Sr
La
Ce
Zr
Hf
Y
Nb
D
T.
T
A basic
A acid
M
M.
P
P.
C

Ce_n/Y_n - Ce_n

These values are chondrite-normalised using Ce=0.865ppm and Y=2.0ppm (Sun et al. 1979).

This diagram is a variation of one used by Gill (1981), in which Y is substituted for Yb. It attempts to discriminate between partial melting and fractional crystallisation mechanisms in the genesis of intermediate magmas. Progressive partial melting of eclogite produces liquid compositions which describe a sub-vertical trend towards lower Ce_n/Y_n values. Y (and Yb) reflect heavy REE behaviour (high Kd for garnet) and would be progessively released into the melt from garnet. Fractional crystallisation of feldspar, orthopyroxene, apatite, biotite and sphene produce sub-horizontal trends, whereas removal of clinopyroxene and amphibole produce sub-vertical trends to higher ratios. This vertical sense is the same as for partial melting, though the evolutionary direction is opposite.

The M. and C groups both define sub-vertical trends. Within C, the trend moves to higher ratios, indicating that fractionation (of hornblende) was operative (clinopyroxene is not found in these rocks). No evolutionary trend is known for the M. rocks, but the fact that they possess very high ratios suggests they may be relatively Y-depleted. Since large quantities of clinopyroxene or amphibole (>50%) would need to be removed from an intermediate source to generate ratios up to 33.5

(RB123), partial melting from a garnet- or amphibole-rich source might be a more feasible mechanism.

The overall trend turns back on itself. D to Q is clinopyroxene ± plagioclase ± orthopyroxene dependent, Q to A can be explained by fractionation of clinopyroxene ±hornblende, while the trend within A and P is related to biotite ± apatite ± sphene. In fact evidence from the Ce/Y vs SiO_2 diagram suggests that the overall trend P to P. is composed of three en-echelon trends which in this diagram are not immediately obvious, but roughly parallel the hornblende vector. The proportion of hornblende in the PSMG gradually falls from P to P. compositions and supports this chemical evidence.

Some of these changes are difficult to explain. The relation between T. and T samples, assumed, on evidence from Harker diagrams to be due to enhanced Ba, La, Ce, Zr and Hf levels, is difficult to rationalise on this plot, even though the two groups are well separated. Apatite or sphene may be responsible . In thin section, T. samples have 0.5mm euhedral crystals of apatite mostly enclosed in biotite, whereas in T samples apatite occurs as smaller, euhedral crystals and laths. Some is enclosed in biotite and some is "free-floating" in plagioclase. Sphene is more abundant in T samples which is not possible if one invokes crystal fractionation from more mafic compositions (Q or T.). It is therefore possible that T and T. represent different magmas.

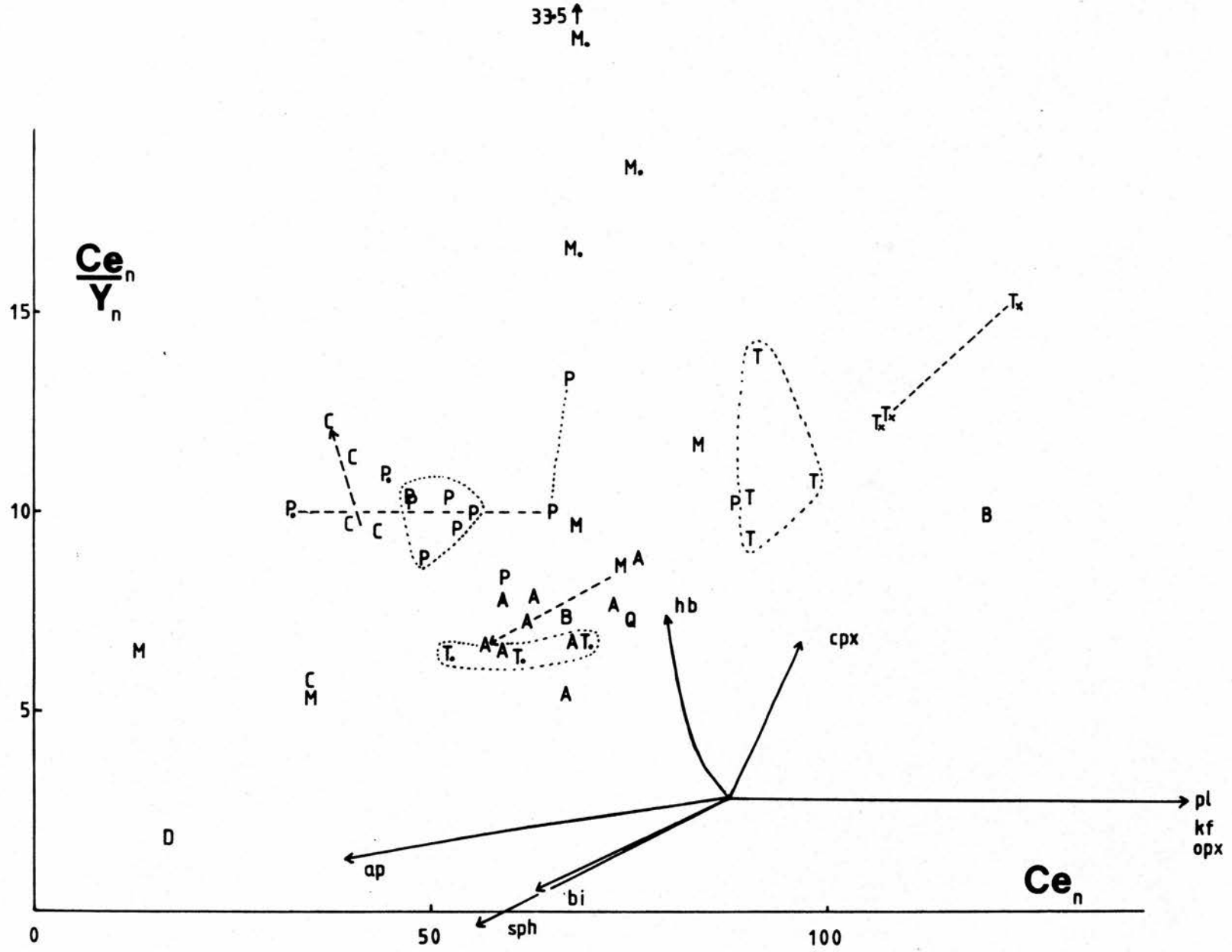
33.5
$\frac{Ce_n}{Y_n}$
15
10
5
0
50
100
Ce_n
hb
cpx
pl
kf
opx
ap
bi
sph

Normative Diopside-Corundum - SiO_2

According to Cawthorn et al.(1976) this diagram will broadly separate I-type from S-type granitoids (as defined by Chappell & White 1974). S-type granites will always be strongly corundum normative (>1%), reflecting their origin from aluminous metasedimentary material. I-types tend to be diopside normative but may fractionate along trends to low corundum normative compositions. In cases where the source may be remelted I-type crust, or mixing of mantle-derived melts with crustal material has taken place, then ambiguities will arise.

The overall trend suggests I-type magmatism with no evidence for S-type granites. The case of M compositions remains unresolved. The widespread presence of hornblende and sphene in Etive rocks confirms the I-type association.
(Chappell and White 1974)

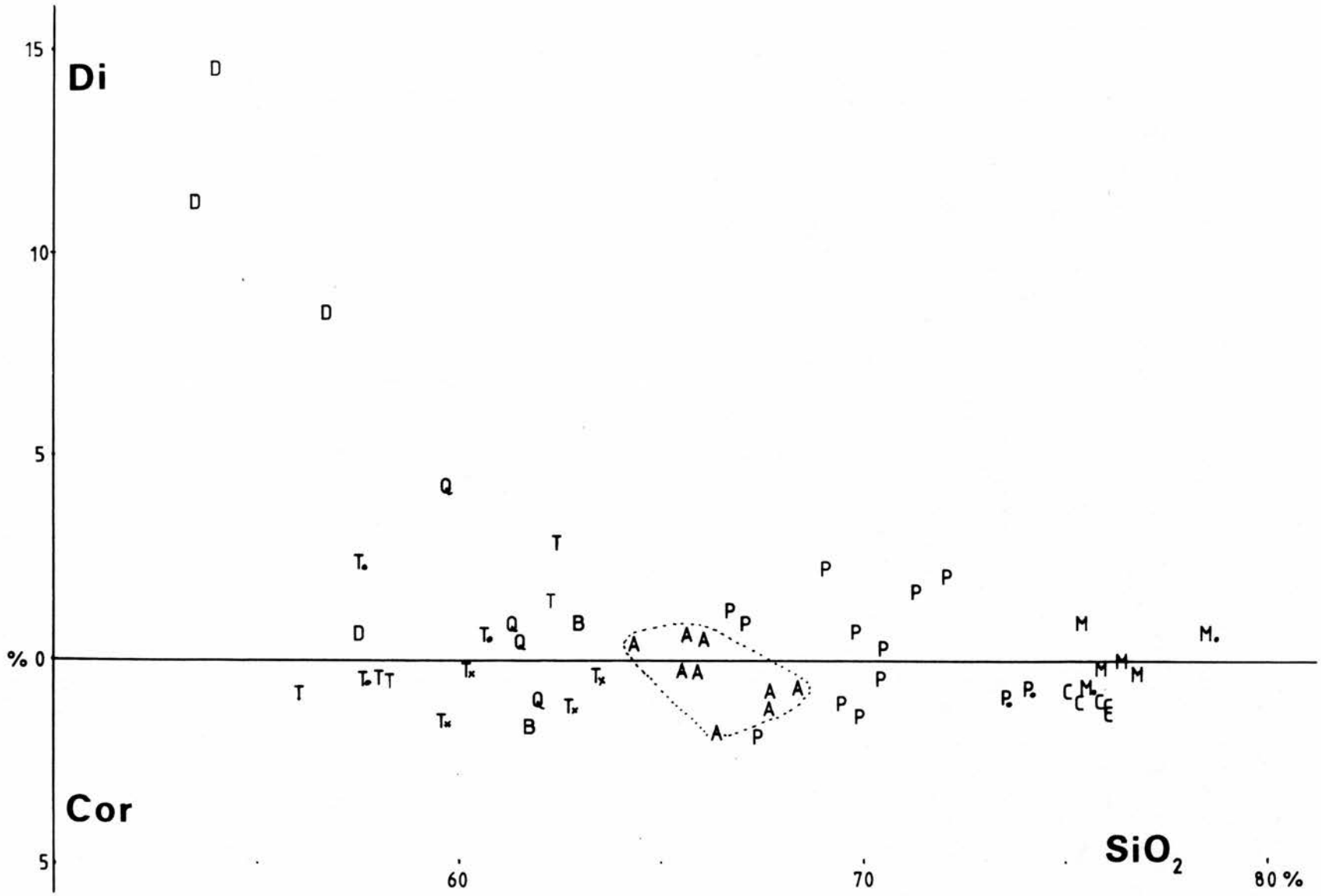
15
Di
10
5
% 0
Cor
5
60
70
80 %
SiO2

Normative Quartz - Albite - Orthoclase

The Thornton and Tuttle (1960) Differentiation Index (DI) represents the sum of normative quartz, albite and orthoclase. Samples with DI>80 are plotted on a triangular diagram with P_{H2O} isobars superimposed: 0.5 to 5kb from Tuttle and Bowen (1958), 10kb from Luth et al. (1964).

The isobaric minima are shown by a '/' and labelled 'm' on the 0.5 kb isobar.

If the normative mineralogy is to be believed, the felsic CMG (A) formed at >5kb P_{H2O}, which would prevent it reaching the surface. However, this granitoid was undoubtedly the sub-volcanic expression of the Glen Coe lavas and the peripheral Fault Intrusion (see Map, Fig 1). Venting off volatiles may have allowed the magma to rise higher into the crust.

The relatively wide spread in P compositions may reflect variation in depth of crystallisation of the feldspar components. Identification of the PSMG phenocrysts as orthoclase (see Section 3.8) makes it feasible that they formed at higher pressures (8kb P_{H2O}) (Kawachi and Sato 1978) though this level of water would prevent the magma from rising high into the crust. Somehow this excess hydrous phase must have been lost to allow the Starav pluton to rise within a few km of the surface (Droop and Treloar 1981).

M. compositions cluster off the main trend between 3 and 5 kb. This grouping resembles the leucosome field from layered migmatites (Johannes 1983) and supports the chemical evidence for these rocks representing crustal partial melts.

C and M (with one exception) lie closer to the field of ternary minimum compositions at 1kb, a field defined by most granites (Carmichael et al. 1974). They represent higher level melts. Chemically M is similar to C but represent a ring dyke of fractionated PSMG injected into the Cruachan during the Starav emplacement.

It is concluded that the felsic mineralogy in the Etive granitoids crystallised under a wide range of confining water pressures, which in turn reflects a wide range in depths of magma generation. The gravity anomaly over the Starav intrusion reaches -46mgal (see Fig 2.1). Such a 'low' anomaly has been interpreted by Brown (1981) as representing an extension of granitic material to more than 12km depth (equivalent to 4kb P_{H2O}).

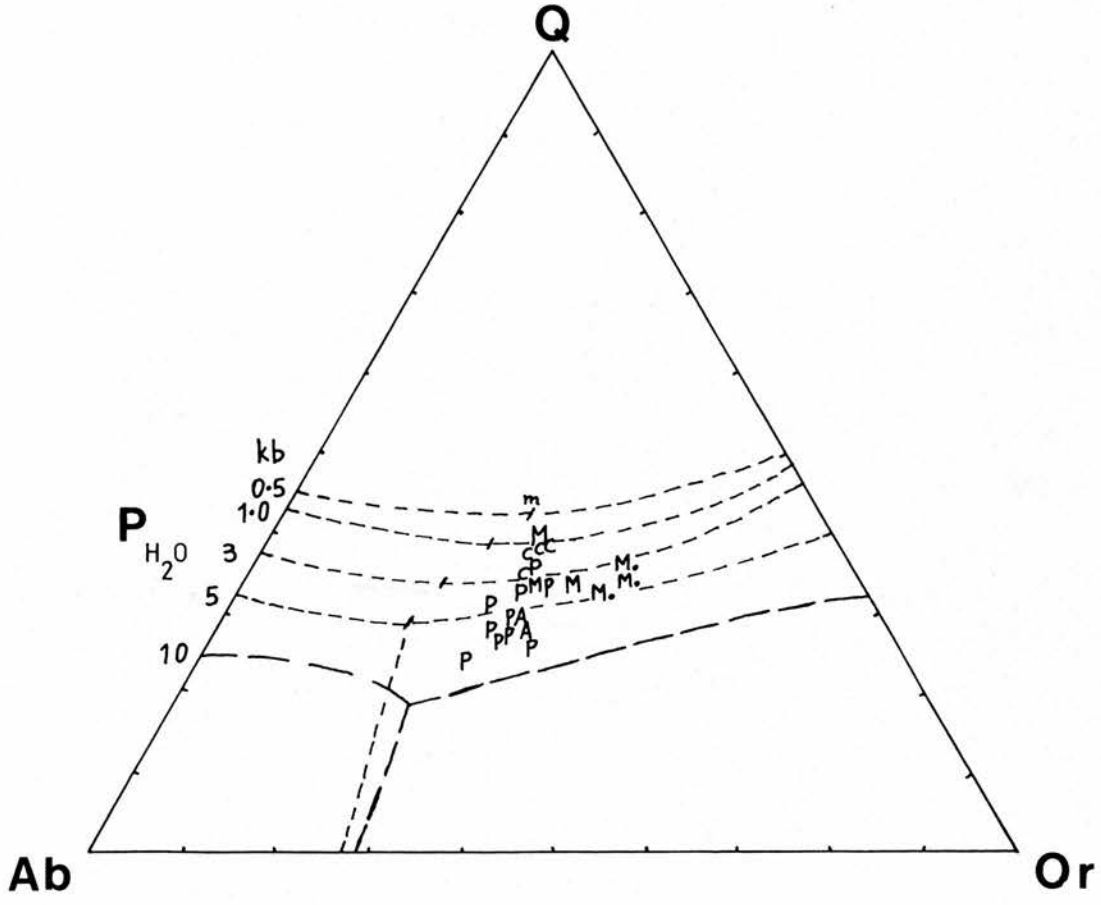
Q
kb
0·5
1·0
3
5
10
P
H_2O
Ab
Or

PETROGENESIS

Diorites

Rocks of dioritic composition are the most mafic types found within the Etive complex, although basalts occur in the neighbouring Lorne lava plateau, an expanse of Lower Old Red Sandstone volcanics (Groome and Hall 1974). The variations in chemistry between dioritic samples, examples of which occur in the NW and SE peripheries of the intrusion, can be ascribed to differences in clinopyroxene and hornblende contents. They are similar in major chemistry to the andesites of the Lorne plateau (Brown 1975; Thirlwall 1979) and it is possible that they share a common origin. The Lorne lavas comprise sequences of basalts, basaltic andesites, andesites and minor trachytes and rhyolites. In considering the possibility that these lavas, penecontemporaneous with the Etive granitoids (c.400Ma, Clayburn et al. (1983)) may have been related to the diorites, recourse is made to some trace element data. Values for Ni in the andesites are very high (c. 190ppm) compared with 3ppm Ni expected if fractionation of olivine ± clinopyroxene from basalt had been the dominant mechanism (Groome and Hall 1974; Ringwood 1975; Thirlwall 1979). Nickel values in the diorites average 100ppm, falling to 40ppm in the quartz diorites (Brown 1975). This change may be explained by clinopyroxene fractionation. Data from Thirlwall (1979) for the Lorne andesites shows a very wide spread in compositions which when considered in conjunction with high Ni values, suggest a mixing origin. Mixing may also

explain the co-existence of orthopyroxene, clinopyroxene and quartz phenocrysts which Thirwall (1979) found in some lava samples. The appinite bodies which occur locally (Kentallen) are thought to be genetically related to the basalts and mafic andesites (Groome and Hall 1974), while the acid extrusives are considered to be independent of both the basalts and the granites of Etive. Pb, Sr and O isotope systematics indicate that while all the granitoids of Etive contain a mantle component, the diorites reflect a greater proportion of mantle-derived melt (Clayburn et al. 1983). The more primitive chondrite-normalised patterns for the diorites (Page 4-69) lend weight to an origin directly from basic parents rather than by mixing mechanisms, which would make them independent of the andesites.

Taking diorite compositions as a theoretical starting point, the whole range of Etive magma compositions can be related to a general fractional crystallisation regime in which clinopyroxene, olivine and orthopyroxene dominated the early stages, and plagioclase and alkali feldpsars dominated the later stages. This apparently continuous trend is seen in most Harker diagrams, log MgO-log K_2O, MgO-Rb, and log Sr-log Rb plots. Such a linear relationship among rocks which are visually and petrographically distinct can only apply if it concerns an inferred source magma which is common to all types. This may not be true for the PSMG, as will be shown later. Strong depletion in chondrite-normalised Y suggests that the Etive source magma originated either as a partial melt from a garnet or amphibole-rich crustal rock, or after fractional crystallisation of hornblende $\pm$ apatite from a

mafic source. A correspondingly strong enrichment in Rb and Th is consistent with an evolved crustal source component to the source magma.

Continued clinopyroxene ± hornblende fractionation changed D to Q compositions (see log Rb/Sr - D.I., Ba/Rb - D.I., CaO - MgO, log Sr - log Ba, Ce_n/Y_n - Ce_n).

Cruachan Granitoids

Magmas of Q compositions appear to have evolved subsequently in three separate directions. Evidence from CaO - MgO, Ce_n/Y_n - Ce_n, V - Ti/1000, and log Sr - log Ba plots strongly suggest that Q compositions gave rise to T. (dark CMD) by either orthopyroxene , hornblende and apatite fractionation or by addition of alkali feldspar, whereas clinopyroxene , hornblende, plagioclase and sphene removal produced A (CMG). A different mechanism produced T compositions. Thus there is a clear divergence in compositions at this point which gave rise to three distinct Cruachan granitoids. Other workers until now have considered that all Cruachan granitoids represent variations within one intrusion, (Bailey and Maufe 1960; Kynaston and Hill 1908; Anderson 1937; Brown 1975). The fact that the northern lobe (denoted A) is more felsic than its southern counterpart (T./T/Tx) led Brown (op.cit.) to invoke a compositionally-zoned pluton showing an increase in silica northwards. Unfortunately crucial areas in the central region (Beinn Sgulaird) are poorly exposed and therefore this chemical change had been assumed to be continuous.

The third Cruachan rock type T(CMD) is characterised by high concentrations of Ba, Al, Zr, Hf, La, Ce, Ti and Na. In most diagrams it stands alone, off the main trend. This anomalous chemistry, with respect to the overall chemical trends seen in Etive has led to the theory that this rock originated from a different source. While fractionation of clinopyroxene from Q compositions gave the correct sense of direction to the liquid vectors on most diagrams, it could not generate the absolute levels of major and trace elements found in T. Removal of 20% clinopyroxene from Q depleted the major components. The removal of 60% to 80% clinopyroxene would be necessary to obtain the observed Ba and Al levels.

The suite of enhanced elements represents the following mineral assemblage: alkali feldspar (Na, Al, Ba, K), biotite (Ba, Ti, Al), zircon (Zr, Hf) and sphene (Ti, La, Ce). Since fractionation could not explain this chemistry, mixing was considered as an alternative mechanism. A study of the R1 - R2 'de la Roche' major oxide projection suggests that to generate T from Q by mixing requires a composition close to the syenite field (lower left on Page 4-30). Syenitic rocks tend to have high Ba, Na, Zr and REE concentrations and such a mildly alkaline composition could provide the necessary elements. An alternative mechanism is that which generates A-type granites, as described by Collins et al. (1982). Partial melting of a felsic granulite could produce a metaluminous or peraluminous melt rich in high field strength elements (Zr, Hf, Nb, Ti, Y, REE) and low in Mg

and Ca. However, A-type granites have high silica values (>75% SiO_2) and low modal plagioclase which do not equate with the monzodioritic composition seen in T samples (54 to 58% SiO_2). Mixing of such a partial melt with more mafic material (host restite?) could move compositions closer to T.

Mixing calculations generated the following composition for an unknown component (X) which when mixed with Q (RB088) in the ratio 60%Q + 40%X yielded T (RB012), provided T represents a liquid composition. The chosen ratio was based on the lowest proportion of X which would not produce negative values for any major constituent.

SiO2	TiO2	Al2O3	Fe2O3	FeO	MnO	MgO
55.45	1.53	24.15	3.21	1.83	0.01	0.23

CaO	Na2O	K2O	P2O5	H2O
4.00	6.05	3.35	0.19	0.00

Li	V	Rb	Sr	Y	Zr	Nb
22	94	37	1724	4	1083	6

Ba	La	Ce	Hf	Pb	Th
3613	91	106	14	-5	8

During anatexis, it is possible that some crystal fractionation may take place which would upset the resultant theoretical composition. Trace elements are particularly susceptible to this process and therefore this calculated assemblage may not strictly represent a true melt or mix composition. With the exception of

Al_2O_3, which is high, the overall chemistry has similarities to syenitic compositions.

A further complication is the occurrence of rocks on the margins of the southern Cruachan lobe which are pale grey granitoids some of which contain pink alkali feldspar crystals. They are denoted Tx or + on chemical diagrams. Samples RB109, RB073, RB076, and JFB157 share physical and chemical characteristics which link them to the northern CMG (A) samples. For example, RB109 and RB056 share pink alkali feldspar and metasedimentary xenoliths, and RB076 has A-group chemistry. They are richer in SiO_2 and Rb, and poorer in Ca and Sr than the neighbouring T samples. Barium levels are not constant and may reflect contact effects due to late-stage fluids. Net-veining occurs close to RB073 and RB091 (1km E of RB109) which may indicate fluid activity. The lighter colour of these rocks contrasts with the dark grey of T rocks. The fact that they occur around the perimeter of the Cruachan intrusion suggests that they belong to a later, annular intrusion related to the northern CMG and linked in time with the CMG extension around the Glen Coe cauldron , the Fault Intrusion (Bailey and Maufe 1960), which was emplaced during the cauldron subsidence at Glen Coe.

The presence of a partial ring fault on the west side of Etive suggests that cauldron subsidence may have affected the southern lobe, and allowed monzogranitic magma to rise, encircling the pre-existing Q and T/T. rocks. The nature of the contact between Cruachan rocks and host Dalradian metasediments,

changes from being steeply dipping in the E, SE and NW, to a gently easterly-dipping interdigitating contact in the W and SW, the area where the CMD (T) predominates. Coincidentally, the fault is only seen in the SW, which suggests that the rest of it has been obliterated by rising magma (? Tx or A). According to Brown (1975) and Droop and Treloar (1981), the SW represents a deeper crustal level. Hence any extensive outer ring intrusion may have been eroded away. Alternatively, the inferred outer monzogranite intrusion was eccentrically emplaced and was pinched out in the SW (see map, Fig 1).

Within A (CMG) compositions, the progressive chemical changes can be explained by in-situ fractionation of hornblende, plagioclase feldspar, apatite, biotite, and alkali feldspar. The most acid member (RB055) occurs in Glen Etive some distance from the external contact. In contrast, contact samples are more mafic (RB051, RB052, RB064); a good case for crystallisation of a magma from the outside inwards (Vance 1961). The presence of greisen veins in Glen Etive (RB058) highlights the presence of residual fluids, concentrated in a cooling pluton.

Porphyritic Starav

Intruding the Cruachan granitoids is the later porphyritic Starav monzogranite (PSMG) which contains distinctive 'pink' alkali feldspar megacrysts and euhedral hornblende. Texturally and chemically it is distinct from its Cruachan neighbour. The most mafic PSMG is more mafic than the most silicic CMG, therefore it cannot be a part of an ongoing Cruachan

fractionating sequence. Nd isotope systematics show that the age of separation of the isotopes for the later PSMG was about 350Ma older than that for the earlier CMG (Hamilton et al. 1980). This strongly suggests that the PSMG magma originated from an older and perhaps deeper source. Within the PSMG, chemistry changes to more silicic compositions inwards. The chemistry indicates that hornblende, plagioclase feldspar, alkali feldspar and apatite crystallisation could account for the overall change in composition. However, evidence from the Ce/Y - SiO_2 diagram shows that within the PSMG, at least three chemically distinct zones can be identified. These show up as three en-echelon trends, with each pulse starting off more mafic than the final composition of the previous one. McBirney (1980) believes that such en-echelon chemical trends are the result of repeated mixing events between hot, rapid-moving crustal melts and pieces of host material. The presence of amphibole-rich mafic knots in PSMG samples does not rule out this hypothesis. This multiple pulse mechanism can also be seen on the R1 - R2 'de la Roche' diagram, K/Rb - D.I., Ba/Rb - D.I. and to a lesser extent, on the V-Ti/1000 plot. There is little petrographic evidence for this subtle change in chemistry, although samples RB015 and RB018 (not analysed) which lie close to an inferred pulse boundary show signs of alteration (chloritised biotite, cloudy plagioclase feldspar and haematised alkali feldspar). There are a number of topographic features which approximately coincide with inferred pulse boundaries. The first pulse (counting from the external contact inwards) covers the area from NE of Cadderlie to south Glen Kinglass and Allt Easach, a valley cut between Beinn Bheag

and Beinn Mheadonach to the E of Beinn Trilleachan. Glen Kinglass itself is a notable feature and centres on the second pulse. The ridge to the north of this valley may mark the boundary between pulses two and three (see Map, Fig 1).

Central Starav

The most silicic PSMG samples (RB014 and RB092) resemble the CSMG in appearance and major chemistry. However, evidence from mostly trace elements shows up important differences, and leads to the conclusion that the inner PSMG (pulse three, P.) and CSMG (C) are separate intrusions or that the CSMG is a pseudo-cumulate mush from the PSMG (McCarthy and Groves 1979)

The important differences are:

1. Chondrite-normalised Th and Nb are enhanced in the CSMG.
2. MgO - K_2O trends are not co-linear
3. Chondrite-normalised Ce/Y - Ce trends are not co-linear
4. K/Rb ratio rate of change is not constant across the P to C 'contact'.
5. Ba/Rb ratio is more constant in CSMG.
6. The R1 - R2 'de la Roche' diagram separates P and C trends.
7. Rb concentrations in CSMG start at lower levels than those in the most evolved PSMG.
8. Ba/K_2O rate of change is smaller in CSMG.
9. log Sr - log Ba shows a large break between P and C.
10. log Rb - log Sr produces a steeper slope for CSMG.
11. Modal trends (fig 3.7) indicate that the CSMG is quartz-dominated while the PSMG is alkali

feldspar-dominated.

Field evidence on the shores of Loch Etive at RB138 (steeply eroded stream gully, haematised fractured rock, pegmatite formation) strongly suggests there is a physical discontinuity between the PSMG and the CSMG.

Meall Odhar

All occurrences of 'pink' granite, as sheets or dykes throughout the Cruachan intrusion have been traditionally defined as Meall Odhar type, after the classic locality at the the hill of that name in the NE area of the Etive complex (Bailey and Maufe 1916). Chemical data shows there to be two distinct types. These have been defined here as 'primitive' (M.) or 'evolved' (M) on the basis of their trace element compositions. 'Primitive' reflects low levels of Rb, Th, La, Y, Nb and higher levels of Ba, Sr, Zr, Hf. 'Evolved' compositions have the reverse assemblage. The classic exposure at Meall Odhar is an arcuate, sheet-like intrusion whose outcrop parallels the Starav contact (Bailey and Maufe 1960). This belongs to the 'evolved' type. Such an evolved trace element signature is compatible with the products of extreme fractionation of mafic minerals and feldspar within a silica-saturated igneous suite (Taylor 1965). It is chemically similar to the CSMG, as seen in the chondrite-normalised Ce/Y - Ce, K/Rb - D.I., Ba/Rb - D.I. and MgO - Rb plots. Modally it is a monzogranite. The evidence is strong enough to state that the 'evolved' MOG in fact represents a ring dyke from the Starav intrusion, an idea put forward by Bailey and Maufe (op cit).

The 'primitive' MOG is an alkali granite (fig 3.7). It has higher Ba and occurs as extensive sheets. The relatively low Rb content, and concomitant high K/Rb ratio of 700 suggests that this rock may have originated from a primitive crustal source (Shaw 1968). That is, it represents a low degree partial melt from a Rb-poor quartzo-feldspathic rock, and is not the result of crystal fractionation. The vertical trend which it describes on the chondrite-normalised Ce/Y - Ce plot also suggests this origin (Gill 1981). In many respects it resembles the A-type assemblages defined by Collins et al. (1982) in which enrichment in high field strength elements can be related to partial melting from a felsic granulite.

Bonawe

Little has been said of the Bonawe intrusion, which Anderson (1937) claimed was a small, separate body isolated from the CMD by a screen of schists. The outcrop is restricted to the working quarry at North Bonawe. Chemically it plots close to the pale CMD (Tx) but it cannot be convincingly fitted into any unique evolutionary model. A very altered red granitoid (RB008) occurs just E of the working quarry. Such alteration is often typical of contacts or discontinuities. In view of the identification of a more felsic peripheral facies to the Cruachan intrusion (Tx), it is suggested that the Bonawe quarry material may represent part of this. The schists noted by Anderson (op cit) may represent country rock down-faulted during the emplacement of the outer granitoid (Tx), and related in time to the Beinn a'Bhuiridh screen.

Discussion

To generate granite magma by fractionation directly from basaltic compositions is volumetrically untenable, since only a small proportion of acid melt can be so produced (Anderson 1976). A two-stage fractionation process has been proposed for the formation of the Sierra Nevada batholiths. It invokes a basalt to andesite fractional crystallisation sequence followed by an andesite to acid melt stage (Presnall and Bateman 1973). Carmichael et al. (1974) were also in favour of a two-stage fractionation mechanism for the formation of granitic melts. Taylor (1969) points out that in a high fO_2 environment, magnetite fractionation could produce calc-alkaline magmas, but the absence of V or Sc depletion in andesites disproves this hypothesis. Fractionation of kaersutitic amphibole could produce andesitic liquids, (Cawthorn and O'Hara 1976), but this would lead to gross depletion in titanium, a feature rarely found in andesites. Wyllie (1982) prefers a multistage process for the production of calc-alkaline magmas, based upon constraints imposed by P_{H2O} on melting of a sub-crustal source. He excludes mantle peridotite, subducted oceanic basic rock, subducted ocean sediment or partial fusion of quartzo-feldspathic rock as sources for generating primary granitic magma (Wyllie et al. 1976).

Winkler (1976) believes that most granites result by anatexis of metasediments. Shales could generate up to 50% granitic melt, while greywackes could yield 70 - 95%. At 2kb P_{H2O} and 800°C, a paragneiss could produce 84% melt consisting of alkali feldspar, quartz, sodic plagioclase and 16% restite, containing opaques, biotite and calcic plagioclase. The latter may disperse or remain as schlieren. A paragneiss could be completely remelted at 900°C and 5kb P_{H2O}, generating a monzogranite composition. At a lower temperature, 675° to 760°C and 2kb P_{H2O}, the melt corresponds to an alkali granite. From the chemical variations seen in Etive rocks, this latter mechanism could have generated M. ('primitive' MOG) compositions while the Starav monzogranites could result by complete melting of a paragneiss. However Pitcher (1979) points out that most anatectic 'granites' show some evidence of the pre- existing structures, be they banding, ghost stratigraphy or schlieren. He does not accept large-scale ultrametamorphism as the cause for cordilleran granitic batholiths though smaller-scale melting could generate the S-type granites which he describes as Hercynotype. The I-type nature of the Starav rocks contradicts the anatexis hypothesis.

In general, trace element behaviour in the Etive suite suggests that fractional crystallisation was a dominant mechanism within each individual intrusion, but it does not rule out the possibility that mixing took place between crustal melts and fractionation- derived magmas of intermediate compositions.

Early measurements on strontium isotopes (Brown 1975) gave large errors on some ages. These were blamed on poor resolution in analytical procedures (eg Cruachan 393±30Ma, I_{Sr} = 0.7049±0.0029). Brown (op cit) explained the high error as due to inhomogeneity in the rock. Similarly large errors for Cruachan have been obtained by Clayburn (1981) using more sensitive techniques (Cruachan 396±61Ma, I_{Sr} =0.70503±0.00040). He ascribed the errors to Sr isotope disturbance by late-stage hydrothermal fluids. However, part of the error for the Cruachan data may be explained by the fact that these values include both CMG and CMD, which this work considers to have separate origins. Hence the Cruachan reflects a mixed assemblage.

I_{Sr} values for all the Etive rocks range from 0.70445 (diorites) to 0.7058 (Meall Odhar, type unspecified) (Clayburn et al. 1983). These low values are taken to indicate the incorporation of a mantle component.Dates obtained for the Lorne lavas (399±5Ma), Meall Odhar (398±6Ma) and Central Starav (389±4Ma) help to constrain the intrusive time interval from a maximum of 19Ma to a minimum of 1Ma (Clayburn 1981).

Data for O^{18} includes 4.1‰ for CMD (Harmon and Halliday 1980), 4.4-8.6‰ for Cruachan, and 8.3-9.7‰ for Meall Odhar and Central Starav (Clayburn 1981). The low values in Cruachan are explained as loss due to circulating hydrothermal fluids. Overall O^{18} values range from 7.2 to 9.8‰, which are slightly below the range for Caledonian granites (10 to 12‰) quoted by Harmon and Halliday (1980).

Lead isotope data for Pb^{206}/Pb^{204} (16.714 to 17.185, Clayburn et al. 1983; 17.5 (Cruachan) Blaxland et al. 1979) has consistently indicated that the crustal component in Etive was from ancient, relatively unradiogenic crust. Clayburn (1981) speculates that the crustal component was of Grenvillian age (c.1100Ma) with little or no upper crustal (Moine and Dalradian) component. Plant et al. (1980) noted only traces of inherited zircons in Etive granitoids (type unspecified) which further suggests the exclusion of ancient, reworked crust. An age of 390±6Ma obtained by U-Pb dating methods on zircons from Etive (type unspecified) shows them to be concordant and hence of primary magmatic origin (Pidgeon and Aftalion 1978).

Neodymium and strontium isotope studies by Hamilton et al. (1980) showed that the combination of negative Δ Nd and positive Δ Sr values gave the Cruachan and PSMG rocks a definite crustal component. (Δ Nd and Δ Sr represent deviations of isotope composition from that of the bulk earth which is set to zero). Values of T_{CHUR} (which represents the minimum age of separation for Sm-Nd isotopes from the mantle, and hence an approximate age of the source) were obtained for CMG (840Ma) and for PSMG (1160 and 1230Ma). An average difference of 350Ma between the ages of the sources for these two magmas is useful evidence to show that they may have originated from different levels in the crust.

The most recent isotopic study on Etive combines Sr, Pb and O data (Clayburn et al. 1983) and observes that:

a). Etive is isotopically the least-evolved of the post-tectonic Caledonian granitoids

b). Emplacement of each unit was over a short time interval

c). The similar behaviour of all three isotopes indicates a common origin for each rock unit

Clayburn et al. (op cit) conclude that the Etive magmas were produced by melting of contemporary enriched mantle and lower crust of Grenville age (c.1100Ma) followed by episodic mixing of these two sources, with limited crystal fractionation within individual intrusive phases. Proportionately more crustal component was incorporated in the PSMG and MOG units.

The point which these authors miss is that the MOG is not part of a sequential magmatic evolution but has independent origins. Therefore their assumption that to generate the later, more mafic PSMG requires an influx of juvenile magma is not necessary. The complex genesis of the CMD (T) will have contributed to the large error in the data.

Fission track dating by Hurford (1977) on zircon and sphene gave ages in good agreement with the generally accepted figure of c.400Ma for Cruachan rocks. The date obtained from apatite was 298±17Ma (for CMD) which indicates the time at which this rock cooled to below 100^{o}C (the apatite blocking temperature). It

therefore took about 100Ma for the CMD to cool from about 800°C (Droop and Treloar 1981) to 100°C, a rate of 7°C/Ma.

Chemical evidence from the Cruachan monzodiorites (T) suggests that mixing may have taken place between quartz diorite compositions and a melt of mildly alkaline nature enriched in certain trace elements (Ba, Zr, La, Ce) to form these rocks. Wyllie (1983) has shown that syenitic liquids would be generated at depths of 50km by melting of crust with granitic composition. A partial melt from a felsic granulite could also yield such an enriched trace element assemblage (Collins et al. 1982) though it does not explain the enhanced Al and Ti levels seen in T samples.

On the whole, Etive granitoids do not show relic structures which might suggest large-scale in-situ anatexis (Pitcher 1979). Being a high-level intrusion (Droop and Treloar 1981) it is more likely that the magmas travelled some distance from their original source, requiring them to be reasonably dry, and therefore unlike anatectic melts.

The concept of magma mixing in the generation of granitoids is preferred by Hall (1972) because it explains the continuity found in the chemistry of Caledonian granites.

On the basis of Sr isotopes and low U levels, Stephens and Halliday (1984) argue that many Caledonian Newer granites originated from continental crust. In particular, they state that the more mafic rocks of the Caledonian eg diorites are the products of high-temperature mantle-derived melts, while the granites have resulted from localised melting at higher levels.

Plate tectonic review

The geochemistry of the Caledonian granites, typified by low Rb/Sr, high K/Na, and low K/Rb ratios, indicates a subduction regime related to the closure of the Iapetus Ocean (Brown 1979) which resulted in continent-continent collision at c.473Ma (Phillips et al. 1976). Since the collision was oblique east to west (Thirwall 1979, 1981) subduction-related magmatism persisted in the west until c.400Ma (Clayburn 1981).

Subduction may have begun 600±50Ma, although evidence for this is confused by metamorphism. The Dalradian trough represented by the deep water Creran Succession continued to expand during the Port Askaig glaciation, an event which deposited the Port Askaig tillite (Litherland 1980). This tillite horizon has been dated at 668±23Ma (Johnson 1983) and thus constrains the period of subduction. A compressional regime persisted throughout Ordovician times, producing metamorphism and anatexis of crustal rocks. This gave rise to the forceful newer granites of northern Scotland whose chemistry is similar to that of the country rocks (Pankhurst 1979). After collision, a period of relaxation ensued which saw the generation of the chemically-distinct late permitted granites of the SW Highlands (eg Cruachan granitoids of Etive). In contrast, the Starav pluton was emplaced forcefully. The chemical contrasts between Ordovician and Lower Old Red Sandstone granites is attributed to the differing nature of the basement rocks (Brown 1979), an idea supported by Stephens and Halliday (1984) who elaborate on it and

suggest that the mantle to the north is old and enriched in K, Ba and Sr by metasomatism.

Brown et al. (1981), from evidence of granulite xenoliths found in Carboniferous volcanics, suggest that the N Caledonides lie over continental crust, while van Breeman and Bluck (1981) emphasised the contribution of subducted sediment in the formation of the late Caledonian granites.

The Etive rocks reflect magmatism associated with syn- and late orogenic tectonics, resulting from continent-continent collision with attendent thickening of the crust.

CONCLUSION

The following diagram summarises the petrogenetic mechanisms which have determined the magma compositions seen in the Etive granitoids. The symbols are those used throughout the text.

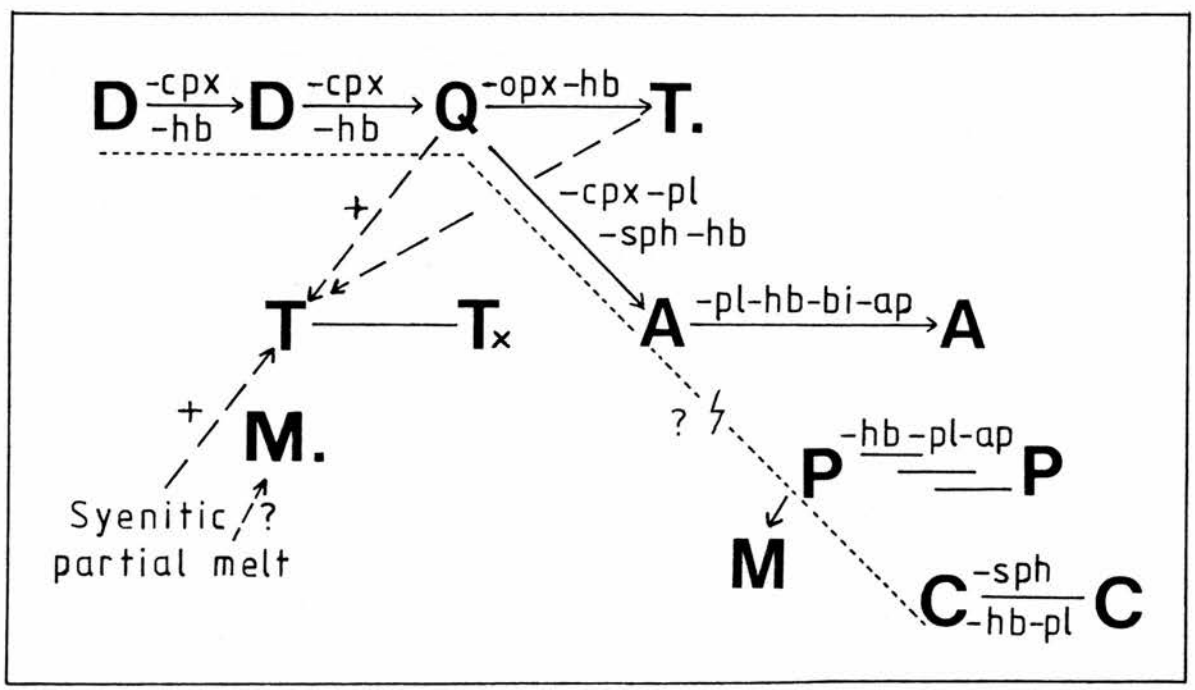

cpx=clinopyroxene, hb=hornblende, opx=orthopyroxene, pl=plagioclase, sph=sphene, bi=biotite, ap=apatite
'-' indicates removal by fractional crystallisation
'+' indicates addition by mixing
'.....' indicates the liquid line of descent of an inferred parental magma.
'——→' indicates liquid lines of descent during fractional crystallisation
'— — — —' indicates mixing paths

The overall trend for all the Etive magmas appears to be the result of fractionation of clinopyroxene, olivine, orthopyroxene, plagioclase and alkali feldspar from a parental magma. This excludes the CMD which lies off this general trend. On the other hand strong yttrium depletion suggests either a partial melting source from garnet or amphibole-rich crust, or fractional crystallisation of amphibole and apatite from a mafic parent. An enrichment in rubidium and thorium indicates the incorportion of a crustal component.

The dioritic rocks are similar to the Lorne Plateau andesites in major chemistry. The level of nickel is lower than in the andesites and may result from clinopyroxene fractionation from a basaltic parent. Variations within the diorites can be related to fractionation of clinopyroxene and hornblende giving rise to quartz diorite compositions. Diorites contain a higher proportion of mantle-derived isotope components and show a primitive chondrite-normalised trace element pattern. This evidence suggests that dioritic rocks originated direct from a mafic parent, unlike the andesites which show chemical and petrographic evidence of mixing.

The quartz diorite compositions developed in three different ways.

1. Orthopyroxene, hornblende and apatite fractionation produced the dark CMD (T.) rocks.

2. Clinopyroxene, hornblende, plagioclase and sphene fractionation produced CMG(A) rocks.

3. Mixing with syenitic melts formed CMD(T) rocks.

The syenitic melts could be produced by partial melting of granitic crust at depths of 50km. Also partial melting of felsic granulites can yield peraluminous melts rich in incompatible elements.

A silica-rich variant of T occurs around the SE, S and SW perimeter of the Cruachan intrusion and is interpreted as an annular intrusion of fractionated T (accumulated in the upper levels of an inferred T reservoir) associated with the Fault Intrusion and cauldron subsidence of Glen Coe. This intrusion has a steep contact with the host metamorphic rocks, in contrast with the area in the W, where T makes a complex interdigitating contact with the metasediments. The A (CMG) composition from the northern part of Etive reflects straightforward in-situ fractional crystallisation of hornblende, plagioclase, apatite, biotite, and alkali feldspar.

The Porphyritic Starav monzogranite intruded the Cruachan by forceful means, not by cauldron subsidence. Contact CMD samples show strong foliation and the Cruachan-Starav contact is sharp and not faulted. Neodymium isotope systematics give an age of separation 350Ma older than for the earlier Cruachan, and suggests that the Starav magma came from a different source. Chemical evidence indicates that the PSMG was intruded as at

least three separate pulses of magma. These chemical divisions can be correlated with topographic features in the field. The overall chemical trend can be related to in-situ fractionation of hornblende, plagioclase feldspar, alkali feldspar and apatite, though within each pulse hornblende is the dominant control. Mafic knots may represent fragments of unassimilated restite material from an earlier partial melting event. Isotope studies and the presnce of schlieren textures confirm the existence of a crustal component.

Chemical and field evidence shows that the late Central Starav monzogranite was a separate intrusion into the PSMG. It is highly fractionated with modal compositions close to the feldspar ternary minimum at 1kb. It is not related to the PSMG by direct fractionation, but is linked to a common Starav source magma.

Pervasive sheets of 'pink' Meall Odhar type granite which are found extensively in the Cruachan granitoids show bimodal chemistry. One type is a monzogranite, has a chemical composition typical of a fractionated calc-alkaline granite and is related to the emplacement of the Starav magmas. The second type is more alkaline, shows unusual trace element assemblages and is most likely a partial melt from a felsic granulite. The distribution of these two types was not investigated in detail and it would make an intriguing sequel to this work. Its field association wiht the CMD raises the question of whether it is related to the inferred partial melts which gave rise to the

CMD(T) compositions.

In conclusion, the Etive granitoid complex is represented by 10 chemically-distinct rock types, varying from diorite to alkali granite. Each group exhibits internal variations in chemistry which can be related to fractioanl crystallisation processes. All the separate types may be related to a common mafic parent but varying degrees of mixing with crustal material has blurred the genealogy. In the case of the 'primitive' Meall Odhar granite (M.), partial melting has been identified as the dominant mechanism, while for the CMD(T) rocks there is evidence for mixing between a crustal partial melt and a dioritic composition.

The whole complex was intruded within a relatively short period of time (between 1 and 19 Ma) at around 400 Ma, during the waning stages of the Caledonian orogenic event. Closure of the Iapetus Ocean at c.473Ma will have created a new tectono-magmatic environment (continent-continent collision) which may have had some bearing on the generation and composition of granitic melts.

The variety of chemistry seen in Etive is ascribed to mixing of mantle-derived and crustal-derived melts in variable proportions, with subsequent modification by fractional crystallisation processes. Further work on Etive might investigate the following:

*Delineation of the chemical discontinuities in

the Porphyritic Starav monzogranite.

*Discrimination and distribution of the Meall Odhar 'pink' granites.

*Delineation of the chemical boundary between CMD(T) and its silicic variant (Tx) and the relationship and contact of the latter with the CMG(A) rocks.

APPENDIX 1

A.1.1 Mineral Separation

Alkali feldspar was separated from a representative sample of each petrographic type.

The clean rock was crushed in a Jaw Crusher, consisting of mild steel jaws, then ground to a coarse powder (for 10 to 20 seconds) in a 100ml 'Tema' Tungsten Carbide mill. This powder was sieved to collect the -150+90 micron fraction (-120+170 mesh), which was washed free of fines with distilled water and then dried.

Magnetic minerals and particles were removed by means of a hand magnet wrapped in a filter paper which was combed through the sieved fraction repeatedly. The remaining material was passed through a 'Frantz Isodynamic Separator' with conditions set to give optimum separation of mafic from felsic minerals. The conditions set on the 'Frantz' separator were: 1.0amp, 20^{o} side slope, 20^{o} forward slope. The fractions were examined under a binocular microscope to check for purity.

For the purpose of determining the structural state of alkali feldspar a heavy liquid separation was carried out on the non-magnetic (felsic) fraction obtained from the preceding stage.

Tetrabromoethane (Sp.Gr. 2.98) was diluted with acetone to yield a liquid with Sp.Gr. 2.58-2.60. The felsic fraction was mixed with this liquid in a separating flask and allowed to stand for 60 minutes. Alkali feldspar (Sp.Gr. 2.56-2.57) floated, allowing the heavier minerals to be removed. The alkali feldspar was removed, washed with acetone and dried. (Hutchison 1974).

A.1.2 X-ray Diffraction

Alkali Feldspar Determination

Conditions

The instrument used was a Philips PW1540 goniometer with PW1010 generator. Conditions used were: Cu Ka radiation at 36kV 18mA. L.L.140, W.250, E.H.T. detector=412v. Dry, fine powder mounts were made and scanned 29-31° 2θ at 1/8th° /min to identify 131 and $1\bar{3}1$ peaks.
KBrO3 was added as internal standard and scans made over 20-52° 2θ at 1/2°/min to identify $\bar{2}01$, 060, $\bar{2}04$ peaks.

A.1.3 Analytical Methods

Rock samples had all surface contamination removed. The clean sample was broken down to small chunks (approximately 4cm cube) which were crushed in a Jaw Crusher with mild steel jaws. 60ml portions of the crushed material were powdered in a "Tema" mill with tungsten carbide mills for 1.5 minutes. The

accumulated portions of powder were mixed, cone and quartered, and opposite quarters were kept for analysis.

A.1.3.1 Wet Chemical Techniques

Major and selected trace elements were determined by a scheme which utilises a combination of published techniques and formed the basis for wet chemical analysis at St.Andrews. (Batchelor 1980).

SiO_2 Determined spectrophotometrically as the reduced blue silicomolybdenic acid complex, after fusion of the sample (0.05g) with NaOH in nickel crucibles.

Al_2O_3, Total Iron as Fe_2O_3, MnO, CaO, MgO Determined by AAS after fusion of 0.1g sample with 0.7g lithium metaborate, and dissolution in 2% v/v HNO_3. Lanthanum chloride hexahydrate (10% La solution) was added to produce a 0.5% La concentration.

TiO_2 Determined spectrophotometrically as the yellow $Ti-H_2SO_4-H_2O_2$ complex after dissolution of 0.5g sample in $HF/HClO_4$.

P_2O_5 Determined spectrophotometrically as the reduced blue phosphomolybdenic acid complex after dissolution of 0.5g sample in $HF/HClO_4$.

Na2O, K2O, Li, Zn Determined by AAS after dissolution of 0.5g sample in HF/HClO4. Ammonia was used to precipitate trivalent cations prior to the determination of Na and K.

FeO Determined volumetrically (redox titration) with potassium dichromate after cold HF attack on 0.2g sample in the presence of ammonium metavanadate.

H2O total Determined gravimetrically as a modified Penfield method.

Precision of major element analysis

	Mean%	Std.Devn.	C.V.%
SiO2	68.0	1.0	1.4
TiO2	0.50	0.02	4.0
Al2O3	15.70	0.10	0.6
Fe2O3t	2.23	0.07	3.2
FeO	2.0	0.03	1.4
MnO	0.03	0.01	33
MgO	1.01	0.01	1.0
CaO	2.56	0.04	1.6
Na2O	4.31	0.06	1.4
K2O	2.74	0.04	1.5
H2O	1.00	0.04	1.5

Precision of trace elements

	mean%	Std.Devn.	C.V.%
Li	43	1.0	2.3
Zn	56	0.8	1.4

A.1.3.2 X-ray Fluorescence

The following elements were determined from a pressed powder disc bonded with 10 drops of a 2% aqueous solution of a p.v.a. resin ("Moviol 66-100").The disc was pressed to 10 tons/sq.in. under vacuum for 1 minute and then dried.

Rb, Sr, Y, Zr, Nb, Th, Pb, V, Ba, Hf, Ce, La.

Instrumental Conditions

Trace Elements

Traces W-A. Programme utilising tungsten-target tube and scintillation counter.

Channel	Line	2θ°	Crystal	Count (secs.)	kV	mA	Coll.
1	bg	20.96	LiF200	100	60	32	coarse
2	Zr Ka	22.51	LiF200	100	60	32	coarse
3	Y Ka	23.76	LiF200	100	60	32	coarse
4	bg	24.24	LiF200	100	60	32	coarse
5	Sr Ka	25.15	LiF200	100	60	32	coarse
6	bg	26.28	LiF200	100	60	32	coarse

7	Rb Ka	26.57	LiF200	100	60	32	coarse
8	bg	27.15	LiF200	100	60	32	coarse
9	bg	20.96	LiF200	100	60	32	fine
10	Nb Ka	21.36	LiF200	100	60	32	fine
11	bg	24.24	LiF200	200	60	32	fine
12	bg	27.22	LiF200	200	60	32	fine
13	Th La1	27.45	LiF200	200	60	32	fine
14	Pb Lb1	28.24	LiF200	200	60	32	fine
15	bg	28.70	LiF200	200	60	32	fine

Traces Au-A. Programme using gold-target tube and gas flow proportional counter.

Channel	Line	2θ°	Crystal	Count (secs.)	kV	mA	coll.
1	bg	96.36	LiF220	40	60	32	coarse
2	Mn Ka	95.08	LiF220	40	60	32	coarse
3	bg	97.98	LiF220	40	60	32	fine
5	bg	120.49	LiF220	100	60	32	fine
6	V Ka	123.09	LiF220	100	60	32	fine
7	bg	130.44	LiF220	100	60	32	fine
8	Ba Lb1	128.64	LiF220	100	60	32	fine
9	bg	46.71	LiF200	100	60	32	fine
10	Hf La1	45.71	LiF200	100	60	32	fine
11	bg	70.61	LiF200	100	60	32	fine
12	Ce La1	71.51	LiF200	100	60	32	fine
13	bg	141.50	LiF220	200	60	32	coarse
14	La La1	138.80	LiF220	200	60	32	coarse
15	TiKb1+2	123.90	LiF220	20	60	32	fine

Multiple regression calibrations were employed for the following elements to account for line interferences.

element	line	interferant
V	Ka	Ti
Ba	Lb1	Ce
Y	Ka	Rb
Zr	Ka	Sr

Precision of trace element analysis(Zaleski,1982)

mean (ppm)	instrument precision		bead variation		combined std.devn.
	S.D.	C.V.%	S.D.	C.V.%	
Nb 27	1.18	4.30	1.59	5.81	2.0
Zr 217	0.92	0.43	6.93	3.20	6.9
Y 26	0.90	3.43	1.32	5.05	1.5
Sr 324	1.45	0.45	1.08	0.33	1.8
Rb 177	1.50	0.85	0.65	0.37	1.4
Th 24	3.03	12.42	0.55	2.27	4.2
V 35	0.78	2.27	0.50	1.45	0.91
Ba 910	8.70	0.96	2.68	0.30	7.5
La 105	1.30	1.25	1.10	1.05	1.3
Ce 129	2.10	1.63	1.11	0.86	2.0
Hf 5.8	0.35	6.00	0.26	4.46	0.41

APPENDIX 2

Sample List

RB001 NN014335

Small sample of contact between 'Cruachan' monzodiorite and a porphyrite dyke. East side of West quarry, Bonawe.

RB002 NN014335

Porphyrite dyke, locality as RB001.

RB003 NN013335

Pink aplite vein (vertical, 90cm. wide) in grey Cruachan monzodiorite, west quarry, Bonawe.

RB004 NN013335

Contact between Cruachan monzodiorite and porphyrite dyke, west Bonawe quarry.

RB005 NN013335

?Bonawe granodiorite? Upper part west Bonawe quarry.

RB006 NN008338

Fine grained ?Bonawe granodiorite? 100m west of Post Office, 20m above road, opposite house entrance, Bonawe. Close to contact with metasediments.

RB007 NN029340

Pale grey coarse Cruachan monzodiorite, in centre of small quarry, 2km ENE of Bonawe, opposite island Sgeir Lag Choan, Loch Etive.

RB008 NN029340

Red, haematised variant of RB007. 5m to east.

RB009 NN032340

Dark dyke, cutting both grey Cruachan monzodiorite and pink veins. Adjacent to track, Bonawe to Craig, west side of Loch Etive.

RB010 NN032340

Pink vein material cutting grey Cruachan monzodiorite. Locality as RB009.

RB011 NN032340

Contact between dark dyke and pink vein. Locality as RB009.

RB012 NN039352

Cruachan monzodiorite, dark grey at track side, 400m NNE Craig, west side of Loch Etive.

RB013 NN050374

Porphyritic Starav monzogranite, track side 600m NE of Cadderlie, west side of Loch Etive.

RB014 NN076407

Less porphyritic Starav type monzogranite on a scarp face, 400m NW from end of Forestry Commission track, 1km N of Barrs, west side of Loch Etive.

RB015 NN067401

Porphyritic Starav monzogranite, showing slight reddening, in river Allt Easach,by bridge on track, 900m WNW of Barrs, west side of Loch Etive.

RB016 NN056395

Aplite vein, cutting coarse porphyritic Starav monzogranite, in river Abhainn Dalach, 600m NW of Dail, west side of Loch Etive.

RB017 NN056395

Coarse porphyritic Starav monzogranite, host to RB016, locality as RB016.

RB018 NN045366

Coarse Porphyritic Starav monzogranite, red alteration. 400m S. of Cadderlie bridge.

RB019 NN037346

Grey Cruachan monzodiorite in trackside cutting, 300m S. of Craig.

RB020 NN032340

Contact between pink veins and grey granite, locality as RB009.

RB021 NN005380

Metasediment 10cm from contact with Cruachan granite, 30m above north bank of Eas a' Chrinlet, 4.3km N. of Bonawe Quarry.

RB022 NN005380

Thermally altered metasediment, as RB021

RB023 NN005380

Contact between metasediments and grey Cruachan granite.

RB024 NN005380

Grey Cruachan granite 10cm from contact, as RB021

RB025 NN017386

Grey Cruachan monzodiorite, 200m below contact with Meall Odhar granite, at "tor" outcrop 1km SW of Meall Dearg.

RB027 NN015386

Coarse grey granite on scarp face, 25m above Eas a' Chrinlet, 1.2km WSW of Meall Dearg.

RB028 NN006380

Pale grey Cruachan monzodiorite 50m above contact with underlying metasediments on N bank of Eas a' Chrinlet, opposite its junction with a multi-channelled tributary, 1.7km WSW of Meall Dearg.

RB029 NN094472

Grey Cruachan monzogranite, 20m above contact with porphyritic Starav granite. on edge of a gully, outer edge of Glen Etive forest, west limb, in Allt a' Bhioran, 1.1km S Lochan na Fola.

RB030 NN095469

Porphyritic Starav granite 350m W of Glen Etive forest, western boundary. 200m S of Allt a' Bhioran, 1.1km NE Lochan na Saobhaidhe.

RB031 NN107461

Aplite vein in Porphyritic Starav granite (RB032) at rounded "roche moutonne" 10m from SW edge of Glen Etive forest, 1km NE Meall nan Gobhar.

RB032 NN107461

Porphyritic Starav granite (crumbly), host to RB031.

RB033 NN108453

Central Starav granite. Boulder at bottom of scree slope, adjacent to stream, 300m N of pier, north end of Loch Etive.

RB034 NN114456

Central Starav monzogranite, by road bridge over Allt a' Bhioran, ajdacent to Gualachulain, Glen Etive.

RB035 NN143484

Grey Cruachan granite, in burn, under bridge in Gleann Charnan, Invercharnan, Glen Etive.

RB036 NN194510

Pink Cruachan granite, on riverside of River Etive, opposite Allt Chaorunn, Glen Etive.

RB037 NN210515

Pink Cruachan granite, jointed, bounded 3m each side by porphyrite dykes, in River Etive, 1.5km NE Allt Chaorunn, Glen Etive.

RB038 NN137566

Cruachan "Fault Intrusion", in road cutting, 50m W of junction of old Glencoe road and new A82(T) on new road, S side. Continues into bed of River Coe, Glen Coe.

RB039 NN256546

Granite, roadside exposure in ditch on N side of A82 road, 400m SE of concrete bridge over River Coe, 700m W of Kingshouse Hotel.

RB040 NN243423

Pink feldspars in green-grey matrix, 800m SE Clashgour, in tributary stream, 3km W Forest Lodge, Victoria Bridge.

RB041 NN256424

Coarse diorite, N side Linne nam Beathach at junction with Allt Toaig opposite green hut, 1.5km W Victoria Bridge.

RB042 NN256424

Darker variant of RB041, E side Allt Toaig, ajdacent to its junction with main river, locality as RB041.

RB043 NN265424

Pink fine grained granite underlying wrinkled metasediments, 1m from contact. Coarsens 2m from contact.

RB044 NN265423

Granitised metasediment, as RB043.

****

RB045 NN061472

Contact between diorite (lower) and metasediments (upper). Contact plane dips 45 S. E side deep gully at end of track from farm, Glen Ure.

RB046 NN064470

Pale grey fine grained granite 5m E of contact with metasediment block. 300m N Stob Gaibhre peak, Glen Ure.

RB047 NN064470

Pale pink coarse grained granite, 10m above RB046.

RB048 NN061473

Coarse quartz diorite from fallen blocks, 5m E of burn, 600m NNW Stob Gaibhre peak, Glen Ure.

RB049 NN063472

Fine grained diorite, 10m S of metasediment contact, 450m NNW Stob Gaibhre, Glen Ure.

RB050 NN227530

Flow banded ignimbrite, 50m above road, at cutting lay-by, Glen Etive.

RB051 NN227525

Pink weathered Cruachan monzogranite. Roof zone. Adjacent to ?felsite dyke or ? thermally altered rhyolite. Contains greisen veins. River Etive.

RB052 NN145494

Cruachan monzogranite, with quartzite and schist xenoliths. At base of crags above Craig na Callich, Glen Etive road.

RB053 NN175511

Pink ?porphyrite or ?chilled granite. Roof zone of Cruachan monzogranite. 700m E. of Dalness, Glen Etive.

RB054 NN182513

Grey porphyrite dyke in Cruachan monzogranite, Glen Etive.

RB055 NN184511

Coarse Cruachan monzogranite with distinct pink alkali feldspar crystals, Glen Etive.

RB056 NN202514

Coarse Cruachan monzogranite with pink alkali feldspar crystals. Hump on N. side of road, W. of bridge, Glen Etive.

RB057 NN215519

Greisenised pink Cruachan monzogranite, containing thin quartz veins, River Etive.

RB058 NN215519

Greisen vein in Cruachan monzogranite, River Etive.

RB059 NN064475

Weathered Cruachan monzogranite in contact with metasediment; outcrop 20m above path, 500m E. of end of track, Glen Ure.

RB060 NN064475

Cruachan monzogranite, 5m E of contact with metasediments, Glen Ure.

RB061 NN080470

Weathered Porphyritic Starav monzogranite, 30m E of its contact with Cruachan monzogranite, 150m W of Airigh nan Lochan, upper Glen Ure.

RB062 NN080470

Reddened Cruachan monzogranite, 2m W of contact with Porphyritic Starav monzogranite, as RB061.

RB063 NN078471

Grey Cruachan monzogranite showing slight foliation, at confluence of two streams 200m W of RB061-RB062 contact.

RB064 NN073473

Grey Cruachan monzogranite, close to aplite veins, upper Glen Ure.

RB064a NN073473

Contact between RB064 and aplite vein.

RB065 NN044433

Coarse Porphyritic Starav monzogranite on E facing ridge, 2km E of Meall Garbh, Creran.

RB066 NN044437

Red MOG-type, 50m over Allt Buidhe watershed, 2km ENE Meall Garbh,Creran.

RB067 NN045438

Dark grey Cruachan granitoid, 10m from inferred contact with Porphyritic Starav monzogranite, 2km ENE Meall Garbh, Creran.

RB068 NN046438

Porphyritic Starav monzogranite, 10m from contact with Cruachan granitoid (RB067), 2km ENE of Meall Garbh, Creran.

RB069 NN041439

Dark Cruachan monzodiorite containing MOG veins. Orientated sample showing slight foliation parallel to the Porphyritic Starav monzogranite contact. 100m W of Allt Buidhe watershed, 2km ENE Meall Garbh, Creran.

RB070 NN040440

Cruachan monzodiorite containing 30mm wide MOG vein, upper reaches of Allt Buidhe, 1.75km NE Meall Garbh, Creran.

RB071 NN040440

Cruachan monzodiorite without MOG veins, as RB070.

RB072 NN035439

Cruachan monzodiorite, Allt Buidhe Stream, 1.5km NE Meall Garbh, Creran.

RB073 NN034439

Pale Cruachan monzodiorite, 100m E of contact with metasediments. Red net veining is common. Slightly weathered. 1km NE Meall Garbh, Creran.

RB074 NN161380

Coarse Porphyritic Starav monzogranite, under footbridge on River Kinglass, 400m SW Glenkinglass Lodge, Glen Kinglass.

RB075 NN152370

Porphyritic Starav monzogranite close to its contact with Cruachan monzodiorite, outcrop on track, 600m SSW of confluence of Allt Hallater and River Kinglass, Glen Kinglass.

RB076 NN146363

Pale Cruachan granitoid , containing pods of finer material, close to contact with Porphyritic Starav monzogranite. River Kinglass, 2.5km SW Glenkinglass Lodge.

RB077 NN134357

Pale Cruachan granitoid showing foliation and containing abundant net veining, close to footbridge, 1.75km S Beinn nan Lus, Glen Kinglass.

RB078 NN110366

Porphyritic Starav monzogranite, 200m up burn from track (by ruin of schoolhouse), 3km ESE Ardmaddy, Glen Kinglass.

RB079 NN101365

Porphyritic Starav monzogranite from river bed, 2.2km ESE of Ardmaddy, Glen Kinglass.

RB080 NN091368

Porphyritic Starav monzogranite from newly blasted track section, 1km SE Ardmaddy, Glen Kinglass.

RB081 NN064357

Cruachan with indurated red zones and containing mafic-rich inclusions. On track-side close to Porphyritic Starav monzogranite - Cruachan monzodioritecontact zone, 400m SW Inverliver.

RB082 NN061356

Cruachan monzodiorite close to contact with Porphyritic Starav monzogranite. Contains large and small red veins. Track side 800m WSW Inverliver.

RB083 NN060356

Dark Cruachan monzodiorite with pink veins in locality. Track side, 900m SW Inverliver

RB083B NN060356

Pink granite sheet in dark Cruachan monzodiorite. Locality as RB083.

RB084 NN054351

Pink granite (?MOG) sheet 70m wide cutting dark Cruachan monzodiorite. On trackside 800m N Glennoe Farm.

RB085 NN053350

Porphyrite dyke close to pink granite sheet. Track side 700m N Glennoe Farm.

RB086 NN053350

Contact of porphyrite dyke with pink granite. Locality as RB085.

RB087 NN052349

Dark Cruachan monzodiorite. Trackside 700m NW Glennoe Farm.

RB088 NN052348

Dark grey, fine grained rock intruding Cruachan monzodiorite. Local spheroidal weathering. On trackside 600m NW Glennoe Farm.

RB089 NN053347

Contact between dark Cruachan monzodiorite and pink granite (MOG) sill. Large amphibole crystals have developed at the contact. Track side, 400m NW Glennoe Farm.

RB090 NN047340

Light coloured Cruachan monzodiorite on track side 200m S mouth of River Noe.

RB091 NN039333

Porphyrite dyke with red veining on track side in Fearnoch Forest, 400m NW Barran Dubh.

RB092 NN082417

Non-porphyritic Porphyritic Starav monzogranite 2km NNE Barrs.

RB093 NN092419

Central Starav monzogranite ? on Loch Etive footpath, NE of Barrs.

RB094 NN089413

Starav granite near inferred contact zone. Contains red veins. On lochside footpath in wood, 2km N Barrs.

RB095 NN087409

Porphyritic Starav monzogranite on lochside, 1.5km NE Barrs.

RB096 NN074403

Porphyritic Starav monzogranite from footpath on loch side, 500m N Barrs.

RB097 NN045361

Porphyrite dyke by track side, 900m S Cadderlie.

RB098 NN044355

Cruachan monzodiorite 1m from contact with pink granite (MOG) intrusion. Promontory 800m NE Craig.

RB098A NN044355

Pink granite (MOG), coarse. Locality as RB098.

RB099 NN135448

Central Starav monzogranite from base of crags, 2.4km NNE Ben Starav summit.

RB100 NN134445

Central Starav monzogranite from base of crags, 2km NNE Ben Starav summit.

RB101 NN132441

Central Starav monzogranite from crags, 1.5km NNE of Ben Starav summit.

RB101a NN132441

Coarse quartz and alkali feldspar pegmatite; locality as 101.

RB102 NN135460

Starav granite in stream by bridge, 500m SW Coileitir, Glen Etive.

RB103 NN132441

Central Starav monzogranite from within convoluted ?weathered joints, on vertical face of crag some 20m below RB101, Ben Starav.

RB104 NN128427

Central Starav monzogranite, fine grained, from 200m below E side of Ben Starav summit.

RB105 NN129426

Central Starav monzogranite scree boulder, coarse grained, from 200m below E side of Ben Starav summit.

RB106 NN127426

Central Starav monzogranite, fine grained, close to Ben Starav summit.

RB107 NN052348

Fine grained, dark ?dioritic composite dyke, veined by coarse felsic crystalline material. Trackside 600m NW Glennoe Farm.

RB107v NN052348

Coarse crystalline material invading RB107.

RB108 NN055345

Porphyritic grey rock,?dioritic, associated with a composite dyke. 200m above Glennoe Farm.

RB109 NN032324

Pink Cruachan 'granitoid' containing metasedimentary xenolith, close to a MOG or aplite intrusion. Cruachan forest, 400m SE Port na Mine, on track to Glen Noe.

RB110 NN032342

Contact between fine grained dark grey dyke, 4m wide, (containing porphyrite xenolith) with grey monzodiorite. Bluff on N side of track from Bonawe Quarry to Craig.

RB111 NN032342

Slightly pinker version of RB110, host to 30cm wide porphyrite dyke with a sinuous mutual contact.

RB112 NN033342

10m E from RB111, slickensided bluff of dark monzodiorite, containing 15cm pink vein which merges into it.

RB113 NN034342

Greyish monzodiorite, in track cutting on N side of bay 750m SW Craig.

RB114 NN035343

200m NNE of RB113 in track cutting. Grey monzodiorite containing fine grained pink dyke.

RB115 NN035343

15m NNE from RB114. Grey monzodiorite.

RB116 NN036344

200m NE from RB114. Fine grained dark sill intruded into pinkish- grey monzodiorite. The contact is sharp, with evidence of chilling in the sill, and the monzodiorite is plucked by the sill. 500m SSW craig.

RB117 NN036344

Grey monzodiorite, host to RB116.

RB118 NN044354

Pinkish-grey fine grained granitoid, in an area of pink granite sheets, containing mafic knots. Bluff on rocky shore, 750m NE Craig.

RB119 NN044354

Greenish-grey dyke 8cm wide cutting granitoid RB118.

RB120 NN044354

Grey granitoid from bluff area 10m N of RB118, further away from the pink granite sheets.

RB121 NN044354

Darker and finer grained than RB120. 50m S of RB120.

RB122 NN042354

Indurated dark grey monzodiorite exhibiting spheroidal weathering. Trackside outcrop 120m E of pink granite bluff, N end of bay N of Craig.

RB123 NN042354

Saccharoidal medium-grained pink granite. Vein in monzodiorite at bluff N end of bay N of Craig.

RB124 NN043357

Medium grained monzodiorite, trackside exposure, 300m N RB123.

RB125 NN043359

Porphyrite sill resting on 'pink' granite. Contact is sinuous with injection of 'pink' granite into sill. Trackside quarry, 160m N of RB124, by Port Mor.

RB126 NN043360

Medium grained pinkish-grey monzodiorite showing spheroidal weathering. 15m N of RB125.

RB127 NN045361

Porphyrite dyke in contact with 'pink' granite, W side of track, 750m S Cadderlie.

RB128 NN045362

Dark grey monzodiorite containing 3cm wide vertical white granophyre vein. Monzodiorite is bounded by 'pink' granite. 200m N of RB127.

RB129 NN045362

Porphyrite dyke in contact with coarse pink granite, 20m N RB128.

RB130 NN045363

Porphyrite dyke, 100m N of RB128.

RB131 NN045364

Coarse grey crystalline rock, rich in amphibole. ?diorite. In stream gully on W side of track 500m S Cadderlie.

RB132 NN039333

Grey monzodiorite adjacent to porphyrite sill/dyke, E side of track, 400m NW Barran Dubh.

RB133 NN067464

'Pink' granite sill, in extensive outcrop of grey granitoid, dipping E towards Starav intrusion. 500m SSE Stob Gaibhre.

RB134 NN067462

Contact between apophysis of Porphyritic Starav (contining 2cm alkali feldspar phenocryst) and Cruachan granitoid. 100m NE of deep stream gully, 750m SSE Stob Gaibhre.

RB135 NN059458

Medium grained pale grey Cruachan granitoid on N side of large stream draining scree-filled corrie of Beinn Sgulaird.

RB136 NN059458

Fine grained pale grey rock adjacent to a massive 'pink' granite sheet, ?hornfels/xenolith. Locality as RB135.

RB137 NN088410

Porphyritic Starav monzogranite, reddened, adjoining coarse quartz-alkali feldspar pegmatite, in burn gully 20m inla from loch side, 1.5km N Barrs.

RB138 NN088411

Starav ?central, reddened, from N bank of burn, as RB137.

RB139 NN088410

Porphyritic Starav monzogranite 20m S burn, on loch shore. As RB137.

RB140 NN088410

Starav ?central, displaying schlieren texture, N of burn, shore outcrop between RB138 and RB139.

APPENDIX 3

Geochemical Modelling

Major elements: A subtractive calculation, listed as FRXTLLN.FOR Fortran programme, was used to calculate liquid compositions after removal of varying proportions of selected rock-forming mineral compositions, noted below, from a high-alumina basalt (de la Roche et al. 1980).

*Plagioclase feldspar (An_{80}), plagioclase feldspar (An_{30}), olivine (Fo_{96}), hornblende, biotite, apatite, sphene, magnetite, and enstatite (from Deer et al. 1966).

*Augite (Haslam 1968).

VECTOR KEY

cpx=clinopyroxene, hb=hornblende, pl=plagioclase, sph=sphene, bi=biotite, ap=apatite, en=enstatite, mt=magnetite, ol=olivine

wt %	H.a.b.	PlagAn80	PlagAn30	OlFo96	Cpx	Horn
SiO2	49.00	49.06	58.10	41.07	51.83	44.99
TiO2	1.23	0.00	0.01	0.05	0.42	1.46
Al2O3	17.23	32.14	26.44	0.56	1.67	11.21
Fe2O3	2.27	0.27	0.04	0.65	2.25	3.33
FeO	6.76	0.00	0.15	3.78	8.55	13.17
MnO	0.16	0.00	0.00	0.23	0.24	0.31
MgO	7.41	0.20	0.03	54.06	14.07	10.41
CaO	11.22	15.38	7.84	0.00	21.04	12.11
Na2O	2.77	2.57	6.48	0.00	0.57	0.97
K2O	0.29	0.17	1.10	0.00	0.12	0.76
P2O5	0.14	0.00	0.00	0.00	0.00	0.17

wt %	Biot	Apat	Sphene	Magnt	Enst
SiO2	34.33	0.00	30.44	0.27	57.73
TiO2	3.63	0.00	39.66	0.00	0.04
Al2O3	14.80	0.00	0.00	0.21	0.95
Fe2O3	2.48	0.00	0.00	68.85	0.42
FeO	19.07	0.21	0.14	30.78	3.57
MnO	0.35	1.52	0.05	0.00	0.08
MgO	11.62	0.54	0.00	0.00	36.13
CaO	1.56	52.40	27.20	0.00	0.23
Na2O	0.65	0.00	0.37	0.00	0.00
K2O	8.16	0.00	0.00	0.00	0.00
P2O5	0.00	40.98	0.00	0.00	0.00

Trace elements: The Rayleigh fractionation model, listed as TRMODEL.FOR Fortran programme, was used to generate vectors for liquid evolution after removal of varying proportions of rock-forming minerals. The table of distribution coefficients was compiled from various literature sources. A theoretical starting trace element composition was used.

Values underlined were extracted from Cox et al. (1979). Other values were compiled from: Wedepohl (1969), Pearce and Norry (1979), Gill (1981), Leeman and Phelps (1982) and Shervais (1982).

Synthetic		Distribution Coefficients								
	(ppm)	Kfeld	Plag	Biot	Horn	Cpx	Apat	Sph	Magt	Opx	Ol
Ti	1000	0.0	0.0	6	4	1.7	0.0	(100)	12	0.4	0.0
V3+	500	0.0	0.0	1.8	13	5	0.0	0.0	67	1.1	0.1
Rb	100	0.4	0.1	3.1	0.4	0.0	0.0	0.0	0.0	0.0	0.0
Sr	200	4.0	4.4	0.1	0.5	0.5	0.0	0.0	0.0	0.0	0.0
Y	20	0.0	0.0	1.1	3.5	2.3	30	10	1.1	0.6	0.0
Zr	200	0.0	0.0	1.2	0.5	0.3	0.0	27	0.4	0.1	0.0
Nb	20	0.0	0.0	6.0	2.0	0.4	0.1	52	1.4	0.4	0.0
Hf	10	0.0	0.0	9.2	0.4	0.7	0.0	(27)	1.9	0.1	0.0
La	50	0.0	0.2	7.7	0.2	1.1	21	8	0.1	0.0	0.0
Ce	50	0.0	0.2	2.8	1.5	0.5	35	53.3	1.7	0.0	0.0
Ba	1000	6.0	0.8	10	0.4	0.0	0.0	0.0	0.0	0.0	0.0

TRMODEL.FOR

```
c       This programme calculates compositions of silicate melts after
c       continuous removal of given % of specified mineral.

        dimension oxide(12),xminl(12),resultox(12),corrox(12)
        real*8 name,minname

        print *, 'This programme calculates compositions
     &   of silicate melts after repeated removal of x %
     &   of a specified mineral'
        read(9,1) name,(oxide(i),i=1,12)
  1     format(a8,11f6.2/f6.2)
         print *, 'Enter mineral name and analysis in
     &   a8,11f6.2/f6.2'
        read(5,2) minname,(xminl(i),i=1,12)
  2     format(a8,11f6.2/f6.2)

        print*, 'Type in value of x in terms of decimal part of 100,
     &  e.g. 0.05 for 5%.'
        read*, x

        write(88,6) name,minname
  6     format(//2x,a8,'-fractionation of',4x,a8)


c       Removal of x% of mineral and summation
  20    sum=0.0
        do 3 i=1,12
        resultox(i)=oxide(i)-(xminl(i)*x)
        sum=sum+resultox(i)
  3     continue


c       Recalculation of products to 100%
        factor=100.0/sum
        do 4 i=1,12
        corrox(i)=resultox(i)*factor
  4     continue


        write(88,5)(corrox(i),i=1,12)
  5     format(/8x,12f6.2)

c       Assign old values to new ones
        do 80 i=1,12
        oxide(i)=corrox(i)
        if(corrox(i).le.0.0) go to 99
 80     continue
        go to 20
 99     call exit
        end
```

FRXTLLN.FOR

```
c       Programme to calculate Rayleigh fractionation trends in trace
c       elements reading distribution coefficients (Kd) from a file
c       and using a hypothetical starting composition.
c
        real dc(13,10),trdat(13),cl(13,10)
        real*8 rocknm,min(10),trtitl(13)
        data trtitl/'Ti','V','Cr','Ni','Rb','Sr','Y','Zr','Nb','Hf','La',
     &  'Ce','Ba'/

c       reads synthetic trace element analysis from TR.DAT assigned for009
        read(9,1) rocknm,(trdat(i),i=1,13)
    1   format(a8,10f6.1/3f6.1)

c       reads table of Kd values stored in file KD.DAT assigned for002

        read(2,2)(min(j),(dc(i,j),i=1,13),j=1,10)
    2   format(a8,10f6.1/3f6.1)

        f=0.95
   90   do 40 j=1,10
        do 40 i=1,13
        cl(i,j)=trdat(i)*(f**(dc(i,j)-1.0))
   40   continue

        z=((1.0-f)*100.0)
        write(13,4) z
    4   format(/2x,'Percentage crystallisation =',f6.2)
        write(13,5)(trtitl(i),i=1,13)
    5   format(9x,7a5/9x,6a5)

        write(13,7)(min(j),(cl(i,j),i=1,13),j=1,10)
    7   format(/9x,a8,7f8.1/6f8.1)

        f=f-0.05
        if(f.le.0.05) go to 99
        go to 90
   99   call exit
        end
```

MAJOR ELEMENT DATA TABLES

Samples prefixed 'A' are taken from Brown (1975)

DIORITIC ROCKS

	RB048	RB049	RB131	A022	A163	RB088
SiO2	54.10	53.50	56.35	57.46	56.54	59.70
TiO2	0.62	0.79	0.89	1.04	1.05	1.06
Al2O3	15.17	16.71	17.89	17.20	16.41	15.93
Fe2O3	1.86	1.33	0.73	2.61	2.33	1.44
FeO	5.80	6.19	5.00	4.42	4.19	4.15
MnO	0.14	0.14	0.09	0.11	0.14	0.11
MgO	7.24	6.47	4.48	4.72	5.98	3.66
CaO	7.88	7.88	5.92	6.86	7.34	5.32
Na2O	3.13	3.13	3.91	2.35	3.53	3.92
K2O	2.66	1.98	2.51	1.92	1.89	2.37
P2O5	0.25	0.16	0.47	0.32	0.28	0.36
H2Ot	1.00	1.00	0.80	0.95	0.98	1.30
Total	99.85	99.28	99.04	99.96	100.66	99.32

	A020	A162	A164
SiO2	61.87	61.44	61.28
TiO2	0.82	0.83	0.82
Al2O3	17.14	17.17	16.63
Fe2O3	2.04	1.39	2.12
FeO	3.27	3.45	3.47
MnO	0.09	0.09	0.10
MgO	3.15	3.51	3.46
CaO	4.79	5.13	4.88
Na2O	2.85	3.41	3.27
K2O	3.14	2.96	3.21
P2O5	0.23	0.27	0.25
H2Ot	0.84	0.60	0.75
Total	100.23	100.25	100.24

CRUACHAN MONZODIORITES

	RB071	RB083	RB087	RB012	RB019	RB025
SiO2	57.60	57.40	60.50	58.00	56.00	58.30
TiO2	1.43	1.37	1.22	1.25	1.39	1.23
Al2O3	18.27	17.80	17.57	19.22	19.87	19.47
Fe2O3	2.51	1.81	1.17	2.15	2.17	1.99
FeO	3.97	4.42	4.02	3.22	3.88	3.14
MnO	0.10	0.06	0.07	0.07	0.08	0.08
MgO	2.66	2.81	2.48	2.29	2.30	2.26
CaO	5.21	5.13	5.32	4.79	5.18	4.64
Na2O	4.35	4.58	3.83	4.77	4.70	4.82
K2O	2.15	2.72	2.51	2.76	2.71	3.01
P2O5	0.44	0.37	0.33	0.29	0.43	0.27
H2Ot	1.20	1.02	0.74	0.78	1.08	0.92
Total	99.89	99.49	99.76	99.59	99.79	100.13

	RB090	RB110	RB122	A155	A156	RB007
SiO2	60.10	56.34	57.47	56.43	55.69	62.60
TiO2	1.38	1.37	1.23	1.20	1.17	1.00
Al2O3	18.38	18.55	20.21	20.41	19.03	17.58
Fe2O3	1.32	2.68	1.73	2.68	2.54	1.50
FeO	3.63	3.80	3.50	3.19	3.58	3.04
MnO	0.08	0.09	0.08	0.10	0.11	0.07
MgO	2.01	3.04	2.57	2.18	2.90	1.81
CaO	4.58	5.86	4.39	5.23	5.54	4.22
Na2O	4.39	4.23	4.79	4.23	4.91	4.48
K2O	3.12	2.57	2.69	2.82	2.79	3.22
P2O5	0.31	0.43	0.38	0.39	0.39	0.23
H2Ot	0.80	0.80	1.00	0.39	1.40	0.76
Total	100.10	99.76	100.04	99.25	100.05	100.51

	RB028	RB073	RB098	RB107V	RB109	A157
SiO2	59.50	63.40	62.40	63.14	62.70	61.46
TiO2	1.04	0.90	0.93	0.69	0.73	0.87
Al2O3	20.19	18.27	16.84	17.09	18.73	19.27
Fe2O3	1.43	0.30	1.58	0.84	1.33	2.12
FeO	2.93	3.25	2.92	2.50	2.03	2.13
MnO	0.06	0.05	0.08	0.05	0.05	0.08
MgO	1.56	1.22	2.56	1.91	0.99	1.49
CaO	3.99	3.10	4.15	3.60	2.69	3.47
Na2O	5.02	5.28	5.24	4.23	5.33	4.11
K2O	3.45	3.17	2.43	3.82	3.97	4.28
P2O5	0.22	0.17	0.25	0.22	0.13	0.17
H2Ot	0.86	0.70	0.86	0.20	0.70	0.87
Total	100.25	99.81	100.24	98.29	99.38	100.32

BONAWE GRANITOID

	RB005	RB006
SiO2	61.70	63.00
TiO2	0.94	0.86
Al2O3	18.25	16.14
Fe2O3	0.20	0.59
FeO	3.95	3.98
MnO	0.07	0.07
MgO	1.78	2.83
CaO	3.76	3.90
Na2O	4.30	4.01
K2O	3.34	3.20
P2O5	0.42	0.29
H2Ot	0.70	0.86
Total	99.41	99.73

CRUACHAN MONZOGRANITES

	RB029	RB035	RB036	RB051	RB052	RB055
SiO2	66.00	65.50	67.60	66.30	65.90	67.60
TiO2	0.72	0.82	0.69	0.66	0.74	0.57
Al2O3	15.67	16.13	15.62	16.18	16.52	15.94
Fe2O3	1.94	2.49	1.46	1.89	0.88	1.58
FeO	1.72	1.32	1.51	1.97	2.41	1.23
MnO	0.06	0.07	0.05	0.07	0.04	0.04
MgO	1.91	2.07	1.48	2.22	1.72	1.43
CaO	2.94	2.61	2.51	2.42	3.25	2.27
Na2O	4.03	4.24	3.67	3.90	3.95	3.66
K2O	4.05	4.11	4.18	3.76	3.78	4.50
P2O5	0.21	0.15	0.19	0.23	0.15	0.15
H2Ot	0.72	0.78	0.70	0.78	0.70	0.68
Total	99.97	100.29	99.66	100.38	100.04	99.65

	RB057	RB064	RB076
SiO2	68.30	64.30	65.60
TiO2	0.57	0.77	0.74
Al2O3	15.17	15.85	15.72
Fe2O3	1.27	1.74	0.89
FeO	1.55	2.32	2.76
MnO	0.05	0.07	0.06
MgO	1.48	2.32	2.05
CaO	2.35	3.50	3.26
Na2O	3.63	4.13	4.07
K2O	4.25	3.36	3.52
P2O5	0.20	0.33	0.21
H2Ot	0.70	0.86	0.80
Total	99.52	99.55	99.68

MEALL ODHAR GRANITES

	RB010	RB066	RB084	A108	RB026	RB083B
SiO2	76.70	75.30	76.30	77.11	75.50	75.80
TiO2	0.15	0.31	0.22	0.13	0.15	0.24
Al2O3	12.52	12.59	12.88	12.88	12.86	12.99
Fe2O3	0.43	0.10	0.60	0.10	0.63	0.42
FeO	0.19	0.74	0.29	0.63	0.34	0.45
MnO	0.01	0.01	0.02	0.05	0.02	0.01
MgO	0.08	0.17	0.12	0.01	0.10	0.11
CaO	0.17	0.49	0.26	0.11	0.17	0.29
Na2O	2.78	3.20	3.98	3.79	2.82	3.50
K2O	6.65	6.31	5.24	5.14	6.62	5.87
P2O5	0.01	0.02	0.01	0.01	0.01	0.01
H2Ot	0.42	0.36	0.32	0.26	0.40	0.36
Total	100.11	99.60	100.24	100.22	99.62	100.05

	RB098A	RB123	RB016
SiO2	78.40	76.17	77.11
TiO2	0.20	0.16	0.06
Al2O3	11.04	13.57	13.23
Fe2O3	0.65	0.40	0.60
FeO	0.06	0.38	0.05
MnO	0.01	0.02	0.01
MgO	0.11	0.28	0.38
CaO	0.23	0.46	0.46
Na2O	3.63	4.04	3.39
K2O	4.74	5.16	5.15
P2O5	0.01	0.01	0.01
H2Ot	0.40	0.20	0.20
Total	99.48	100.85	100.65

PORPHYRITIC STARAV MONZOGRANITES

	RB013	RB015	RB017	RB065	RB074	RB075
SiO2	66.70	69.80	69.40	67.00	69.70	70.40
TiO2	0.56	0.51	0.43	0.60	0.49	0.43
Al2O3	15.46	14.65	16.06	15.41	14.76	14.97
Fe2O3	1.42	1.26	1.07	1.59	0.63	0.19
FeO	1.90	1.92	1.29	1.60	1.58	1.91
MnO	0.04	0.05	0.04	0.06	0.05	0.04
MgO	1.55	1.45	0.94	1.65	0.91	0.91
CaO	2.94	1.67	2.29	2.56	2.00	2.00
Na2O	3.97	3.54	3.84	4.43	4.13	4.03
K2O	4.13	4.28	4.36	3.94	4.50	3.97
P2O5	0.16	0.18	0.12	0.19	0.12	0.13
H2Ot	0.60	0.56	0.52	0.82	0.64	0.60
Total	99.43	99.87	100.36	99.85	99.51	99.58

	RB078	RB080	RB095	RB096	RB014	RB092
SiO2	70.50	69.00	71.20	72.00	73.50	73.90
TiO2	0.54	0.49	0.38	0.27	0.22	0.35
Al2O3	14.43	15.72	14.09	14.09	14.05	13.70
Fe2O3	0.72	1.00	0.52	0.54	0.01	0.86
FeO	1.30	1.61	1.11	1.03	1.19	0.64
MnO	0.04	0.04	0.03	0.01	0.01	0.04
MgO	0.91	1.16	0.63	0.60	0.43	0.54
CaO	1.62	2.42	1.23	1.43	0.97	1.08
Na2O	4.34	4.73	4.18	4.41	3.63	3.63
K2O	4.37	4.54	5.41	4.86	5.03	4.66
P2O5	0.12	0.15	0.07	0.07	0.04	0.05
H2Ot	0.70	0.66	0.68	0.66	0.44	0.66
Total	99.59	101.52	99.53	99.97	99.52	100.11

CENTRAL STARAV MONZOGRANITES

	RB034	RB093	RB101	RB104	RB106
SiO2	75.00	75.30	76.00	76.00	75.80
TiO2	0.16	0.31	0.14	0.18	0.16
Al2O3	13.35	13.35	13.35	13.23	13.23
Fe2O3	0.25	1.18	0.61	0.26	0.87
FeO	0.67	0.08	0.32	0.71	0.17
MnO	0.02	0.02	0.04	0.03	0.04
MgO	0.31	0.35	0.22	0.32	0.25
CaO	0.61	0.95	0.51	0.60	0.65
Na2O	3.81	3.49	3.61	3.47	3.60
K2O	4.74	4.44	4.83	4.68	4.65
P2O5	0.03	0.04	0.02	0.03	0.03
H2Ot	0.46	0.60	0.56	0.62	0.60
Total	99.41	100.11	100.21	100.13	100.05

TRACE ELEMENT DATA TABLES

Samples prefixed 'A' are taken from Brown (1975)

DIORITIC ROCKS

	RB049	A022	A163	RB131	RB088	A020
Li	24				25	
V	182	128	122	146	106	80
Zn	78	98	85		86	80
Rb	52	40	40	75	74	66
Sr	920	1218	1235	1058	872	944
Y	18	32	19	17	19	24
Zr	83	196	188	152	203	219
Nb	2			6	11	
Ba	545	701	801	1406	793	1383
La	14			33	39	
Ce	15			64	61	
Hf	2			3	4	
Pb	8			26	12	
Th	5			1	5	

	A162	A164
Li		
V	99	93
Zn	90	76
Rb	59	67
Sr	1012	943
Y	17	27
Zr	224	237
Nb		
Ba	1257	1363
La		
Ce		
Hf		
Pb		
Th		

CRUACHAN MONZODIORITES

	RB071	RB083	RB087	RB012	RB019	RB025
Li	42	37	32	24	15	17
V	158	146	137	101	117	97
Zn	86	81	75	80	108	87
Rb	67	74	104	59	64	66
Sr	1133	1330	1210	1213	1094	1175
Y	16	19	20	13	18	17
Zr	127	106	117	555	434	573
Nb	7	9	10	9	9	9
Ba	880	943	860	1921	1750	1875
La	33	34	33	60	54	49
Ce	45	53	60	79	85	78
Hf	3	3	3	8	6	8
Pb	13	8	12	5	8	11
Th	4	7	3	6	2	2

	RB090	RB110	RB122	A155	A156	RB007
Li	23					28
V	99	155	99	93	124	97
Zn	75			90	75	80
Rb	90	73	63	55	77	100
Sr	1038	990	1237	1167	1128	794
Y	17	19	14	26	24	22
Zr	393	124	661	493	284	338
Nb	12	11	11			15
Ba	2240	2035	2986	2769	1662	1716
La	62	54	61			71
Ce	93	78	94			120
Hf	5	2	10			5
Pb	6	9	10			16
Th	4	4	6			10

	RB028	RB073	RB098	RB107V	RB109	A157
Li	28	27	25		23	
V	70	60	101	59		74
Zn	70	65	77		48	69
Rb	69	88	100	58	86	75
Sr	1065	1018	814	882	834	865
Y	16	17	24	15		21
Zr	600	617	158	270		447
Nb	9	9	23	11		
Ba	1969	2020	850	2649	2766	1346
La	70	60	55	44		
Ce	106	92	81	73		
Hf	10	9	3	4		
Pb	6	11	16	12		
Th	2	5	15	9		

BONAWE GRANITOID

	RB005	RB006
Li	36	16
V	84	98
Zn	52	54
Rb	81	82
Sr	934	853
Y	24	18
Zr	327	193
Nb	12	10
Ba	1304	867
La	56	36
Ce	104	58
Hf	6	4
Pb	18	18
Th	4	7

CRUACHAN MONZOGRANITES

	RB029	RB035	RB036	RB051	RB052	RB055
Li	27	38	12	23	27	21
V	64	68	52	75	57	50
Zn	52	56	34	60	50	34
Rb	77	93	107	111	124	118
Sr	707	668	610	695	763	543
Y	17	16	18	19	20	17
Zr	172	192	193	189	188	172
Nb	13	10	11	8	12	7
Ba	1000	1000	812	875	1063	735
La	47	43	42	47	40	41
Ce	58	55	51	63	59	49
Hf	4	3	4	3	3	3
Pb	15	15	16	9	17	14
Th	8	6	20	10	5	13

	RB057	RB064	RB076
Li	11	29	29
V	55	78	72
Zn	37	50	67
Rb	114	76	103
Sr	571	766	727
Y	17	17	15
Zr	190	203	178
Nb	8	12	11
Ba	735	1000	1122
La	41	41	40
Ce	54	66	51
Hf	3	3	4
Pb	16	15	19
Th	14	7	9

MEALL ODHAR GRANITES

	RB010	RB066	RB084	A108	RB026	RB083B
Li	2	5	5		2	5
V	5	8	5	4	12	8
Zn	16	15	23	26	16	10
Rb	118	116	150	130	78	133
Sr	45	83	37	36	144	155
Y	13	17	14	14	8	4
Zr	93	154	109	100	175	65
Nb	6	13	13	13	3	8
Ba	220	600	270	100	688	165
La	23	39	50	47	36	28
Ce	30	64	72	59	58	11
Hf	1	2	1	3	3	1
Pb	18	20	27	30	2	25
Th	14	19	25	21	6	27

	RB098A	RB123
Li	4	
V	7	6
Zn	20	
Rb	85	59
Sr	140	56
Y	8	4
Zr	89	124
Nb	6	3
Ba	1070	532
La	53	41
Ce	65	58
Hf	1	1
Pb	22	27
Th	14	7

PORPHYRITIC STARAV MONZOGRANITES

	RB013	RB015	RB017	RB065	RB074	RB075
Li	27	33	33	34	36	32
V	54	47	36	56	35	34
Zn	53	66	39	55	41	41
Rb	96	110	98	117	130	96
Sr	766	402	646	711	528	598
Y	13	17	10	14	10	9
Zr	152	211	138	149	126	122
Nb	9	16	8	11	10	9
Ba	1098	688	825	1055	1234	1055
La	45	54	43	43	38	35
Ce	56	76	58	51	45	41
Hf	3	3	2	3	3	3
Pb	17	25	17	13	23	18
Th	18	15	9	6	12	8

	RB078	RB080	RB095	RB096	RB014	RB092
Li	29	35	35	38	23	40
V	32	44	21	21	15	19
Zn	41	41	34	33	31	32
Rb	103	105	135	129	143	150
Sr	460	709	324	304	282	264
Y	10	11	11	9	6	8
Zr	127	14	113	112	69	110
Nb	13	11	10	8	8	15
Ba	920	1120	600	720	667	500
La	43	37	34	39	33	41
Ce	48	42	46	41	28	38
Hf	3	3	2	1	1	2
Pb	22	18	28	26	33	29
Th	16	12	18	13	11	13

CENTRAL STARAV MONZOGRANITES

	RB034	RB093	RB101	RB104	RB106
Li	25	23	16	16	16
V	8	11	1	10	11
Zn	25	28	29	29	26
Rb	170	135	186	157	143
Sr	77	171	106	106	88
Y	8	9	6	12	7
Zr	82	89	78	92	77
Nb	13	10	10	7	9
Ba	200	250	190	223	190
La	27	37	26	26	30
Ce	34	37	32	30	35
Hf	1	1	1	1	1
Pb	33	28	34	27	29
Th	24	18	18	20	18

CIPW NORMATIVE MINERALOGY DATA TABLES

Note: TTDI represents the Thornton and Tuttle (1960) Differentiation Index (Q+Or+Ab)

TOTDI represents Total Diopside

TOTHY represents Total Hypersthene

DIORITIC ROCKS

CIPW Norm of Sample	RB048
Quartz	0.00
Orthoc	15.72
Albite	26.47
Anorth	19.49
Corndm	0.00
Di %Wo	7.50
Di %En	4.79
Di %Fs	2.22
Hy %En	10.38
Hy %Fs	4.81
Ol %Fo	2.00
Ol %Fa	1.02
Mag.	2.70
Haem.	0.00
Ilm.	1.18
Rutile	0.00
Titan.	0.00
Apatit	0.59
Water	1.00
Total	99.87
TTDI=	42.19
TOTDI=	14.51
TOTHY=	15.19

CIPW Norm of Sample	RB049
Quartz	0.13
Orthoc	11.70
Albite	26.47
Anorth	25.70
Corndm	0.00
Di %Wo	5.15
Di %En	3.10
Di %Fs	1.78
Hy %En	13.01
Hy %Fs	7.45
Ol %Fo	0.00
Ol %Fa	0.00
Mag.	1.93
Haem.	0.00
Ilm.	1.50
Rutile	0.00
Titan.	0.00
Apatit	0.38
Water	1.00
Total	99.29
TTDI=	38.30
TOTDI=	10.03
TOTHY=	20.45

CIPW Norm of Sample	RB131
Quartz	3.20
Orthoc	14.83
Albite	33.07
Anorth	23.86
Corndm	0.00
Di %Wo	1.02
Di %En	0.59
Di %Fs	0.38
Hy %En	10.57
Hy %Fs	6.89
Ol %Fo	0.00
Ol %Fa	0.00
Mag.	1.06
Haem.	0.00
Ilm.	1.69
Rutile	0.00
Titan.	0.00
Apatit	1.11
Water	0.80
Total	99.07
TTDI=	51.10
TOTDI=	1.99
TOTHY=	17.46

CIPW Norm of Sample	A022
Quartz	13.87
Orthoc	11.34
Albite	19.88
Anorth	30.72
Corndm	0.00
Di %Wo	0.51
Di %En	0.34
Di %Fs	0.13
Hy %En	11.41
Hy %Fs	4.32
Ol %Fo	0.00
Ol %Fa	0.00
Mag.	3.78
Haem.	0.00
Ilm.	1.98
Rutile	0.00
Titan.	0.00
Apatit	0.76
Water	0.95
Total	99.98
TTDI=	45.09
TOTDI=	0.98
TOTHY=	15.73

CIPW Norm of Sample	A163
Quartz	5.42
Orthoc	11.17
Albite	29.86
Anorth	23.35
Corndm	0.00
Di %Wo	4.69
Di %En	3.32
Di %Fs	0.96
Hy %En	11.57
Hy %Fs	3.34
Ol %Fo	0.00
Ol %Fa	0.00
Mag.	3.38
Haem.	0.00
Ilm.	1.99
Rutile	0.00
Titan.	0.00
Apatit	0.66
Water	0.98
Total	100.68
TTDI=	46.44
TOTDI=	8.97
TOTHY=	14.90

CIPW Norm of Sample	RB088
Quartz	10.90
Orthoc	14.00
Albite	33.15
Anorth	18.88
Corndm	0.00
Di %Wo	2.15
Di %En	1.32
Di %Fs	0.71
Hy %En	7.79
Hy %Fs	4.18
Ol %Fo	0.00
Ol %Fa	0.00
Mag.	2.09
Haem.	0.00
Ilm.	2.01
Rutile	0.00
Titan.	0.00
Apatit	0.85
Water	1.30
Total	99.34
TTDI=	58.06
TOTDI=	4.19
TOTHY=	11.97

CIPW Norm of Sample A020

Quartz	17.56
Orthoc	18.55
Albite	24.10
Anorth	22.26
Corndm	0.90
Di %Wo	0.00
Di %En	0.00
Di %Fs	0.00
Hy %En	7.84
Hy %Fs	3.13
Ol %Fo	0.00
Ol %Fa	0.00
Mag.	2.96
Haem.	0.00
Ilm.	1.56
Rutile	0.00
Titan.	0.00
Apatit	0.55
Water	0.84
Total	100.24
TTDI=	60.21
TOTDI=	0.00
TOTHY=	10.97

CIPW Norm of Sample A162

Quartz	13.21
Orthoc	17.49
Albite	28.84
Anorth	22.81
Corndm	0.00
Di %Wo	0.37
Di %En	0.23
Di %Fs	0.11
Hy %En	8.50
Hy %Fs	3.88
Ol %Fo	0.00
Ol %Fa	0.00
Mag.	2.02
Haem.	0.00
Ilm.	1.58
Rutile	0.00
Titan.	0.00
Apatit	0.64
Water	0.60
Total	100.27
TTDI=	59.54
TOTDI=	0.71
TOTHY=	12.38

CIPW Norm of Sample A164

Quartz	13.81
Orthoc	18.97
Albite	27.66
Anorth	21.22
Corndm	0.00
Di %Wo	0.56
Di %En	0.37
Di %Fs	0.15
Hy %En	8.24
Hy %Fs	3.30
Ol %Fo	0.00
Ol %Fa	0.00
Mag.	3.07
Haem.	0.00
Ilm.	1.56
Rutile	0.00
Titan.	0.00
Apatit	0.59
Water	0.75
Total	100.26
TTDI=	60.43
TOTDI=	1.09
TOTHY=	11.54

CRUACHAN MONZODIORITES

CIPW Norm of Sample	RB007	CIPW Norm of Sample	RB012
Quartz	12.10	Quartz	5.85
Orthoc	19.02	Orthoc	16.31
Albite	37.89	Albite	40.34
Anorth	18.36	Anorth	21.86
Corndm	0.00	Corndm	0.38
Di %Wo	0.45	Di %Wo	0.00
Di %En	0.26	Di %En	0.00
Di %Fs	0.16	Di %Fs	0.00
Hy %En	4.24	Hy %En	5.70
Hy %Fs	2.66	Hy %Fs	2.20
Ol %Fo	0.00	Ol %Fo	0.00
Ol %Fa	0.00	Ol %Fa	0.00
Mag.	2.17	Mag.	3.12
Haem.	0.00	Haem.	0.00
Ilm.	1.90	Ilm.	2.37
Rutile	0.00	Rutile	0.00
Titan.	0.00	Titan.	0.00
Apatit	0.55	Apatit	0.69
Water	0.76	Water	0.78
Total	100.52	Total	99.61
TTDI=	69.01	TTDI=	62.50
TOTDI=	0.87	TOTDI=	0.00
TOTHY=	6.90	TOTHY=	7.90

CIPW Norm of Sample	RB019	CIPW Norm of Sample	RB025
Quartz	3.55	Quartz	5.20
Orthoc	16.01	Orthoc	17.78
Albite	39.75	Albite	40.77
Anorth	22.89	Anorth	21.25
Corndm	0.82	Corndm	0.50
Di %Wo	0.00	Di %Wo	0.00
Di %En	0.00	Di %En	0.00
Di %Fs	0.00	Di %Fs	0.00
Hy %En	5.73	Hy %En	5.63
Hy %Fs	3.19	Hy %Fs	2.24
Ol %Fo	0.00	Ol %Fo	0.00
Ol %Fa	0.00	Ol %Fa	0.00
Mag.	3.15	Mag.	2.89
Haem.	0.00	Haem.	0.00
Ilm.	2.64	Ilm.	2.34
Rutile	0.00	Rutile	0.00
Titan.	0.00	Titan.	0.00
Apatit	1.02	Apatit	0.64
Water	1.08	Water	0.92
Total	99.81	Total	100.15
TTDI=	59.31	TTDI=	63.75
TOTDI=	0.00	TOTDI=	0.00
TOTHY=	8.91	TOTHY=	7.87

CIPW Norm of Sample	RB028	CIPW Norm of Sample	RB090
Quartz	5.69	Quartz	9.14
Orthoc	20.38	Orthoc	18.43
Albite	42.46	Albite	37.13
Anorth	18.35	Anorth	20.69
Corndm	1.47	Corndm	0.20
Di %Wo	0.00	Di %Wo	0.00
Di %En	0.00	Di %En	0.00
Di %Fs	0.00	Di %Fs	0.00
Hy %En	3.88	Hy %En	5.00
Hy %Fs	2.59	Hy %Fs	3.45
Ol %Fo	0.00	Ol %Fo	0.00
Ol %Fa	0.00	Ol %Fa	0.00
Mag.	2.07	Mag.	1.91
Haem.	0.00	Haem.	0.00
Ilm.	1.98	Ilm.	2.62
Rutile	0.00	Rutile	0.00
Titan.	0.00	Titan.	0.00
Apatit	0.52	Apatit	0.74
Water	0.86	Water	0.80
Total	100.26	Total	100.12
TTDI=	68.53	TTDI=	64.71
TOTDI=	0.00	TOTDI=	0.00
TOTHY=	6.48	TOTHY=	8.45

CIPW Norm of Sample	RB110	CIPW Norm of Sample	RB122
Quartz	5.31	Quartz	5.75
Orthoc	15.18	Orthoc	15.89
Albite	35.78	Albite	40.51
Anorth	24.04	Anorth	19.29
Corndm	0.00	Corndm	2.35
Di %Wo	0.92	Di %Wo	0.00
Di %En	0.63	Di %En	0.00
Di %Fs	0.22	Di %Fs	0.00
Hy %En	6.94	Hy %En	6.40
Hy %Fs	2.45	Hy %Fs	3.12
Ol %Fo	0.00	Ol %Fo	0.00
Ol %Fa	0.00	Ol %Fa	0.00
Mag.	3.89	Mag.	2.51
Haem.	0.00	Haem.	0.00
Ilm.	2.60	Ilm.	2.34
Rutile	0.00	Rutile	0.00
Titan.	0.00	Titan.	0.00
Apatit	1.02	Apatit	0.90
Water	0.80	Water	1.00
Total	99.79	Total	100.06
TTDI=	56.27	TTDI=	62.16
TOTDI=	1.78	TOTDI=	0.00
TOTHY=	9.39	TOTHY=	9.51

CIPW Norm of Sample	RB071	CIPW Norm of Sample	RB083
Quartz	8.82	Quartz	4.86
Orthoc	12.70	Orthoc	16.07
Albite	36.79	Albite	38.74
Anorth	22.97	Anorth	19.98
Corndm	0.37	Corndm	0.00
Di %Wo	0.00	Di %Wo	1.27
Di %En	0.00	Di %En	0.74
Di %Fs	0.00	Di %Fs	0.47
Hy %En	6.62	Hy %En	6.26
Hy %Fs	3.04	Hy %Fs	4.00
Ol %Fo	0.00	Ol %Fo	0.00
Ol %Fa	0.00	Ol %Fa	0.00
Mag.	3.64	Mag.	2.62
Haem.	0.00	Haem.	0.00
Ilm.	2.72	Ilm.	2.60
Rutile	0.00	Rutile	0.00
Titan.	0.00	Titan.	0.00
Apatit	1.04	Apatit	0.88
Water	1.20	Water	1.02
Total	99.92	Total	99.51
TTDI=	58.31	TTDI=	59.67
TOTDI=	0.00	TOTDI=	2.48
TOTHY=	9.66	TOTHY=	10.25

CIPW Norm of Sample	RB087	CIPW Norm of Sample	RB073
Quartz	12.60	Quartz	10.63
Orthoc	14.83	Orthoc	18.73
Albite	32.39	Albite	44.66
Anorth	23.34	Anorth	14.27
Corndm	0.00	Corndm	0.93
Di %Wo	0.37	Di %Wo	0.00
Di %En	0.21	Di %En	0.00
Di %Fs	0.15	Di %Fs	0.00
Hy %En	5.97	Hy %En	3.04
Hy %Fs	4.38	Hy %Fs	4.33
Ol %Fo	0.00	Ol %Fo	0.00
Ol %Fa	0.00	Ol %Fa	0.00
Mag.	1.70	Mag.	0.43
Haem.	0.00	Haem.	0.00
Ilm.	2.32	Ilm.	1.71
Rutile	0.00	Rutile	0.00
Titan.	0.00	Titan.	0.00
Apatit	0.78	Apatit	0.40
Water	0.74	Water	0.70
Total	99.78	Total	99.82
TTDI=	59.82	TTDI=	74.02
TOTDI=	0.73	TOTDI=	0.00
TOTHY=	10.35	TOTHY=	7.36

CIPW Norm of Sample	RB098
Quartz	10.23
Orthoc	14.36
Albite	44.32
Anorth	15.26
Corndm	0.00
Di %Wo	1.54
Di %En	1.01
Di %Fs	0.42
Hy %En	5.36
Hy %Fs	2.25
Ol %Fo	0.00
Ol %Fa	0.00
Mag.	2.29
Haem.	0.00
Ilm.	1.77
Rutile	0.00
Titan.	0.00
Apatit	0.59
Water	0.86
Total	100.25
TTDI=	68.90
TOTDI=	2.97
TOTHY=	7.61

CIPW Norm of Sample	A155
Quartz	6.86
Orthoc	16.66
Albite	35.78
Anorth	23.39
Corndm	1.83
Di %Wo	0.00
Di %En	0.00
Di %Fs	0.00
Hy %En	5.43
Hy %Fs	1.85
Ol %Fo	0.00
Ol %Fa	0.00
Mag.	3.89
Haem.	0.00
Ilm.	2.28
Rutile	0.00
Titan.	0.00
Apatit	0.92
Water	0.39
Total	99.27
TTDI=	59.30
TOTDI=	0.00
TOTHY=	7.28

CIPW Norm of Sample	A156
Quartz	0.84
Orthoc	16.48
Albite	41.53
Anorth	21.65
Corndm	0.00
Di %Wo	1.37
Di %En	0.92
Di %Fs	0.35
Hy %En	6.30
Hy %Fs	2.40
Ol %Fo	0.00
Ol %Fa	0.00
Mag.	3.68
Haem.	0.00
Ilm.	2.22
Rutile	0.00
Titan.	0.00
Apatit	0.92
Water	1.40
Total	100.07
TTDI=	58.85
TOTDI=	2.64
TOTHY=	8.70

BONAWE GRANITOIDS

CIPW Norm of Sample	RB005	CIPW Norm of Sample	RB006
Quartz	11.82	Quartz	13.36
Orthoc	19.73	Orthoc	18.91
Albite	36.37	Albite	33.92
Anorth	15.91	Anorth	16.60
Corndm	1.73	Corndm	0.00
Di %Wo	0.00	Di %Wo	0.36
Di %En	0.00	Di %En	0.19
Di %Fs	0.00	Di %Fs	0.15
Hy %En	4.43	Hy %En	6.85
Hy %Fs	5.67	Hy %Fs	5.38
Ol %Fo	0.00	Ol %Fo	0.00
Ol %Fa	0.00	Ol %Fa	0.00
Mag.	0.29	Mag.	0.86
Haem.	0.00	Haem.	0.00
Ilm.	1.79	Ilm.	1.63
Rutile	0.00	Rutile	0.00
Titan.	0.00	Titan.	0.00
Apatit	1.00	Apatit	0.69
Water	0.70	Water	0.86
Total	99.43	Total	99.75
TTDI=	67.92	TTDI=	66.18
TOTDI=	0.00	TOTDI=	0.70
TOTHY=	10.10	TOTHY=	12.23

CRUACHAN MONZOGRANITES

CIPW Norm of Sample	RB029
Quartz	18.42
Orthoc	23.93
Albite	34.08
Anorth	12.71
Corndm	0.00
Di %Wo	0.21
Di %En	0.17
Di %Fs	0.02
Hy %En	4.59
Hy %Fs	0.46
Ol %Fo	0.00
Ol %Fa	0.00
Mag.	2.81
Haem.	0.00
Ilm.	1.37
Rutile	0.00
Titan.	0.00
Apatit	0.50
Water	0.72
Total	99.98
TTDI=	76.43
TOTDI=	0.39
TOTHY=	5.05

CIPW Norm of Sample	RB035
Quartz	16.88
Orthoc	24.28
Albite	35.86
Anorth	11.97
Corndm	0.32
Di %Wo	0.00
Di %En	0.00
Di %Fs	0.00
Hy %En	5.15
Hy %Fs	0.00
Ol %Fo	0.00
Ol %Fa	0.00
Mag.	2.11
Haem.	1.04
Ilm.	1.56
Rutile	0.00
Titan.	0.00
Apatit	0.36
Water	0.78
Total	100.30
TTDI=	77.02
TOTDI=	0.00
TOTHY=	5.15

CIPW Norm of Sample	RB036
Quartz	22.99
Orthoc	24.70
Albite	31.04
Anorth	11.21
Corndm	0.95
Di %Wo	0.00
Di %En	0.00
Di %Fs	0.00
Hy %En	3.68
Hy %Fs	0.52
Ol %Fo	0.00
Ol %Fa	0.00
Mag.	2.12
Haem.	0.00
Ilm.	1.31
Rutile	0.00
Titan.	0.00
Apatit	0.45
Water	0.70
Total	99.67
TTDI=	78.73
TOTDI=	0.00
TOTHY=	4.20

CIPW Norm of Sample	RB109
Quartz	8.97
Orthoc	23.46
Albite	45.08
Anorth	12.49
Corndm	1.09
Di %Wo	0.00
Di %En	0.00
Di %Fs	0.00
Hy %En	2.46
Hy %Fs	1.52
Ol %Fo	0.00
Ol %Fa	0.00
Mag.	1.93
Haem.	0.00
Ilm.	1.39
Rutile	0.00
Titan.	0.00
Apatit	0.31
Water	0.70
Total	99.39
TTDI=	77.50
TOTDI=	0.00
TOTHY=	3.98

CIPW Norm of Sample	A157
Quartz	11.62
Orthoc	25.29
Albite	34.76
Anorth	16.10
Corndm	1.98
Di %Wo	0.00
Di %En	0.00
Di %Fs	0.00
Hy %En	3.71
Hy %Fs	0.87
Ol %Fo	0.00
Ol %Fa	0.00
Mag.	3.07
Haem.	0.00
Ilm.	1.65
Rutile	0.00
Titan.	0.00
Apatit	0.40
Water	0.87
Total	100.33
TTDI=	71.67
TOTDI=	0.00
TOTHY=	4.58

CIPW Norm of Sample	RB051
Quartz	20.90
Orthoc	22.21
Albite	32.98
Anorth	10.50
Corndm	1.85
Di %Wo	0.00
Di %En	0.00
Di %Fs	0.00
Hy %En	5.53
Hy %Fs	1.10
Ol %Fo	0.00
Ol %Fa	0.00
Mag.	2.74
Haem.	0.00
Ilm.	1.25
Rutile	0.00
Titan.	0.00
Apatit	0.55
Water	0.78
Total	100.39
TTDI=	76.10
TOTDI=	0.00
TOTHY=	6.62

CIPW Norm of Sample	RB052
Quartz	18.21
Orthoc	22.33
Albite	33.41
Anorth	15.14
Corndm	0.38
Di %Wo	0.00
Di %En	0.00
Di %Fs	0.00
Hy %En	4.28
Hy %Fs	2.55
Ol %Fo	0.00
Ol %Fa	0.00
Mag.	1.28
Haem.	0.00
Ilm.	1.41
Rutile	0.00
Titan.	0.00
Apatit	0.36
Water	0.70
Total	100.05
TTDI=	73.95
TOTDI=	0.00
TOTHY=	6.83

CIPW Norm of Sample	RB055
Quartz	22.50
Orthoc	26.59
Albite	30.96
Anorth	10.28
Corndm	1.28
Di %Wo	0.00
Di %En	0.00
Di %Fs	0.00
Hy %En	3.56
Hy %Fs	0.09
Ol %Fo	0.00
Ol %Fa	0.00
Mag.	2.29
Haem.	0.00
Ilm.	1.08
Rutile	0.00
Titan.	0.00
Apatit	0.36
Water	0.68
Total	99.66
TTDI=	80.04
TOTDI=	0.00
TOTHY=	3.65

CIPW Norm of Sample	RB057
Quartz	23.83
Orthoc	25.11
Albite	30.70
Anorth	10.35
Corndm	0.81
Di %Wo	0.00
Di %En	0.00
Di %Fs	0.00
Hy %En	3.68
Hy %Fs	0.95
Ol %Fo	0.00
Ol %Fa	0.00
Mag.	1.84
Haem.	0.00
Ilm.	1.08
Rutile	0.00
Titan.	0.00
Apatit	0.47
Water	0.70
Total	99.53
TTDI=	79.64
TOTDI=	0.00
TOTHY=	4.63

CIPW Norm of Sample	RB064
Quartz	16.74
Orthoc	19.85
Albite	34.93
Anorth	14.79
Corndm	0.00
Di %Wo	0.17
Di %En	0.12
Di %Fs	0.04
Hy %En	5.65
Hy %Fs	1.65
Ol %Fo	0.00
Ol %Fa	0.00
Mag.	2.52
Haem.	0.00
Ilm.	1.46
Rutile	0.00
Titan.	0.00
Apatit	0.78
Water	0.86
Total	99.57
TTDI=	71.52
TOTDI=	0.33
TOTHY=	7.30

CIPW Norm of Sample	RB076
Quartz	17.68
Orthoc	20.80
Albite	34.42
Anorth	14.24
Corndm	0.00
Di %Wo	0.24
Di %En	0.14
Di %Fs	0.09
Hy %En	4.97
Hy %Fs	3.14
Ol %Fo	0.00
Ol %Fa	0.00
Mag.	1.29
Haem.	0.00
Ilm.	1.41
Rutile	0.00
Titan.	0.00
Apatit	0.50
Water	0.80
Total	99.69
TTDI=	72.90
TOTDI=	0.46
TOTHY=	8.10

MEALL ODHAR GRANITES

CIPW Norm of Sample	RB010
Quartz	34.64
Orthoc	39.29
Albite	23.51
Anorth	0.78
Corndm	0.47
Di %Wo	0.00
Di %En	0.00
Di %Fs	0.00
Hy %En	0.20
Hy %Fs	0.00
Ol %Fo	0.00
Ol %Fa	0.00
Mag.	0.21
Haem.	0.28
Ilm.	0.28
Rutile	0.00
Titan.	0.00
Apatit	0.02
Water	0.42
Total	100.11
TTDI=	97.44
TOTDI=	0.00
TOTHY=	0.20

CIPW Norm of Sample	RB066
Quartz	31.16
Orthoc	37.28
Albite	27.06
Anorth	1.36
Corndm	0.00
Di %Wo	0.39
Di %En	0.14
Di %Fs	0.26
Hy %En	0.28
Hy %Fs	0.52
Ol %Fo	0.00
Ol %Fa	0.00
Mag.	0.14
Haem.	0.00
Ilm.	0.59
Rutile	0.00
Titan.	0.00
Apatit	0.05
Water	0.36
Total	99.60
TTDI=	95.50
TOTDI=	0.79
TOTHY=	0.80

CIPW Norm of Sample	RB084
Quartz	32.41
Orthoc	30.96
Albite	33.66
Anorth	1.22
Corndm	0.22
Di %Wo	0.00
Di %En	0.00
Di %Fs	0.00
Hy %En	0.30
Hy %Fs	0.00
Ol %Fo	0.00
Ol %Fa	0.00
Mag.	0.36
Haem.	0.35
Ilm.	0.42
Rutile	0.00
Titan.	0.00
Apatit	0.02
Water	0.32
Total	100.24
TTDI=	97.03
TOTDI=	0.00
TOTHY=	0.30

CIPW Norm of Sample	A108
Quartz	34.76
Orthoc	30.37
Albite	32.05
Anorth	0.48
Corndm	0.91
Di %Wo	0.00
Di %En	0.00
Di %Fs	0.00
Hy %En	0.02
Hy %Fs	0.95
Ol %Fo	0.00
Ol %Fa	0.00
Mag.	0.14
Haem.	0.00
Ilm.	0.25
Rutile	0.00
Titan.	0.00
Apatit	0.02
Water	0.26
Total	100.22
TTDI=	97.18
TOTDI=	0.00
TOTHY=	0.98

CIPW Norm of Sample	RB026
Quartz	33.29
Orthoc	39.11
Albite	23.85
Anorth	0.78
Corndm	0.77
Di %Wo	0.00
Di %En	0.00
Di %Fs	0.00
Hy %En	0.25
Hy %Fs	0.00
Ol %Fo	0.00
Ol %Fa	0.00
Mag.	0.73
Haem.	0.13
Ilm.	0.28
Rutile	0.00
Titan.	0.00
Apatit	0.02
Water	0.40
Total	99.62
TTDI=	96.26
TOTDI=	0.00
TOTHY=	0.25

CIPW Norm of Sample	RB083B
Quartz	32.19
Orthoc	34.68
Albite	29.60
Anorth	1.37
Corndm	0.38
Di %Wo	0.00
Di %En	0.00
Di %Fs	0.00
Hy %En	0.27
Hy %Fs	0.10
Ol %Fo	0.00
Ol %Fa	0.00
Mag.	0.61
Haem.	0.00
Ilm.	0.46
Rutile	0.00
Titan.	0.00
Apatit	0.02
Water	0.36
Total	100.05
TTDI=	96.48
TOTDI=	0.00
TOTHY=	0.38

CIPW Norm of Sample	RB098A
Quartz	38.84
Orthoc	28.00
Albite	30.40
Anorth	0.00
Corndm	0.00
Di %Wo	0.27
Di %En	0.23
Di %Fs	0.00
Hy %En	0.04
Hy %Fs	0.00
Ol %Fo	0.00
Ol %Fa	0.00
Mag.	0.00
Haem.	0.56
Ilm.	0.15
Rutile	0.00
Titan.	0.30
Apatit	0.02
Water	0.40
Total	99.48
TTDI=	97.24
TOTDI=	0.51
TOTHY=	0.04

CIPW Norm of Sample	RB123
Quartz	31.51
Orthoc	30.49
Albite	34.17
Anorth	2.22
Corndm	0.53
Di %Wo	0.00
Di %En	0.00
Di %Fs	0.00
Hy %En	0.70
Hy %Fs	0.14
Ol %Fo	0.00
Ol %Fa	0.00
Mag.	0.58
Haem.	0.00
Ilm.	0.30
Rutile	0.00
Titan.	0.00
Apatit	0.02
Water	0.20
Total	100.85
TTDI=	96.16
TOTDI=	0.00
TOTHY=	0.84

CIPW Norm of Sample	RB016
Quartz	36.18
Orthoc	30.43
Albite	28.67
Anorth	2.22
Corndm	1.27
Di %Wo	0.00
Di %En	0.00
Di %Fs	0.00
Hy %En	0.95
Hy %Fs	0.00
Ol %Fo	0.00
Ol %Fa	0.00
Mag.	0.02
Haem.	0.59
Ilm.	0.11
Rutile	0.00
Titan.	0.00
Apatit	0.02
Water	0.20
Total	100.65
TTDI=	95.28
TOTDI=	0.00
TOTHY=	0.95

PORPHYRITIC STARAV MONZOGRANITES

CIPW Norm of Sample	RB013	CIPW Norm of Sample	RB015
Quartz	19.29	Quartz	26.83
Orthoc	24.40	Orthoc	25.29
Albite	33.58	Albite	29.94
Anorth	12.17	Anorth	7.11
Corndm	0.00	Corndm	1.59
Di %Wo	0.57	Di %Wo	0.00
Di %En	0.38	Di %En	0.00
Di %Fs	0.15	Di %Fs	0.00
Hy %En	3.48	Hy %En	3.61
Hy %Fs	1.32	Hy %Fs	1.74
Ol %Fo	0.00	Ol %Fo	0.00
Ol %Fa	0.00	Ol %Fa	0.00
Mag.	2.06	Mag.	1.83
Haem.	0.00	Haem.	0.00
Ilm.	1.06	Ilm.	0.97
Rutile	0.00	Rutile	0.00
Titan.	0.00	Titan.	0.00
Apatit	0.38	Apatit	0.43
Water	0.60	Water	0.56
Total	99.44	Total	99.88
TTDI=	77.27	TTDI=	82.05
TOTDI=	1.10	TOTDI=	0.00
TOTHY=	4.80	TOTHY=	5.35

CIPW Norm of Sample	RB017	CIPW Norm of Sample	RB065
Quartz	24.04	Quartz	18.63
Orthoc	25.76	Orthoc	23.28
Albite	32.48	Albite	37.47
Anorth	10.57	Anorth	10.53
Corndm	1.15	Corndm	0.00
Di %Wo	0.00	Di %Wo	0.39
Di %En	0.00	Di %En	0.29
Di %Fs	0.00	Di %Fs	0.05
Hy %En	2.34	Hy %En	3.82
Hy %Fs	0.85	Hy %Fs	0.69
Ol %Fo	0.00	Ol %Fo	0.00
Ol %Fa	0.00	Ol %Fa	0.00
Mag.	1.55	Mag.	2.31
Haem.	0.00	Haem.	0.00
Ilm.	0.82	Ilm.	1.14
Rutile	0.00	Rutile	0.00
Titan.	0.00	Titan.	0.00
Apatit	0.28	Apatit	0.45
Water	0.52	Water	0.82
Total	100.37	Total	99.86
TTDI=	82.28	TTDI=	79.37
TOTDI=	0.00	TOTDI=	0.73
TOTHY=	3.19	TOTHY=	4.51

CIPW Norm of Sample	RB074	CIPW Norm of Sample	RB075
Quartz	22.56	Quartz	25.27
Orthoc	26.59	Orthoc	23.46
Albite	34.93	Albite	34.08
Anorth	8.45	Anorth	9.07
Corndm	0.00	Corndm	0.72
Di %Wo	0.29	Di %Wo	0.00
Di %En	0.16	Di %En	0.00
Di %Fs	0.12	Di %Fs	0.00
Hy %En	2.11	Hy %En	2.27
Hy %Fs	1.55	Hy %Fs	2.71
Ol %Fo	0.00	Ol %Fo	0.00
Ol %Fa	0.00	Ol %Fa	0.00
Mag.	0.91	Mag.	0.28
Haem.	0.00	Haem.	0.00
Ilm.	0.93	Ilm.	0.82
Rutile	0.00	Rutile	0.00
Titan.	0.00	Titan.	0.00
Apatit	0.28	Apatit	0.31
Water	0.64	Water	0.60
Total	99.52	Total	99.59
TTDI=	84.08	TTDI=	82.81
TOTDI=	0.56	TOTDI=	0.00
TOTHY=	3.66	TOTHY=	4.98

CIPW Norm of Sample	RB078
Quartz	23.68
Orthoc	25.82
Albite	36.71
Anorth	6.99
Corndm	0.00
Di %Wo	0.11
Di %En	0.07
Di %Fs	0.03
Hy %En	2.20
Hy %Fs	0.94
Ol %Fo	0.00
Ol %Fa	0.00
Mag.	1.04
Haem.	0.00
Ilm.	1.03
Rutile	0.00
Titan.	0.00
Apatit	0.28
Water	0.70
Total	99.60
TTDI=	86.20
TOTDI=	0.21
TOTHY=	3.14

CIPW Norm of Sample	RB080
Quartz	17.61
Orthoc	26.82
Albite	40.00
Anorth	8.26
Corndm	0.00
Di %Wo	1.15
Di %En	0.73
Di %Fs	0.35
Hy %En	2.16
Hy %Fs	1.04
Ol %Fo	0.00
Ol %Fa	0.00
Mag.	1.45
Haem.	0.00
Ilm.	0.93
Rutile	0.00
Titan.	0.00
Apatit	0.36
Water	0.66
Total	101.53
TTDI=	84.43
TOTDI=	2.23
TOTHY=	3.20

CIPW Norm of Sample	RB095
Quartz	22.77
Orthoc	31.96
Albite	35.35
Anorth	3.71
Corndm	0.00
Di %Wo	0.81
Di %En	0.46
Di %Fs	0.31
Hy %En	1.11
Hy %Fs	0.73
Ol %Fo	0.00
Ol %Fa	0.00
Mag.	0.75
Haem.	0.00
Ilm.	0.72
Rutile	0.00
Titan.	0.00
Apatit	0.17
Water	0.68
Total	99.53
TTDI=	90.09
TOTDI=	1.58
TOTHY=	1.84

CIPW Norm of Sample	RB096
Quartz	24.05
Orthoc	28.71
Albite	37.30
Anorth	4.31
Corndm	0.00
Di %Wo	0.97
Di %En	0.55
Di %Fs	0.38
Hy %En	0.94
Hy %Fs	0.64
Ol %Fo	0.00
Ol %Fa	0.00
Mag.	0.78
Haem.	0.00
Ilm.	0.51
Rutile	0.00
Titan.	0.00
Apatit	0.17
Water	0.66
Total	99.97
TTDI=	90.06
TOTDI=	1.90
TOTHY=	1.58

CIPW Norm of Sample	RB092
Quartz	31.99
Orthoc	27.53
Albite	30.70
Anorth	5.03
Corndm	0.84
Di %Wo	0.00
Di %En	0.00
Di %Fs	0.00
Hy %En	1.34
Hy %Fs	0.00
Ol %Fo	0.00
Ol %Fa	0.00
Mag.	1.18
Haem.	0.05
Ilm.	0.66
Rutile	0.00
Titan.	0.00
Apatit	0.12
Water	0.66
Total	100.11
TTDI=	90.23
TOTDI=	0.00
TOTHY=	1.34

CIPW Norm of Sample	RB014
Quartz	29.71
Orthoc	29.72
Albite	30.70
Anorth	4.55
Corndm	0.97
Di %Wo	0.00
Di %En	0.00
Di %Fs	0.00
Hy %En	1.07
Hy %Fs	1.83
Ol %Fo	0.00
Ol %Fa	0.00
Mag.	0.01
Haem.	0.00
Ilm.	0.42
Rutile	0.00
Titan.	0.00
Apatit	0.09
Water	0.44
Total	99.52
TTDI=	90.13
TOTDI=	0.00
TOTHY=	2.90

CENTRAL STARAV MONZOGRANITES

CIPW Norm of Sample	RB034
Quartz	32.67
Orthoc	28.00
Albite	32.22
Anorth	2.83
Corndm	0.92
Di %Wo	0.00
Di %En	0.00
Di %Fs	0.00
Hy %En	0.77
Hy %Fs	0.80
Ol %Fo	0.00
Ol %Fa	0.00
Mag.	0.36
Haem.	0.00
Ilm.	0.30
Rutile	0.00
Titan.	0.00
Apatit	0.07
Water	0.46
Total	99.41
TTDI=	92.90
TOTDI=	0.00
TOTHY=	1.57

CIPW Norm of Sample	RB093
Quartz	35.58
Orthoc	26.23
Albite	29.52
Anorth	4.45
Corndm	1.17
Di %Wo	0.00
Di %En	0.00
Di %Fs	0.00
Hy %En	0.87
Hy %Fs	0.00
Ol %Fo	0.00
Ol %Fa	0.00
Mag.	0.00
Haem.	1.18
Ilm.	0.21
Rutile	0.20
Titan.	0.00
Apatit	0.09
Water	0.60
Total	100.11
TTDI=	91.33
TOTDI=	0.00
TOTHY=	0.87

CIPW Norm of Sample	RB101
Quartz	35.17
Orthoc	28.54
Albite	30.53
Anorth	2.40
Corndm	1.31
Di %Wo	0.00
Di %En	0.00
Di %Fs	0.00
Hy %En	0.55
Hy %Fs	0.00
Ol %Fo	0.00
Ol %Fa	0.00
Mag.	0.76
Haem.	0.09
Ilm.	0.27
Rutile	0.00
Titan.	0.00
Apatit	0.05
Water	0.56
Total	100.21
TTDI=	94.24
TOTDI=	0.00
TOTHY=	0.55

CIPW Norm of Sample	RB104
Quartz	35.86
Orthoc	27.65
Albite	29.35
Anorth	2.78
Corndm	1.44
Di %Wo	0.00
Di %En	0.00
Di %Fs	0.00
Hy %En	0.80
Hy %Fs	0.85
Ol %Fo	0.00
Ol %Fa	0.00
Mag.	0.38
Haem.	0.00
Ilm.	0.34
Rutile	0.00
Titan.	0.00
Apatit	0.07
Water	0.62
Total	100.13
TTDI=	92.86
TOTDI=	0.00
TOTHY=	1.64

CIPW Norm of Sample	RB106
Quartz	35.40
Orthoc	27.47
Albite	30.45
Anorth	3.03
Corndm	1.17
Di %Wo	0.00
Di %En	0.00
Di %Fs	0.00
Hy %En	0.62
Hy %Fs	0.00
Ol %Fo	0.00
Ol %Fa	0.00
Mag.	0.21
Haem.	0.72
Ilm.	0.30
Rutile	0.00
Titan.	0.00
Apatit	0.07
Water	0.60
Total	100.05
TTDI=	93.32
TOTDI=	0.00
TOTHY=	0.62

REFERENCES

ANDERSON A T (1976) Magma mixing: petrological process and volcanological tool. J.VOLC.GEOTHERM.RES. 1, 3-33.

ANDERSON J G C (1937) The Etive Granite Complex. QUART.J.GEOL.SOC. 93, 487-533.

BAILEY E B and MAUFE A B (1916,1960) The Geology of Ben Nevis and Glen Coe. MEM.GEOL.SURV.SCOT. Sheet 53.

BATCHELOR R A (1980) Analysis of major, minor, and selected trace elements in silicate rocks and minerals. INT.PUBL.80/1., DEPT OF GEOLOGY, UNIV. OF ST.ANDREWS.

BLAXLAND A B, AFTALION M, and van BREEMAN O (1979) Lead isotopic composition of feldspars from Scottish Caledonian granites, and the nature of the underlying crust. SCOTT.J.GEOL. 15, 139-151.

BORG I Y and SMITH D K (1969) Calculated X-ray powder patterns for silicate minerals. MEM.GEOL.SOC.AMER. 122.

BOWEN N L and TUTTLE O F (1950) The system $NaAlSi_3O_8$ - $KAlSi_3O_8$ - H_2O. J.GEOL. 58,489-511.

BROWN G C (1979) Geochemical and geophysical constraints on the origin and evolution of Caledonian granites. In:A.L.Harris, C.H.Holland, and B.E.Leake (eds.), "The Caledonides of the British Isles - reviewed". GEOL.SOC.LOND.SPEC.PUBL.No.8. pp.645-651.

BROWN G C, CASSIDY J, LOCKE C A, PLANT J and SIMPSON P R (1981) Caledonian plutonism in Britain: A summary. J.GEOPHYS.RES. 86, 10502-10514.

BROWN J F (1975) Rb-Sr studies and related chemistry on the Caledonian calc-alkaline igneous rocks of NW Argyllshire. UNPUBL.Ph.D., UNIV. OF OXFORD, ENGLAND.

CARMICHAEL I S E, TURNER F J and VERHOOGEN J (1974) Igneous Petrology. McGRAW-HILL, NEW YORK.

CAWTHORN R G and O'HARA M J (1976) Amphibole fractionation in calc-alkaline magma genesis. AMER.J.SCI. 276, 309-329.

CAWTHORN R G, STRONG D F and BROWN P A (1976) Origin of corundum-normative intrusive and extrusive magmas. NATURE 259, 102-104.

CHAPPELL B W and WHITE A J R (1974) Two contrasting granite types. PACIFIC GEOLOGY 8, 173-174.

CHINNER G A (1978) Metamorphic zones and fault displacement in the Southern Highlands. GEOL.MAG. 115, 37-45.

CLAYBURN J A P (1981) Age and petrogenetic studies of some magmatic and metamorphic rocks in the Grampian Highlands. UNPUBL. D.Phil., UNIV. OF OXFORD.

CLAYBURN J A P, HARMON R S, PANKHURST R J and BROWN J F (1983) Sr, O and Pb isotopic evidence for the origin and evolution of the Etive complex, Scotland. NATURE 303, 492-497.

COLLINS W J, BEAMS S D, WHITE A J R and CHAPPELL B W (1982) Nature and origin of A-type granites with particular reference to SE Australia. CONT.MIN.PET. 80, 189-200.

COX K G, BELL J D and PANKHURST R J (1979) The Interpretation of Igneous Rocks. GEORGE,ALLEN & UNWIN, 450pp.

CULBERT R R (1972) Abnormalities in the distribution of K, Rb, and Sr in the Coast Mountains batholith, British Columbia. GEOCHIM.COSMO.ACTA 36, 1091-1100.

DEER W A, HOWIE R A and ZUSSMAN J (1966) Introduction to the Rock-Forming Minerals. LONGMAN GROUP LTD., LONDON. 528pp.

de la ROCHE H, LETERRIER J, GRANDE CLAUDE P and MARCHAL M (1980) A classification of volcanic and plutonic rocks using R1 - R2 diagrams and major element analyses - its relationships with current nomenclature. CHEM.GEOL. 29, 183-210.

DROOP G T R and TRELOAR P J (1981) Pressures of metamorphism in the thermal aureole of the Etive Granite Complex. SCOTT.J.GEOL. 17, 85-102.

FOURCADE S and ALLEGRE C J (1981) Trace element behaviour in granite genesis: a case study. The calc-alkaline plutonic association from Querigut Complex, pyrenees, France. CONT.MIN.PET. 76, 177-195.

GILL J (1981) Orogenic andesites and plate tectonics. SPRINGER-VERLAG p. 97-167.

GOLDSMITH J R and LAVES F (1954) The microcline - sanidine stability relations. GEOCHIM.COSMO.ACTA. 5, 1-19.

GROOME D R and HALL A (1974) The geochemistry of the Devonian lavas of the Northern Lorne plateau, Scotland. MIN.MAG. 39, 621-640.

HALL A (1972) New data on the composition of Caledonian granites. MIN.MAG. 38 847-862.

HALL D H and DAGLEY P (1970) Regional magnetic anomalies: Analysis of the smoothed aeromagnetic maps of Great Britain and Northern Ireland. REP.INST.GEOL.SCI,U.K., 70/10, 8pp.

HAMILTON P J, O'NIONS R K and PANKHURST R J (1980) Isotopic evidence for the provenance of some Caledonian granites. NATURE 287, 279-284.

HARKER A (1909) The Natural History of Igneous Rocks. MACMILLAN, NEW YORK.

HARMON R S and HALLIDAY A N (1980) Oxygen and strontium isotope relationships in the British late Caledonian granites. NATURE 283, 21-25.

HARMON R S, HALLIDAY A N, STEPHENS W E and CLAYBURN J A P (1983) Chemical and isotope systematics of the Caledonian intrusions of Scotland and Northern England: a guide to magma source region and magma-crust interaction. PHIL.TRANS.ROY.SOC.LOND. (in press).

HASLAM H W (1968) The crystallisation of intermediate and acid magmas at Ben Nevis, Scotland. J.PET. 9, 84-104.

HELLMAN P L, SMITH R E and HENDERSON P (1976) The mobility of the rare earth elements: evidence and implications from selected terrains affected by burial metamorphism. CONT.MIN.PET. 71, 23-44.

HIPKIN R G and HUSSAIN A (1983) Regional gravity anomalies. 1.Northern Britain. REP.INST.GEOL.SCI.,U.K., 82/10, 45pp.

HURFORD A J (1977) A preliminary fission track dating survey of Caledonian Newer and Later Granites from the Highlands of Scotland. SCOTT.J.GEOL. 13, 271-284.

HUTCHISON C (1974) Laboratory Handbook of Petrographic Techniques. WILEY INTESCIENCE, 527pp.

ISHIHARA S (1977) The magnetite-series and ilmenite-series granitic rocks. MING.GEOL. 27, 293-305.

JIRANEK J (1982) A rapid X-ray method of assessing the structural state of monoclinic K-feldspars. LITHOS 15, 85-87.

JOHANNES W (1983) On the origin of layered migmatites. In: M.P. Atherton and C.D.Gribble (eds.) "Migmatites, Melting and Metamorphism". SHIVA p234-248.

JOHNSON M R W (1983) Dalradian. In: G.Y.Craig (ed) "The Geology of Scotland". Oliver and Boyd, Edinburgh.

KAWACHI Y and SATO T (1978) Orthoclase megacrysts in the Yakashima granite, southern Kyushu, Japan. NEUES JAHR.MIN.ABH. 132, 136-152.

KYNASTON H and HILL J B (1908) The geology of the country near Oban and Dalmally. MEM.GEOL.SURV.SCOT. Sheet 45.

LAMEYRE J and BOWDEN P (1982) Plutonic rock type series: discrimination of various granitoid series and related rocks. J.VOLC.GEOTHERM.RES. 14, 169-186.

LEEMAN W P and PHELPS D W (1982) Partitioning of rare earth and other trace elements between sanidine and co-existing volcanic glass. J.GEOPHYS.RES. 86, 10193-10199.

LIN T H and YUND R A (1972) Potassium and sodium self-diffusion in alkali feldspar. CONT.MIN.PET. 34, 177-184.

LITHERLAND M (1980) The stratigraphy of the Dalradian rocks around Loch Creran, Argyll. SCOTT.J.GEOL. 16, 105-124.

LITHERLAND M (1982) The structure of the Loch Creran Dalradian and a new model for the SW Highlands. SCOTT.J.GEOL. 18, 205-225.

LUTH W C, JAHNS R H and TUTTLE O F (1964) The granite system at pressures of 4 to 10 kilobars. J.GEOPHYS.RES. 69, 759-773.

MacCULLOCH J (1817) Observations on the mountain Cruachan in Argyllshire, with some remarks on the surrounding country. TRANS.GEOL.SOC. 4, 117-138.

MANN A C (1983) Trace element geochemistry of high-alumina basalt - andesite - dacite - rhyodacite lavas of the main volcanic series of Santorini volcano, Greece. CONT.MIN.PET. 84, 43-57.

MARTIN R F (1974) Controls of ordering and sub-solidus phase relations in the alkali feldspars. In: W.J.Mackenzie and J.Zussman "The Feldspars". Manchester Univ. Press, p. 313-336.

MASON R (1978) Petrology of the Metamorphic Rocks. GEORGE, ALLEN and UNWIN. 254pp.

MASUDA Y and AOKI K (1979) Trace element variations in the volcanic rocks from the Nasu zone, NE Japan. EARTH.PLANET.SCI.LETT. 44, 139-149.

MASUDA A and NAGASAWA S (1975) Rocks with negative cerium anomalies dredged from the Shatsky rise. GEOCHEM.J. 9, 227-233.

McBIRNEY A R (1980) Mixing and unmixing of magmas. J.VOLC.GEOTHERM.RES. 7, 357-371.

McCARTHY T S and GROVES D I (1979) The Blue Tier Batholith, NE Tasmania - A cumulate-like product of fractional crystallisation. CONT.MIN.PET. 71, 193-209.

McCARTHY T S and ROBB L J (1978) On the relationship between cumulus mineralogy and trace and alkali element chemistry in an Archaean granite from the Barberton region, South Africa. GEOCHIM.COSMO.ACTA. 42, 21-26.

MEIGHAN I (1979) The acid igneous rocks of the British Tertiary province. In: "Mesozoic and Tertiary volcanism in the North Atlantic and neighbouring regions; Proceedings of the Flett Symposium. G.B.GEOL.SURV.BULL. No.70, 10-22.

NOCKOLDS S R and ALLEN R (1953) The geochemistry of some igneous rock series. Part 1. Calc-alkaline. GEOCHIM.COSMO.ACTA. 4, 105-142.

PANKHURST R J (1979) Isotope and trace element evidence for the origin and evolution of Caledonian granites in the Scottish Highlands. In: M.P.Atherton and J.Tarney (eds) "Origin of Granite Batholiths; geochemical evidence". SHIVA, p.18-33.

PEACOCK M A (1931) Classification of igneous rock series. J.GEOL. 39, 65-67.

PEARCE J A and NORRY M J (1979) Petrogenetic implications of Ti, Zr, Y and Nb variations in volcanic rocks. CONT.MIN.PET. 69, 33-47.

PECCERILLO A and TAYLOR S R (1976) Geochemistry of Eocene calc-alkaline volcanic rocks from the Kastamonu area, Northern Turkey. CONT.MIN.PET. 58, 63-81.

PHILLIPS W E A, STILLMAN C J and MURPHY T (1976) A Caledonian plate tectonic model. J.GEOL.SOC.LOND. 132, 579-609.

PIDGEON R T and AFTALION M (1980) Cogenetic and inherited zircon U-Pb systems in granites: Palaeozoic granites of Scotland and England. In: D.R.Bowes and B.E.Leake (eds) "Crustal evolution in NW Britain and adjacent regions". GEOL.SOC.LOND.SPEC.PUBL.No.10, p.183-220.

PITCHER W S (1979) The nature, ascent and emplacement of granitic magmas. J.GEOL.SOC.LOND. 136, 627-663.

PLANT J, BROWN G C, SIMPSON P R and SMITH R T (1980) Signatures of metalliferous granites in the Scottish Caledonides. TRANS.INST.MIN.METALL. 89B, 198-210.

PRESNALL D C and BATEMAN P C (1973) Fusion relations in the system $NaAlSi_3O_8$ - $CaAl_2Si_2O_8$ - $KAlSi_3O_8$ - SiO_2 - H_2O and the generation of granitic magmas of the Sierra Nevada batholith. GEOL.SOC.AM.BULL. 84, 3181-3202.

RAGLAND P C (1970) Composition and structural state of the potassic phase in perthites as related to petrogenesis of granitic plutons. LITHOS 3, 167-189.

READ H H (1961) Aspects of Caledonian magmatism in Britain. LIVERPOOL and MANCHESTER GEOL.J. 2, 653-683.

RINGWOOD A E (1975) Composition and Petrology of the Earth's Mantle. McGRAW-HILL, NEW YORK. 618pp.

ROBERTS J L (1966) The emplacement of the Main Glen Coe Fault Intrusion at Stob Mhic Mhartuin. GEOL.MAG. 103, 299-316.

ROBERTS J L (1974) The evolution of the Glen Coe cauldron. SCOTT.J.GEOL. 10, 269-282.

SENDEROV E E, YAS'KIM G M and BYCHOV A M (1975) Effects of alkaline solutions on Si-Al ordering in potash feldspar. GEOCHEM.INT. 12, 116-125.

SHAW D M (1968) A review of K-Rb trends by covariance analysis. GEOCHIM.COSMO.ACTA 32, 573-601.

SHERVAIS J W (1982) Ti-V plots and the petrogenesis of modern and ophiolitic lavas. EARTH PLANET.SCI.LETT. 59, 101-118.

SMITH J V (1974) Feldspar Minerals. 1.Crystal Structure and Physical Properties. SPRINGER-VERLAG, NEW YORK.

STEPHENS W E and HALLIDAY A N (1984) Contrasts between late Caledonian granites of Northern, Central and Southern Scotland. TRANS.ROY.SOC.EDIN. (in press).

STRECKEISEN A (1976) To each plutonic rock its proper name. EARTH SCI.REV. 12, 1-33.

SUN S-S, NESBITT R W and SHARASKIN A Ya (1979) Geochemical characteristics of Mid-Ocean Ridge Basalts. EARTH PLANET.SCI.LETT. 44, 119-138.

TAUSON L V and KOSLOV V D (1973) Distribution functions and ratios of trace element concentrations as estimators of the ore-bearing potential of granites. PROC.INTERNL.GEOCHEM.EXPL.SYMP. 4, 37-44. (Inst. Min.Metall., London).

TAYLOR S R (1965) The application of trace element data to problems in petrology. PHYS.CHEM.EARTH 6, 133-212.

TAYLOR S R (1969) Trace element chemistry of andesites and associated calc-alkaline rocks. In: A.R.McBirney (ed) "Proceedings of the Andesite conference", BULL.OREG.DEP.GEOL.MIN.IND. 65, 43-64.

THIRLWALL M F (1979) The petrochemistry of the British Old Red Sandstone volcanic province. UNPUBL. Ph.D., UNIV. OF EDINBURGH.

THIRLWALL M F (1981) Implications for Caledonian plate tectonic models of chemical data from volcanic rocks of the British Old Red Sandstone. J.GEOL.SOC.LOND. 138, 123-138.

THOMPSON R N (1982) Magmatism of the British Tertiary Volcanic Province. SCOTT.J.GEOL. 18, 49-107.

THORNTON C P and TUTTLE O F (1960) Chemistry of igneous rocks. 1. Differentiation Index. AMER.J.SCI. 258, 664-684.

TREUIL M and VARET J (1973) Criteres volcanologiques, petrologiques et geochimiques de la genese et la differenciation des magmas basaltiques; exemple de l'Afar. SOC.GEOL.FR.BULL. 15, 506-540.

TUTTLE O F and BOWEN N L (1958) Origin of granite in the light of experimental studies in the system $NaAlSi_3O_8$ - $KAlSi_3O_8$ - SiO_2 - H_2O. GEOL.SOC.AM.MEM. 74, 153pp.

van BREEMAN O and BLUCK B J (1981) Episodic granite plutonism in the Scottish Caledonides. NATURE 291, 113-117.

VANCE J A (1961) Zoned granitic intrusions - an alternative hypothesis of origin. BULL.GEOL.SOC.AM. 72, 1723-1728.

WEDEPOHL K H (1969,1970) Handbook of Geochemistry SPRINGER-VERLAG.

WHITNEY J A (1975) The effects of P, T and X_{H2O} on phase assemblage in four synthetic rock compositions. J.GEOL. 83, 1-31.

WINKLER H G F (1976) Petrogenesis of Metamorphic Rocks. SPRINGER-VERLAG. p.278-324.

WRIGHT T L (1968) X-ray and optical study of alkali feldspars. II. An x-ray method for determining the composition and structural state from measurement of 2θ values for three reflections. AM.MINER. 53, 88-104.

WYLLIE P J (1977) From crucibles through subduction to batholiths. In:S.K.Saxena and S.Battacharji, "Energetics of Geological Processes", SPRINGER-VERLAG, NEW YORK. p.389-433.

WYLLIE P J (1983) Experimental studies on biotite- and muscovite-granites and some crustal magmatic sources. In: M.P.Atherton and C.D.Gribble (eds) "Migmatites, Melting and Metamorphism" SHIVA. p 12-26.

WYLLIE P J, HUANG W L, STERN C R and MAALØE S (1976) Granitic magmas: possible and impossible sources, water contents and crystallisation sequences. CAN.J.EARTH SCI. 13, 1007-1019.

YODER H S and TILLEY C E (1964) Origin of basalt magmas: an experimental study of natural and synthetic rock systems. J.PET. 3, 342-532.

ZALESKI E (1982) The geology of Speyside and lower Findhorn granitoids. UNPUBL. M.Sc., UNIV. OF ST.ANDREWS.